Aus der Klinik für Allgemein-, Viszeral- und Transplantationschirurgie

Klinik der Ludwig-Maximilians-Universität München

Direktor: Prof. Dr. J. Werner

mTORC1 and mTORC2 converge at the Arp2/3 complex-mediated actin rearrangement in oncogenic Kras^{G12D}-induced acinar-to-ductal metaplasia

Dissertation

zum Erwerb des Doktorgrades der Humanbiologie

an der Medizinischen Fakultät der

Ludwig-Maximilians-Universität Zu München

vorgelegt von

Yamin Zhao

aus Yongcheng, China

2020

Mit Genehmigung der Medizinischen Fakultät

der Ludwig-Maximilians-Universität München

Berichterstatter:	PD Dr. Jan D'Haese
	_____
Mitberichterstatter:	PD Dr. Helga Török
	Prof. Dr. Dolores Schendel
Dekan:	Prof. Dr. med. dent. Reinhard Hickel
Tag der mündlichen Prüfung:	04.11.2020

TABLE OF CONTENTS

Affidavit

I hereby declare, the submitted thesis entitled ‘mTORC1 and mTORC2 converge at the Arp2/3 complex-mediated actin rearrangement in oncogenic $Kras^{G12D}$-induced acinar-to-ductal metaplasia’ is my own work, all of the present work embodied in this thesis was carried out between 11/2015 and 03/2020 under the supervision of PD. Dr. Dr. Bo Kong, Department of Surgery, Klinikum rechts der Isar, Technical University of Munich. This project is carried out within the frame of scientific collaboration with PD. Dr. Jan G. D’Haese at the Department of Surgery, Ludwig-Maximilians-Universität München.

I have only used the sources indicated and have not made unauthorized use of services of a third party. Where the work of others has been quoted or reproduced, the source is always given. This work has not been submitted in part or full to any other university or institute for any degree or diploma.

I further declare that the submitted thesis or parts thereof have not been presented as part of an examination degree to any other university.

Part of the work was done by Miss. Vivien Tissen, master student of Technical University of Munich, Germany. She has performed the *in vitro* studies to investigate the role of mTORC2 signaling in ADM formation. The data is presented in the results part (section 4.14).

Munich, 05.11.2020	Zhao Yamin
……..	……...
Place, date	Signature doctoral candidate

Zusammenfassung

Onkogene $Kras^{G12D}$-Expression transformiert adulte Azinuszellen irreversibel in duktale Zellen. Die sogenannte azinär-duktale Metaplasie (ADM) ist entscheidend bei der Entwicklung des duktalen Pankreaskarzinoms (PDAC). Jüngste Studien zeigen, dass diese metaplastische Veränderung eine spezielle Umlagerung des Zytoskeletts erfordert, welche wiederum eine Umverteilung der apiko-basalen Spannung innerhalb der Azinuszellen erzeugt. Der genaue Mechanismus für diese apiko-basale Spannungsumverteilung ist jedoch noch unbekannt. mTOR (mechanistisches Ziel der Rapamycinkinase), eine Zielstruktur von onkogenem Kras, beruht auf der Funktion von Rptor (regulatorisch assoziiertes Protein von mTOR, Komplex 1) und Rictor (RPTOR-unabhängiger Begleiter von mTOR, Komplex 2), um die mutmaßlichen PDAC-onkogenen Komplexe, mTORC1 und mTORC2, zu bilden. Der Actin-verwandte Protein 2/3 (Arp2/3) -Komplex ist ein Actin-Keimbildner, der die neuartige Actin-Polymerisation und die Erzeugung mechanischer Spannungen in anderen biologischen Zusammenhängen fördert.

Ein gut etabliertes Mausmodell der entzündungsbeschleunigten $Kras^{G12D}$-gesteuerten frühen Pankreaskarzinogenese wurde verwendet. Ebenfalls wurden Rptor und Rictor in Azinuszellen spezifisch ausgeschaltet, um mTORC1 und mTORC2 zu deaktivieren, während Arpc4 (Aktin-verwandte Protein 2/3 Komplexuntereinheit 4) deletiert wurde, um die Funktion des Arp2/3-Komplex zu verhindern. Ein 3D-Kultursystem wurde appliziert, um die ADM-Bildung in vitro zu untersuchen. Die Ergebnisse der präklinischen Modelle wurden an menschlichen Materialien bestätigt. Massenspektrometrische Proteomanalyse wurde zum Screening auf nachgeschaltete Ziele von mTORC1 und mTORC2 verwendet.

Sowohl mTORC1 als auch mTORC2 sind insbesonders in ADM-Läsionen bei

Menschen und Mäusen aktiviert. Funktionell hemmt die alleinige Deaktivierung von mTORC1 oder mTORC2 nur vorübergehend die onkogene $Kras^{G12D}$-gesteuerte ADM-Bildung. Eine gleichzeitige Deaktivierung von mTORC1 und mTORC2 ist erforderlich, um die onkogene $Kras^{G12D}$-gesteuerte ADM-Entwicklung dauerhaft zu unterdrücken. Somit existiert eine synergistische Wechselwirkung zwischen ihnen. Die Proteomanalysen identifizieren Arp2/3-Komplex als den gemeinsamen nachgeschalteten Effektor von mTORC1 und mTORC2. Die genetische Deaktivierung des Arp2/3-Komplexes blockiert die onkogene $Kras^{G12D}$-gesteuerte ADM-Entwicklung vollständig und ahmt den Phänotyp von Mäusen, bei denen sowohl mTORC1 als auch mTORC2 fehlen, nach. Insbesondere $Kras^{G12D}$-Azinuszellen mit deaktiviertem Arp2/3-Komplex sind nicht in der Lage, eine apiko-basale Spannungsumverteilung zu erzeugen. Mechanistisch gesehen ist mTORC1 für die direkte Proteinsynthese von Rac1 (kleine GTPase 1 der Rac-Familie) und Arp3 verantwortlich, während mTORC2 die Aktivität des Arp2/3-Komplexes durch Akt / Rac1-Signalübertragung fördert.

Nun identifizieren wir eine gleichzeitige, jedoch nicht redundante regulatorische Rolle von mTORC1 und mTORC2 bei der Förderung der Arp2/3-Komplexfunktion, die für die $Kras^{G12D}$-gesteuerte ADM-Bildung unverzichtbar ist. Die durch den Arp2/3-Komplex vermittelte Aktinpolymerisation ist für die Erzeugung einer Umverteilung der apiko-basalen Spannung verantwortlich und instruiert Azinuszellen eine duktale Morphologie anzunehmen.

Abstract

Upon oncogenic $Kras^{G12D}$ expression, adult acinar cells assume an irreversible phenotype of acinar-to-ductal metaplasia (ADM), playing a crucial role in pancreatic ductal adenocarcinoma (PDAC) development. Recent studies demonstrate that this metaplastic change requires a specific cytoskeleton rearrangement generating apical-basal tension redistribution within acinar cells. However, the exact mechanism for this apical-basal tension redistribution is still unknown. mTOR (mechanistic target of rapamycin kinase), a downstream target of oncogenic Kras, relies on the function of Rptor (regulatory associated protein of mTOR, complex 1) and Rictor (RPTOR independent companion of mTOR, complex 2) to form putative oncogenic complexes of PDAC: mTORC1 and mTORC2. The actin-related protein 2/3 (Arp2/3) complex is an actin nucleator promoting novel actin polymerization and generation of mechanical tension in other biological contexts.

A well-established mouse model of inflammation-accelerated $Kras^{G12D}$-driven early pancreatic carcinogenesis was used. At the same time, Rptor and Rictor were conditionally ablated in acinar cells to deactivate mTORC1 and mTORC2, while Arpc4 (actin related protein 2/3 complex subunit 4) was deleted to ablate the function of Arp2/3 complex. A 3D-culture system was applied to investigate ADM formation in vitro. Results from the preclinical models were confirmed on human materials. Mass spectrometry-based proteomic analysis was used for screening downstream targets of mTORC1 and mTORC2.

Both mTORC1 and mTORC2 are mainly activated in human and mouse ADM lesions. Functionally, mTORC1 or mTORC2 deactivation alone only transiently inhibits oncogenic $Kras^{G12D}$-driven ADM formation. A dual deactivation of mTORC1 and mTORC2 is required to persistently suppress oncogenic $Kras^{G12D}$-driven ADM

development, demonstrating a synergistic interaction between them. The proteomic analyses identify the Arp2/3 complex as the common downstream effector of mTORC1 and mTORC2. Genetic deactivation of Arp2/3 complex completely blocks oncogenic $Kras^{G12D}$-driven ADM development in mice, photocopying the phenotype of mice deficient for both mTORC1 and mTORC2. In particular, $Kras^{G12D}$ acinar cells with deactivated Arp2/3 complex are not capable of generating apical-basal tension redistribution. Mechanistically, mTORC1 is responsible for the direct protein synthesis of Rac1 (Rac family small GTPase 1) and Arp3 while mTORC2 promotes the activity of Arp2/3 complex by Akt/Rac1 signalling.

Now, we identify a dual, yet non-redundant, regulatory role of mTORC1 and mTORC2 in promoting Arp2/3 complex function, which is indispensable for $Kras^{G12D}$-driven ADM formation. The Arp2/3 complex-mediated actin polymerization is responsible for generating apical-basal tension redistribution, acting as an “incipient” instruction cue for ductal morphology of acinar cells.

1. Introduction

1.1 Pancreatic ductal adenocarcinoma

Pancreas cancer is highlighted by a similar morbidity and mortality.[1] Though surgical resection leads to more prolonged survival compared with chemotherapy, radiation therapy and palliative care, only a small part of patients are eligible for curative resection due to the late diagnosis.[2] Furthermore, a majority of patients succumb to recurrence in the end.[1, 3, 4] Total deaths due to pancreas cancer are predicted to increase dramatically to become one of the top cancer killers before 2030 in the USA.[5] Early diagnosis and treatment of pancreatic cancer is the only way to reduce mortality.

Pancreatic ductal adenocarcinoma (PDAC) is the most common entity of malignant pancreatic tumours, which also include solid-pseudopapillary neoplasms (SPNs), pancreatic neuroendocrine tumours (PanNETs), acinar cell carcinomas (ACC), pancreatoblastomas, classified according to tumour morphology and immunohistochemical features.[6, 7] Risk factors for PDAC consist of cigarette smoking, chronic pancreatitis, diabetes, obesity, races and inherited risk factors.[8] But the most vital driver factor of PDAC is gene alteration, generally including genetic mutations in kirsten rat sarcoma viral oncogene homolog (KRAS), cyclin-dependent kinase inhibitor 2A (CDKN2A), tumor protein p53 (TP53) and small mothers against decapentaplegic (SMAD4).[9] KRAS is the most universal mutated oncogene, usually co-exists with genetic alternations on putative tumour suppressers such as CDKN2A, TP53 and SMAD4.[7, 10, 11] There are three well-established PDAC precursor lesions: pancreatic intraepithelial neoplasias (PanINs), intraductal papillary mucinous neoplasms (IPMNs), and mucinous cystic neoplasms (MCNs).[12] Every precursor lesion is different from each other with their unique features in pathology.

In the adult pancreas, more than 90% of it are acinar cells, and the rest are ductal and

endocrine cells, including α, β, δ, PP and ε cells.[13] It was thought that PDAC originates from ductal cells in the pancreas because of their similar morphologies. Recently, results from genetically engineered mouse models (GEMMs) revealed that PDAC can be initiated from different cell types in the pancreas.[14] Lineage tracing studies demonstrate that PanIN lesions mainly arise from the acinar cell.[15] However, IPMNs might develop from the ductal epithelium within the so-called progenitor niche; the origin of MCN is still unknown.[14] Thus, the cell of origin for PDAC remains elusive. It was reported that insulin-expressing cells could also be transformed to develop PanINs and PDAC in the context of Kras mutation, p53 mutation and caerulein-induced pancreatitis.[16]

1.2 GEMM of PDAC

1.2.1 $Kras^{G12D}$ mouse model

To identify the molecular mechanism of initiation and development of pancreatic cancer, develop novel diagnostic and therapeutic strategies, GEMMs are employed to recapitulate several pancreatic tumour subtypes. In GEMMs of PDAC, a so-called "$Kras^{G12D}$ strain" was used as the backbone mouse model (see below). This mouse model relies on the Lox-Stop-Lox-$Kras^{G12D}$ mouse strain (referred to as LSL-$Kras^{G12D}$) and the Cre recombinase-dependent tissue-specific system. In the LSL-$Kras^{G12D}$ mouse, the expression of knock-in mutant $Kras^{G12D}$ allele is blocked by STOP cassette flanked by LoxP sites. In the presence of Cre recombinase driven by Pdx1 or Ptf1a (also known as p48), the pancreas-specific promoter, mutant Kras is activated by removing STOP cassette and by Cre recombinase. These mice developed precursor lesions and partially progressed to PDAC after a long latency. Based on the $Kras^{G12D}$ mouse model, one of the most used GEMMs of PDAC was generated by crossing with the LSL-$Trp53^{R172H}$ mouse strain. It displayed invasive and metastatic carcinomas.[17, 18]

1.2.2 Inducible system

However, there is a limitation of these mouse models. The Cre-mediated recombination occurs in embryo, which means Kras is activated in a very early stage, the pancreas develops PanINs rapidly after birth, which is different from the PDAC development in humans. Here, PDAC occurs in the mature gland of adult subjects through random mutations in the pancreas. To overcome these shortcomings, an inducible system was developed in which genes of interest can be knocked in or knocked out temporally and spatially. As such, one of frequently used system is CreER technology which was firstly described by Feil et al. in 1996. In this new version of the Cre-loxp system, Cre recombinase is fused to a mutated ligand-binding domain (LBD) of the human estrogen receptor (ER), which is so-called CreER. The CreER recombinase can be activated by tamoxifen instead of estradiol *in vivo*.[19] Once induced by tamoxifen, CreER recombinase translocates from the cytoplasm into the nucleus, where it mediates the genetic recombination of LoxP sites.[20] Currently, the most effective CreER recombinase is $CreER^{T2}$ version. The LBD of $CreER^{T2}$ harbours G400V/M543A/L544A triple mutations to avoid possible unexpected side effects induced by tamoxifen[21, 22] In the field of PDAC modelling, the inducible systems include ElastasCreERT2, $Ptf1a^{Cre\text{-}ERTM}$, and Pdx1-CreERT,[23-25] where the CreER recombinase expression is driven by cell-type-specific promotors in pancreas. To monitor the recombination efficiency of these inducible systems, a reporter gene has been developed and used as a critical tool. The most widely used reporters are autofluorescent proteins (AFPs), such as green fluorescent protein (GFP) and red fluorescent protein (RFP). The expression of AFPs can be detected by fluorescence-activated cell sorting (FACS) at the single living cell level, fluorescence microscopy and fluorometer without any invasive treatment and exogenous substrates. The ubiquitous expression of AFPs can be achieved by inserting the reporter gene into the Rosa26 locus, which is transcriptionally active across the majority of organs. The temporal and tissue-specific expression of Rosa26-targeted reporter proteins can be realized by the Cre-loxp system using the above mentioned Loxp_Stop_Loxp strategy.[26]

1.3 Acinar-to-ductal metaplasia

In the pancreas, acinar cells are highly plastic which have the potential of dedifferentiating to other cell types such as ductal cells and endocrine cells.[15, 27]. The acinar-to-ductal metaplasia (ADM) is a process that acinar cells acquire a duct-like phenotype.[28] *In vivo*, ADM can be induced by oncogenic Kras and pancreatitis.[29] *In vitro*, the factors that are applied to promote ADM formation include mutant Kras,[30] transforming growth factor-α (TGF-α), hepatocyte growth factor (HGF) in rodent[31] and transforming growth factor-β (TGF-β) in human.[32] During the process of ADM, gene expression profile changes dramatically. Part of genes are downregulated, such as Ptf1a, Mist1, Gata6. These are transcription factors which maintain the morphology and functions of acinar cells. Genetic ablation of any of these genes in acinar cells leads to ADM formation.[33-35] Other genes like p120 catenin, an intracellular protein, which supports cell-cell adhesion, its deletion in the pancreas lead to ADM formation.[36] Part of genes are upregulated. Transcription factors Sox9 and Pdx1 are required for acinar cell dedifferentiation. Sox9 mainly expresses in human and mouse centroacinar cells, also in acinar cells and some ductal cells, but at a low level.[37, 38] In the context of inflammation, Sox9 expression increased dramatically in acini which proceed to ADM.[39] The expression of Pdx1 is mostly in islets, but few in acinar cells of adult mouse pancreas, in pancreatitis, Pdx1 is upregulated.[40, 41] Furthermore, the sustained Pdx1 expression in acinar cells induced also ADM phentype.[42] Besides, the matrix-degrading metalloproteinases (MMP)-9 was strongly upregulated in the inflamed pancreas. Inflammatory macrophages secret several cytokines to activate nuclear factor (NF)-κB, which regulates the degradation of the extracellular matrix through MMP-9. It is proved that the MMP inhibitor completely blocked the pancreatitis-induced ADM formation *in vivo*.[43]

1.4 Pancreatic regeneration

ADM is common after acute pancreatitis or injury. In wild-type animals, ADM formation is a transient process that resolves itself in 7 days post caerulein treatment. During this process, pancreatic regeneration is achieved by ADM redifferentiation and acinar cell proliferation.[44-46] Some genes are essential for pancreas regeneration; for example, Hes1 is expressed in the centroacinar cells; the loss of Hes1 leads to persistent ADM after acute caerulein-induced pancreatitis.[47] Knock out of ARID1A, which altered most frequently in PDAC, leads to impaired recovery of the exocrine compartment.[48] Hedgehog (Hh) pathway maintains progenitor cell number in adult tissues, genetic inhibition of Hh Signaling results in impaired pancreatic regeneration.[49] Numb, a multifunctional protein, is vital for cell division and maintaining progenitor cell. Deletion of Numb in pancreatic acinar cells leads to abundant duct structures 7 days post caerulein injection.[45]

1.5 ADM driven by oncogenic Kras^{G12D}

In the presence of Kras^{G12D}, ADM lesions do not differentiate back to acinar cells, but they further progress into pre-neoplastic lesions and eventual PDAC. This is mediated by a number of downstream pathways of oncogenic Kras^{G12D} (see below).

1.5.1 MAPK pathway

Mitogen-activated protein kinase (MAPK) pathway is well studied as a downstream pathway of Kras. It regulates cell growth, proliferation, differentiation and other biological processes. The classical MAPK pathway is Ras → Raf → MEK → ERK; Firstly, the activated Kras phosphorylates the serine/threonine kinase Raf, continuously, MAPK kinase (MEK1/2) is activated by Raf, which proceeds on phosphorylating extracellular signal-regulated kinase (ERK1/2).[50] In wild-type mice, the MAPK pathway is upregulated but only for a short time during acute pancreatitis, in the context of oncogenic Kras^{G12D}, the upregulation is consistent. A pharmacological inhibition of MAPK signalling prevents the ADM and PanIN formation in Kras^{G12D} mice 1 week

after caerulein injection. Interestingly, under the inhibition of Mek1/2, PanIN lesions are capable of redifferentiating back to acinar cells.[51] Above all, the sustained activation of MAPK pathway is partially accountable for ADM, PanIN and PDAC development caused by oncogenic $Kras^{G12D}$ and pancreatitis.

1.5.2 PI3K pathway

Phosphoinositide 3-kinase (PI3K) is another downstream effector of Kras. It is proved in mice that PI3K p110α isoform is activated in pancreatic precursor lesion induced by oncogenic $Kras^{G12D}$ and pancreatitis. A pharmacological inhibition of p110α block the ADM formation *in vivo*. Moreover, the genetic inactivation of p110α prevents the formation of pre-neoplastic lesion in these models. Further analysis revealed that the p110α signalling regulates the ADM plasticity through actin cytoskeleton.[29] Consistently, Payne SN et al. proved the similar finding, he generated a $Pc^{l}Pik3cap^{110*}$ mouse model in which PI3K signalling is persistently activated, and observed that this persistently activated PI3K signalling accelerated the ADM development *in vivo*. ERK1/2, the downstream of PI3K, is involved in such process.[52] Sustained activation of Akt signalling, the downstream of PI3K, drives the formation of "ductal structures": a portion of these ductal structures is the result of proliferative ductal epithelium, ADM lesions and β cells also contribute partially to these "ductal structures". [53] Rac family small GTPase 1 (Rac1), a guanosine triphosphatase (GTPase) of rhodopsin (Rho) family, is also a downstream effector of PI3K, regulating actin dynamics. It is proposed that the deactivation of PI3K pathway and the Rac1 ablation prevent the $Kras^{G12D}$-driven ADM development *in vivo* by affecting the similar cellular machinery-actin remodelling.[54]

1.5.3 Other pathways

Other upregulated signalling pathways include polycystic kidney disease 1 (PKD1), Notch and nuclear factor kappa-light-chain-enhancer of activated B cells (NF-κB). It

was reported that the expression of oncogenic Kras cause san oxidative stress in ADM and PanIN leions. In 3D culture, the pharmacological inhibition of mitochondrial reactive oxygen species (mROS) reduced the capacity of isolated $Kras^{G12D}$ acinar cells in promoting ADM lesions in vitro. The further study revealed that mROS activated PKD1, which triggers the NF-κB pathway. Collectively, it led to the increased expression of epidermal growth factor receptor (EGFR) and its ligands TGF-α and a disintegrin and metalloptroteinase-17 (ADAM 17).[55] *In vitro* data from the same researchers proved that TGF-α induced ADM formation through Kras activation, PKD1 is activated as a downstream target of Kras, however, inhibition of Notch pathway block ADM formation under activated TGF-α-Kras-PKD1 signalling.[56] In another study, the TGFα-induced ADM relies on the function of matrix metalloproteinase (MMP) 7, which is important in maintaining the pro-ADM function of Notch signalling *vitro*.[57]

1.6 Pancreatic injury

Oncogenic $Kras^{G12D}$ promotes ADM and PanIN formation in mouse model, however few of them develop PDAC, to accelerate this procedure, extra events are required. Such additional events include mutation of p53,[58] CDKN2A,[59] inactivations of Smad4.[60]

The widely used method to accelerate oncogenic Kras-driven pancreatic carcinogenesis is the caerulein-induced pancreatitis. Caerulein, an analogue of cholecystokinin (CCK), stimulates the secretion of digestive enzymes in rodents, resulting in the severe autodigestion by pancreatic protease.[61] According to the commonly used protocol for acute pancreatitis induction, mice are administered caerulein at supramaximal levels, seven doses hourly one day, 50 μg/kg body weight, but in pancreatic regeneration research, two consecutive days intraperitoneal injection are required.[62, 63] However, in the presence of oncogenic $Kras^{G12D}$, the organ regeneration in acinar cell compartment is blocked, instead, the acinar cell acquired non-reversible ADM phenotype and some of them further progress into PanIN lesions and PDAC after caerulein-induced

pancreatitis.[64]

1.7 mTOR signalling

Mechanistic target of rapamycin (mTOR) is a serine/threonine protein kinase which belongs to the PI3K-related kinase (PIKK) family. mTOR is involved in two complexes, mTOR complex 1 (mTORC1) and 2 (mTORC2), which play crucial roles in growth, metabolism and disease.

1.7.1 mTORC1 signalling

Components of mTORC1

mTORC1 is composed of mTOR, the regulatory-associated protein of mTOR (Rptor), mammalian lethal with Sec13 protein 8 (mLST8, also known as GβL),[65, 66] proline-rich Akt substrate of 40 kDa (PRAS40)[67, 68] and DEP domain-containing mTOR-interacting protein (DEPTOR).[69] Rptor is required for mTORC1 kinase activity.[70, 71] mLST8 keeps the kinase activation loop stable.[72] However, the other two subunits play an inhibitory role in the signalling.

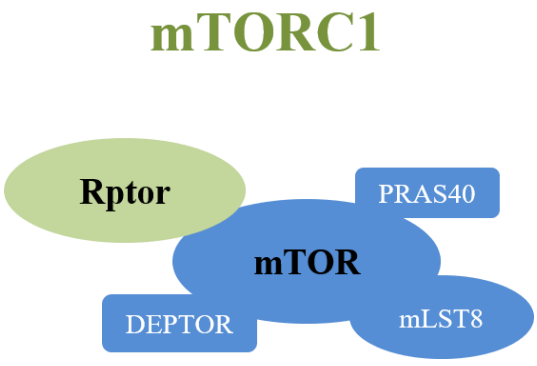

Figure 1. The simplified structure of mTORC1

mTORC1 upstreams

mTORC1 is activated by the small GTPase ras homolog enriched in brain (Rheb),[73] which is the downstream effector of Tuberous Sclerosis Complex (TSC). Many growth factor pathways such as insulin/insulin-like growth factor-1 (IGF-1) pathway, receptor

tyrosine kinase-dependent Ras signalling, Wnt signalling and the inflammatory cytokine TNFα activate mTORC1 via phosphorylating TSC.[74] For example, insulin promotes the PI3K activity that converts phosphatidylinositol 4,5-bisphosphate (PIP2) to phosphatidylinositol 3,4,5 trisphosphate (PIP3). By the function of PIP3, Akt is recruited to the plasma membrane where it is phosphorylated by pyruvate dehydrogenase kinase 1 (PDK1) at Thr308, leading to the partial activation of Akt This partially activated Akt, in turn, phosphorylates TSC2, which further activate the mTORC1.[75]

mTORC1 signalling is inhibited under the circumstances of glucose deprivation, hypoxia and DNA damage through either the direct phosphorylation of Rptor or the indirect activation of TSC.[76-78] mTORC1 is also tightly regulated by the concentration of amino acid. It was reported that Rag GTPases could be converted to be activated state once stimulated by amino acids, which allows them to bind to Rptor, then mTORC1 is recruited to the lysosomal surface and activated by Rheb. This discovery was considered as a breakthrough by unraveling the mechanism underlying amino acid sensing by mTORC1.[79, 80]

mTORC1 downstream

p70S6 Kinase 1 (S6K1) and eIF4E Binding Protein (4EBP) are two main downstream targets of mTORC1. S6K1 is phosphorylated by mTORC1 on Thr 389 and further phosphorylated by PDK1. Activated S6K1 subsequently phosphorylates eukaryotic translation initiation factor 4B (eIF4B) to promote the mRNA translation initiation. At the meantime, it also phosphorylates programmed Cell Death 4 (PDCD4), an inhibitor of eIF4B, to accelerate the degradation of PDCD4.[81, 82] The 40S ribosomal protein S6 (S6) can also be phosphorylated by S6K1, it is linked to the mRNA translation and cell growth.[83] The other substrate-4EBP binds to eukaryotic translation initiation factor 4E (eIF4E), as such, it prevents the assembly of Eukaryotic initiation factor 4F (eIF4F) complex. When phosphorylated by mTORC1, 4EBP dissociates from eIF4E, promoting the mRNA translation initiation.[84] mTORC1 promotes the protein synthesis mainly

through these two key effectors.

mTORC1 also activates the sterol responsive element binding protein (SREBP) which is a transcription factor regulating the expression of metabolic proteins associated with fatty acid and cholesterol biosynthesis.[85] S6K1 can activate carbamoyl-phosphate synthetase (CAD), which governs the pyrimidine synthesis pathway.[86] mTORC1 also regulates the transcription factor hypoxia-inducible factor 1 (HIF1α), which promote the glucose metabolism by increasing the expression of glycolytic enzymes.[87] Thus, mTORC1 signalling activates lipid, nucleotideand glucose metabolism to support cell growth.

Unc-51-like kinase 1 (ULK1) can also be phosphorylated by mTORC1 when the nutrient is sufficient. This phosphorylation of ULK1 prevents the initiation of autophagy.[88] Transcription factor EB (TFEB) can also be phosphorylated by mTORC1, which inhibits the process of autophagy.[89, 90] In this way, mTORC1 promotes cell growth via the inhibition of protein catabolism.

1.7.2 mTORC2 signalling

Components of mTORC2

mTORC2 shares the component of mTOR, mLST8 and DEPTOR with mTORC1. However, mLST8 is required to maintain the rictor-mTOR binding instead of the rptor-mTOR interaction.[91] Rapamycin insensitive companion of mTOR (Rictor) is specific to mTORC2, and it is essential for its activity.[92] mTORC2 also contains the unique regulatory subunits of mammalian stress-activated protein kinase interacting protein 1 (mSin1) and protein observed with rictor 1 and 2 (Protor1/2).[93, 94]

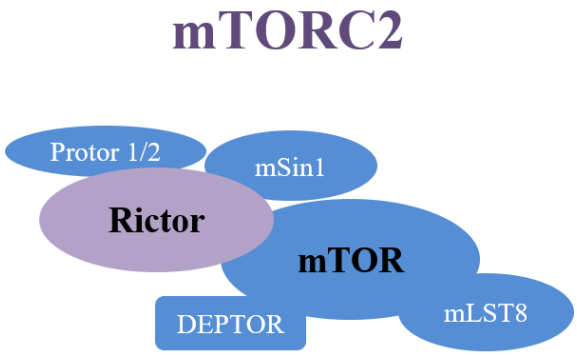

Figure 2. The simplified structure of mTORC2

mTORC2 upstream

mTORC2 is the downstream of insulin/PI3K signalling. One subunit of mTORC2 is mSin1 which has a pleckstrin homology (PH) domain. Via this PH domain, it interacts with mTOR kinase domain to prevent the activation of mTORC2, when insulin is not available. However, this inhibition can be released upon the SIN1-PH binding to PIP3 (generated by PI3K) at plasma membrane.[95] It is also reported that PI3K promotes the binding of mTORC2 to ribosomes, which are necessary for the mTORC2 activity; however, how ribosomes activate mTORC2 is elusive.[96] mTORC2 can also be activated by phosphorylated Akt at T308, and this partial activation of Akt phosphorylates mSin1, which drives the mTORC2 activity.[97]

mTORC2 downstream

The first identified substrate of mTORC2 was protein kinase C alpha (PKCα), regulating the actin cytoskeleton.[98] After that, it is reported that several other members of PKC protein kinase can also be phosphorylated by mTORC2, such as PKCδ, PKCζ, PKCγ and PKCε,[99-101] involved in cytoskeleton organization and cell migration regulation. Another important downstream effector of mTORC2 is Akt.[102] Akt is phosphorylated at Ser473 by mTORC2, leading to fully activated AKT signaling.[103] Furthermore, the serum- and glucocorticoid-induced protein kinase (SGK)1 is be activated by mTORC2 to regulate the ion transport and to promote cell survival.[104]

1.7.3 Physiological functions of mTOR signalling

Both mTORC1 and mTORC2 are involved in various biological processes and they play essential roles in physiological procedures. Using well-established mouse models, more and more functions of these two mTOR complexes are being uncovered in mammalians.

The regulation of mTORC1 signalling is critical for glucose homeostasis. The hyperactivation of mTORC1 in the liver inhibits autophagy and gluconeogenesis, resulting in hypoglycemia.[105, 106] Sustained mTORC1 activity in the pancreas improves glucose tolerance at the beginning, but reduces β-cell mass and leads to hyperglycemia in the end.[107, 108] mTORC1 signalling also promotes muscle growth. Activated mTORC1 signalling is correlated with muscle hypertrophy,[109] impaired mTORC1 signalling leads to severe muscle atrophy.[110] Both mTORC1 and mTORC2 signalling play important roles in adipogenesis and lipid homeostasis. Inhibition of mTORC1 blocks adipogenesis and suppresses lipogenesis in the adipocyte.[111] mTORC2 activation has been shown to accelerate lipogenesis in the liver.[112] In the immune system, mTORC1 promotes T-cell activation and expansion via facilitating anabolic metabolism.[113] Recent studies found that mTORC1 plays a complicated role in T-cell maturation.[114, 115] In nervous system development, the loss of mTORC1 or mTORC2 leads to smaller neuron and early death. Conversely, the hyperactivation of mTORC1 signalling in the brain is associated with various brain disorders.[116]

1.7.4 Oncogenic functions of mTOR signalling

mTOR is widely involved in tumorigenesis of multiple diseases including breast cancer, head and neck cancer, colorectal cancer, intestinal cancer, prostate cancer, pancreatic cancer and so on.[117-122] Sustained mTORC1 signalling in tumours can be achieved in different ways. As the downstream of PI3K/Akt and MAPK pathways, which are frequently mutated in cancers, mTORC1 is activated subsequently.[123] Besides, the mutated p53 negatively regulates the lysosomal TSC2, which leads to the hyperactive

mTORC1.[124] Furthermore, mTOR itself is found to be mutated in a variety of cancers, leading to the hyperactivation of mTORC1.[125] Sustained mTORC1 signalling promotes cell growth and proliferation and accelerates cancer development. mTORC2 is also required in prostate cancer in the mouse model and essential for human prostate epithelial cells to develop tumours.[126] Researchers have also shown that specific mTORC2 inhibitor blocks breast cancer cell growth and survival *in vivo* and *in vitro*.[127] Also, the loss of mTORC2 signalling inhibits PDAC tumour growth in mouse models.[128]

1.7.5 mTOR inhibitor

Rapamycin is the typical inhibitor of mTORC1. It binds the peptidyl-prolyl-isomerase FKBP12 to inhibit mTORC1 activation.[129] mTORC2 is not sensitive to acute rapamycin treatment, but its inhibition can be achieved by the prolonged Rapamycin treatment, potentially due to an impaired mTORC2 assembly disturbed by the rapamycin-FKBP12 complex.[130]

Previously, a number of rapamycin analogues, namely rapalogs, have been tested by clinical trials.[131-134] Unfortunately, none of them were as successful as expected from pre-clinical research.[135] It was found that mTORC2 is activated due to negative feedback on insulin/PI3K/Akt signalling when mTORC1 is inhibited alone.[97] This explanation is proved by increased Akt signalling detected in tumour biopsies from the clinical trial.[136] It was also reported that the rapalogs only partially inhibited the downstream activity of mTORC1, for example, the phosphorylation of S6 was indeed inhibited whereas the 4EBP1 activity was resistant in a majority of clinical settings.[137, 138] Moreover, the mTORC1 inhibition promotes the autophagy and micropinocytosis which again support cancer growth and survival.[139] Therefore, the combination of rapalogs and autophagy inhibitors is being tested in clinical trials. The preliminary results in melanoma patients showed an improved efficacy compared with the rapalog monotherapy.[140]

Recently, inhibitors targeting both mTORC1 and mTORC2 are developed and tested in clinical trials. These novel inhibitors are ATP-competitive catalytic inhibitors against mTOR, which suppress both mTORC1 and mTORC2 catalytic activity directly. Although these new mTOR inhibitor were more effective than rapalogs in preclinical research, the feedback activation of PI3K also took place after the long-term treatment with ATP-competitive mTOR inhibitors.[141] Thus, the dual PI3K/mTOR inhibitors are currently under development to overcome this feedback activation.

1.8 Arp2/3 complex

1.8.1 Physiological function of Arp2/3 complex

The actin-related protein 2/3 (Arp2/3) complex is composed of seven subunits, two of which are Arp2 and Arp3, actin-related proteins, the other five of which are Arpc1 to 5. Arpc1 can be encoded by paralogous genes Arpc1a and Arpc1b, Arpc5 also has two isoforms: Arpc5 and Arpc5l.[142] In the inactive conformation of Arp2/3 complex, Arp2 and Arp3 are separated,[143] when it is activated, Arp2/3 complex binds to the pre-existing actin filaments, also called mother filaments, Arp2 and Arp3 move close and form a dimmer on the sides of mother filaments, promoting a new filament (daughter filament) nucleation on the dimmer.[144] Therefore, the Arp2/3 complex function as generating branched actin networks. Its activity is mainly regulated by nucleation-promoting factors (NPFs) such as N-WASP or WAVE.[145, 146] Different paralogous subunits in Arp2/3 complex also show different activity in promoting actin polymerization, Arpc1b and Arpc5l are more efficient.[142] Besides, the phosphorylation of Arp2 is also essential for the activity of the Arp2/3 complex.[147] Small molecules CK-666 and CK-869 are commonly used inhibitors specifically for Arp2/3 complex. CK-666 binds between Arp2 and Arp3, stabilizing Arp2/3 inactive conformation. CK-869 has a different binding site on Arp3, which reduces the stability of Arp2-Arp3 dimmer and inhibits Arp2/3 activation.[143]

1.8.2 Oncognic function of Arp2/3 complex

Arp2/3 subunits were studied in different diseases in past decades. In PDAC cell lines, Arpc1a gene is overexpressed, the silencing of Arpc1a in AsPC-1 cell line suppresses cell migration and invasion.[148] Besides, Arpc3 and Arpc4 are also overexpressed, especially the silencing of Arpc4 inhibits cell migration in all tested PDAC cell lines.[149] In colorectal cancer, the expression of Arp2 and its regulator WAVE2 is positively correlated with the liver metastasis.[150] Similarly, the co-expression of Arp2 and WAVE2 in lung adenocarcinoma and breast ductal carcinoma predicts shorter survival time.[151, 152]

2. Hypothesis

Previously, we and others have provided genetic evidence defining the oncogenic function of both mTORC1 and mTORC2 in overt PDAC.[128, 153-156] However, it remains unknown whether these two mTOR complexes are involved early pancreatic carcinogenesis, especially in ADM and PanIN formation. To address this, a well-established mouse model of inflammation-accelerated $Kras^{G12D}$-driven early pancreatic carcinogenesis was used.

3. Material and Methods

3.1 Instruments and chemicals

3.1.1 Instruments

Analytic Balance	Sartorius, Goettingen, Germany
PH meter	Peqlab Biotechnologie GmbH, Erlangen, Germany
Biometra TOne	Analytic Jena AG, Jena, Germany
X-RAY CASSETTE	X-ray GmbH, Augsburg, Germany
Microtome RM2255	Leica, Wetzlar, Germany
GLOMA multi detection system	Promega, Madison, USA
Nanodrop 2000	Thermo Fisher Scientific, Waltham, USA
HERA safe	Thermo Scientific, Langenselbold, Germany
HERA cell 150	Thermo Scientific, Langenselbold, Germany
Axiovert 40 CFL	Zeiss, Oberkochen, USA
Electrophoresis chamber	Bio-Rad, Carlifonia, USA
Vortex mixer	Neolab, Heiderburg, Germany
TissueLyser	QIAGEN, Hilden, Germany
Centrifuge 5415 R	Eppendorf, Hamburg, Germany
Centrifuge 5424	Eppendorf, Hamburg, Germany
Titromax 100	Heidolph Instruments GmbH, Schwabach, Germany
Multifuge 3SR+	Thermo Fisher Scientific, Waltham, USA
Roller mixer	Merck, Darmstadt, Germany
Cryostat CM 3000	Leica Microsystems, Bensheim, Germany

3.1.3 Miscellaneous

Hypodermic-needle	Braun, Melsungen, Germany
PAP Pen	Kisker, Steinfurt, Germany
Star Seal Advanced Polyolefin Film	Starlab, Hamburg, Germany
SafeSeal micro tube	SARSTEDT, Nuembrecht, Germany
Cell strainer 100 µm	Corning Incorporated, New York, USA
RT-PCR primers	Merck, Darmstadt, Germany
Vasofix Safety	BRAUN, Melsungen, Germany
Weighing tray	Carl Roth GmbH+Co.KG, Karlsruhe, Germany
Disposable Pasteur pipettes	Carl Roth GmbH+Co.KG, Karlsruhe, Germany
Feather disposable scalpel	Daigger Scientific, Vernon Hills, USA
Medical examination gloves	Critical Environment Solutions Ltd, Swindon, England
Pipetboy	INTEGRA Biosciences GmbH, Biebertal, Germany
Multiply-uStrip 0.2 ml chain	SARSTEDT AG, Nuembrecht, Germany
8-Lid chain, flat	SARSTEDT AG, Nuembrecht, Germany
96-well PCR microplate	STARLAB, Hamburg, Germany
Filter Tip	STARLAB, Hamburg, Germany
Embedding cassettes	Carl Roth, Karlsruhe, Germany
Vacuum Filter	Sarstedt, Newton, USA
12-well cell culture plate	Merck, Darmstadt, Germany
Cell culture dishes, 60*15mm	Merck, Darmstadt, Germany
Disposable forceps	Megro GmbH, Wesel, Germany
Syringe 1ml and 5ml	BRAUN, Melsungen, Germany
Serological pipette 5ml-50ml	Merck, Darmstadt, Germany
Syringe Filter 0.2 µm	Thermo Scientific, Waltham, USA
Cell strainer 100 µm	Corning Incorporated, New York, USA
Medical X-ray film	Agfa HealthCare, NV, Mortsel, Belgium
Nitrocellulose blotting membrane	GE Healthcare, Germany
Parafilm	Merck, Darmstadt, Germany
Tube 15 ml and 50 ml	Merck, Darmstadt, Germany
Insulin syringe	BRAUN, Melsungen, Germany

Micro tube	Sarstedt, Nuembrecht, Germany

3.1.2 Chemicals and reagents

RNeasy Mini Kit	Qiagen GmbH, Hilden, Germany
BCA Protein Assay Kit	Thermo Fisher Scientific, Waltham, USA
Tamoxifen	Merck, Darmstadt, Germany
Phosphatase inhibitor cocktail tablet	Roche, Mannheim, Germany
Protease inhibitor cocktail tablet	Roche, Mannheim, Germany
Western Blotting detection reagents	GE Healthcare, Buckinghamshire, UK
SignalStain Ab Diluent	Cell signaling, Frankfurt, Germany
Sample reducing agent (10x)	Invitrogen, Carlsbad, USA
LDS sample buffer (4x)	Invitrogen, Carlsbad, USA
Ethonal absolut	Otto Fischar GmbH, Saarbrucken, Germany
Roticlear	ROTH, Karlsruhe, Germany
Aqua	BRAUN, Melsungen, Germany
Isofluran	CP-Pharma Handelsgesellschaft mbH, Burgdorf, Germany
Saline	Fresenius Kabi Deutschland GmbH, Homburg, Germany
Powdered milk	Carl Roth GmbH+Co.KG, Karlsruhe, Germany
Agarose	VWR, Radnor, USA
Bovines Serum Albumin	Roche Diagnostics, Mannheim, Germany
DMSO	Roche Diagnostics, Mannheim, Germany
30% Acrylamide	Carl Roth GmbH, Karlsruhe, Germany
TEMED	Carl Roth GmbH, Karlsruhe, Germany
Eosin	Merck, Darmstadt, Germany
Hamotoxylin	Roche Diagnostics, Mannheim, Germany
HCl (5N)	Merck, Darmstadt, Germany
Isopropanol	Merck, Darmstadt, Germany
Chloroform	Merck, Darmstadt, Germany

Citrate	Merck, Darmstadt, Germany
DMEM-medium	Merck, Darmstadt, Germany
FSC	Merck, Darmstadt, Germany
Dulbecco's PBS (1×)	Merck, Darmstadt, Germany
Trypsine/EDTA (10×)	Merck, Darmstadt, Germany
Penicillin/Streptomycin (1×)	Merck, Darmstadt, Germany
PBS powder	Merck, Darmstadt, Germany
Protein ladder	Thermo Fisher Scientific, Waltham, USA
Collagen Type I	Corning Incorporated, New York, USA
Hanks' salt solution	Biochrom GmbH, Berlin, Germany
Waymouth's MB 752/1 Medium (1×)	Gibco, Waltham, USA
Collagenase P	Roche, Mannheim, Germany
Soybean trypsin inhibitor	Gibco, Waltham, USA
HEPES	Gibco, Waltham, USA
Caerulein	Merck, Darmstadt, Germany

3.2 Patient material and tissue collection

PDAC and chronic pancreatitis tissues were obtained from patients who carried out pancreatic resections. All the diagnoses were histologically confirmed. Samples were either partially snap-frozen in liquid nitrogen or partially fixed in paraformaldehyde (PFA) solution for 24 hours and then embedded in paraffin for histological analysis. Normal pancreas tissues were obtained through an organ donor program from previously healthy donors; all the samples had previously been collected at Technical University Munich and written informed consent had been obtained from these patients. The use of pancreatic tissues for this study was approved by the local Ethics committee (approval number: 80/17s).

3.3 Experimental procedures

3.3.1 Animals

Mice line harbouring floxed allele of $Rptor^{loxp/loxp}$($Rptor^{fl/fl}$, stock number: 013188), $Rictor^{loxp/loxp}$ ($Rictor^{fl/fl}$, stock number: 020649), the pancreas-specific inducible Cre recombinase line $Ptf1a^{CreERTM}$ (also known as $p48^{CreERTM}$, stock number: 019378) and LSL-$Rosa26^{CAG\text{-}tdTomato}$ (stock number: 007914) were purchased from The Jackson Laboratory (Bar Harbor, Maine, USA). $Ptf1a^{Cre/+}$ (also known as $p48^{Cre/+}$) mice and LSL-$Kras^{G12D}$ mice have been described previously.[153] The wild type C57BL/6J mice were obtained from Charles River Laboratory (Sulzfeld, Germany). The $Arpc4^{flox/flox}$ line was generated by R.K. and M.I. as previously described.[157]

3.3.2 Animal breeding

All mice were housed at pathogen-free mouse facility with normal housing conditions under a 6 am-6 pm hour light cycle at the Technical University of Munich. Mouse husbandry and breeding were maintained for the complete duration of the research. All mouse experiments described here were approved by the Technical University of Munich and the Institutional Animal Care and Use Committees (Proposal number: ROB-55.2-2532.Vet_02-17-83). All experimental procedures were in compliance with the German Federal Animal Protection Laws.

3.3.3 Tamoxifen (TAM) induction

Tamoxifen suspension was prepared according to the following procedure:

1. Weigh 80 mg tamoxifen powder in 2 ml micro tube.
2. Add 200 µl pure ethanol to the micro tube.
3. Add 1800 µl oil to the micro tube to gain a final concentration of 40 mg/ml, shake it up and down for several times.

4. Oscillate the micro tube for 5 min at room temperature until tamoxifen powder is completely dissolved.
5. Centrifuge the tube shortly to get rid of the air bubbles inside.
6. Seal the tube with parafilm and store at -20°C for no longer than 4 months.

Induction procedure:

1. Warm the stored tamoxifen solution to room temperature. Once thawed, store at 4°C no longer than one week.
2. Fill 1 ml syringe with 600 µl tamoxifen working solution, connect it to Vasofix Safety tube and fill up the tube with a working solution.
3. Fix the mouse from the back with one hand, and softly insert the Vasofix Safety tube into the stomach with the other hand, administer 100 µl tamoxifen solution slowly.
4. Label the mouse card with date and treatments.
5. Each mouse was treated with tamoxifen three times per week at the age of 5-6 weeks (Day1, Day3, Day5). Treatment had to be stopped once mice showed apparent adverse effects.

3.3.4 Caerulein-induced acute pancreatitis

Acute pancreatitis was induced at 8-9 weeks of age by consecutive caerulein injections for two days. All mice were treated with eight hourly intraperitoneal (i.p.) caerulein injections (2 µg per mouse each dose).[63] Control mice were treated with saline. The time point and the day of the last dose were considered as hour 0 and day 0, respectively.

3.4 Genotype identification

3.4.1 Tissue collection for genotyping of transgenic mouse

Earmarking is carried out using a ear tag puncher to with a consecutive number. The

marking scheme is demonstrated in Figure 3. Gather all the ear punch tissue samples in a single micro tube for DNA isolation and genotype identification.

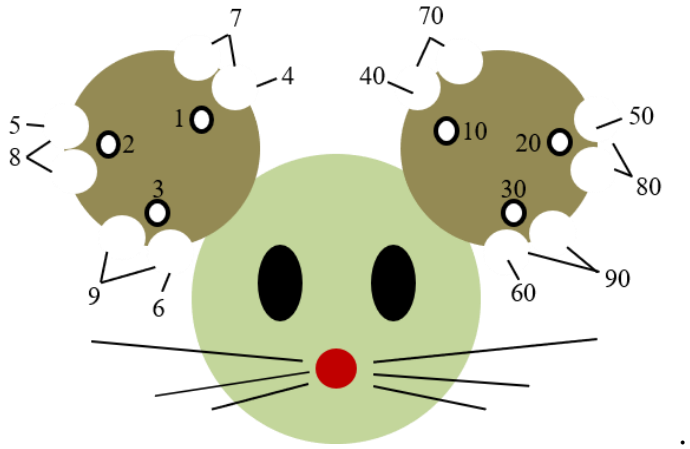

Figure 3. Earmarking system of transgenic mouse models

3.4.2 DNA isolation

Add 150 µl STE buffer and 5 µl proteinase K to each micro tube containing ear tissue sample, cap the tube tightly and shake at 55°C overnight to lyse the tissue. Centrifuge at 12000 rpm at room temperature for 10 min. Transfer the supernatant to a new micro tube. Add 400 µl 100% Isopropanol to each sample and mix by pipetting. Incubate at room temperature for 10 min to precipitate gDNA. Centrifuge at 12000 rpm at room temperature for 10 minutes. Discard the supernatant, wash the gDNA pellet with 500 µl 70% ethanol 2 times. Remove the supernatant and incubate at 37°C for 10 minutes. Add 50 ul ddH_2O to each tube and incubate at 55°C for 15 minutes. Store DNA solution at 4°C.

Recipe

1 L STE buffer

Dissolve 5.84 g NaCl, 1.21 g Tris, 0.29 g EDTA in 900 ml ddH_2O, adjust the pH to 8.0, fill up with ddH_2O to 1 liter, store at room temperature.

3.4.3 Polymerase chain reaction (PCR)

1. Prepare the following mixture on ice. The primer sequences are displayed in Table 1.

Components	Volume per sample (µl)
Master mix	12.5
Primer mixture (forward and reverse)	1
H_2O	10.5

Table 1. Genotyping Primer list for mouse strains

Mouse Strain	Primer Type	Sequence 5' - 3'
$p48^{Cre-ERTM}$	Forward	GAA GGC ATT TGT GTA GGG TCA
	Reverse	GGC TGA GTG AGG GTT GTG AG
$Rptor^{fl/fl}$	Forward	CTC AGT AGT GGT ATG TGC TCA G
	Reverse	GGG TAC AGT ATG TCA GCA CAG
$Rictor^{fl/fl}$	Forward	CAA GCA TCA TGC AGC TCT TC
	Reverse	TCC CAG AAT TTC CAG GCT TA
LSL-$Kras^{G12D}$	Wild type Forward	TGT CTT TCC CCA GCA CAG T
	Common	CTG CAT AGT ACG CTA TAC CCT GT
	Mutant Forward	GCA GGT CGA GGG ACC TAA TA
LSL-$Rosa26^{CAG-tdTomato}$	Wild type Forward	AAG GGA GCT GCA GTG GAG TA
	Wild type Reverse	CCG AAA ATC TGT GGG AAG TC
	Mutant Forward	CTG TTC CTG TAC GGC ATG G
	Mutant Reverse	GGC ATT AAA GCA GCG TAT CC
$p48^{Cre}$	Transgene Reverse	GGT TCT TGC GAA CCT CAT CA
	Common	GAG CAG CCC ATT CGT CCT

	Wild type Reverse	GTC GCG GTA GCA GTA TTC GT
$Arpc4^{fl/fl}$	Forward	AAG CCT TGC CCG AGA TAA TG
	Reverse	AAG CAA AGC CAG TCC CTC AC

2. Vortex the mixture shortly and transfer to PCR tube on ice.

3. Add 1 µl DNA solution into PCR tube from last step. Positive and negative control are necessary.

4. Put tubes in PCR machine under certain thermal conditions as follows:

Temperature (°C)	Duration	Repetition
95	10 min	1×
95	15 sec	30
55	30 sec	
72	40 sec	
72	5 min	1×
4	-∞	1×

3.4.4 Agarose gel electrophoresis

1. Add 3 g agarose powder into 200 µl TBE buffer, microwave at 600 W for 10 min until agarose totally dissolve.

2. Cool down briefly, add 5 µl ethidium bromide in and shake well.

3. Cast agarose gel in the mold. Cool down at room temperature until the gel gets solidified.

4. Load 10 µl reaction outcome into well.

5. Run the gel at 150 volts for 30 min in TBE buffer. TBE buffer must cover the gel.

6. Image under UV and save image for record.

3.5 Three-dimensional (3D) culture

3.5.1 3D and 2D culture medium preparation

1. Add all the components together and wait until Soybean Trypsin Inhibitor and $NaHCO_3$ totally dissolved, sterilize 3D culture medium with disposable vacuum filter. Store at 4°C for up to 2 months.
2. 3D culture medium was mainly used for 3D collagen gel preparation, 2D culture medium was mainly for acinar cell cluster culture.
3. 3D culture medium composition for total volume of 200 ml is as follows:

Components	Volume/Amount	Concentration
Waymouth's MB 752/1 media	154 ml	-
FBS	40 ml	20%
Penicillin/streptomycin	4 ml	2%
Soybean Trypsin Inhibitor	40 mg	0.2 mg/ml
5000× Dexamethasone	40µl	4 µg/ml
HEPES	2 ml	10 mM
$NaHCO_3$	0.52 g	2.6 mg/ml

4. 2D culture medium composition for total volume of 200 ml is as follows:

Components	Volume/Amount	Concentration
Waymouth's MB 752/1 media	177 ml	-
FBS	20 ml	10%
Penicillin/streptomycin	2 ml	1%
Soybean Trypsin Inhibitor	20 mg	0.1 mg/ml
5000× Dexamethasone	20 µl	2 µg/ml
HEPES	1 ml	5 mM
$NaHCO_3$	0.26 g	1.3 mg/ml

Recipe

5000× Dexamethasone

Dissolve 20 mg dexamethasone powder in Waymouth's MB 752/1 media, fill up to 1 ml to generate a 20 mg/ml stock. Aliquot and store at -20°C.

3.5.2 Acinar cell isolation

Pancreas dissection and harvest (Day -1)

A rapid organ harvest is crucial for sufficient extraction of viable acinar cells.

1. Euthanize mouse with isoflurane.
2. Fix the mouse supinely on the dissection plate. Sterilize mouse abdomen with 70% ethanol spray. Median laparotomy with sterile scissors and forceps to expose the whole abdominal cavity.
3. Grab and pull the spleen with forceps to expose the mesentery between stomach and pancreas and cut it with scissors to dissect the pancreas from stomach.
4. Pull the spleen vertically, liberate the head of pancreas from the beginning of small intestine with scissors carefully and rapidly and resect the lifted pancreas.
5. Hold the spleen with forceps and dissect the pancreas.
6. Transfer the pancreas to chilled 5% FBS/Hank’s solution on ice immediately.
7. Fix the rest part of the pancreas in 4% formalin overnight for recombination efficiency calculation.

Recipe

5% FBS/Hanks’ solution

Add 25 ml FBS to 475 ml Hanks’ balanced salt solution, store at 4°C.

4% Formalin

Mix the same amount of 8% formalin stock and ddH_2O to get 4% formalin, store at room temperature.

Enzymatic digestion of pancreas (Day -1)

From this step, the rest procedures were performed with sterile dissection tools in a

hood with laminar flow.

1. Pick the pancreas with sterile disposable plastic forceps from chilled 5% FBS/Hanks' solution and transfer it to a 6 cm culture dish containing 5 ml collagenase P solution (1mg/ml, prepared with 5% FBS/Hanks' solution, filtered with 0.2 μm sterile strainer).
2. Mince the pancreas into 1 mm small pieces and keep the dish in a 37℃ incubator for 15 min.
3. Remove pancreas tissue together with the collagenase P solution to a 50 ml sterile Falcon tube with 10 ml 5% FBS/Hanks' solution and centrifuge at 300 rpm for 5 min.
4. Aspirate the supernatant, wash pancreatic tissue with 10 ml 5% FBS/Hanks' solution, swirl the washing solution until tissue cluster disperse and centrifuge at 300 rpm for 5min.
5. Discard the supernatant, re-suspend the pellet in 25 ml 5% FBS/Hanks' solution added in another 5 ml FBS by pipetting gently up and down with 25 ml pipet.
6. Transfer the tissue suspension with 25 ml pipet to a new 50 ml Falcon tube through a 10 cm sterile mesh. Keep the tip of the pipet on the mesh while rotating and pipetting to grind pancreatic tissue into the acinar cell cluster. Centrifuge at 300 rpm for 5 min.
7. Remove the supernatant, wash the pellet with 10 ml 5% FBS/Hanks' solution by swirling to resuspension. Centrifuge at the same speed with last step for 5 min.
8. Aspirate the supernatant, re-suspend the pellet with 10 ml 2D culture medium by pipetting softly up and down.
9. Dilute 5 μl 20 ug/ml caerulein stock solution in 495 μl 2D culture medium evenly, add 100 μl diluent to cell suspension.
10. Mix acinar cell suspension gently and transfer to a sterile 10 cm culture dish.
11. Incubate acinar cells in 2 ng/ml caerulein-included 2D culture medium under 37℃, 5% CO_2 condition for 24 hours.

Recipe

Collagenase P solution

Dissolve 50 mg collagenase P powder in 5% FBS/Hanks' solution, fill up to 50 ml to generate 1 mg/ml collagenase P solution, sterilize with 0.2 μm filter, store at 4°C less than 2 weeks.

Caerulein stock solution

Dissolve 2 mg caerulein powder in sterile saline, fill up to 100 ml to get 20 μg/ml concentration, sterilize by passing through 0.2 μm filter, aliquot in 2 ml or 1.5 ml sterile micro tube, store at -80°C.

3.5.3 Collagen gel preparation and 12-well plates coating (Day 0)

1. Prepare collagen gel on ice for the first and second layer according to the following list.

Collagen Gel	Final Collagen Concentration (Con)	Final Volume for One Well in 12-Well Plate
First Layer	1.5 mg/ml	1.5 ml
Second Layer	1.0 mg/ml	0.5 ml

Components of Collagen Gel	Volume (V)
10× PBS	$V_{PBS} = 10\% V_{Final Volume}$
Collagen	$V_{Collagen} = V_{Final Volume} * Con_{Final Collagen Concentration} / Con_{Original Collagen Concentration}$
NaOH (1 M)	$V_{NaOH} = V_{Collagen} * 0.023$
3D Culture Medium	$V_{3D culture medium} = V_{Final Volume} - V_{Collagen} - V_{PBS} - V_{NaOH}$
$NaHCO_3$ (7.5%)	$V_{NaHCO3} = V_{Final Volume} / 60$

V: volume; Con: concentration

2. Pipet 500 μl mixture to each well of 12-well plate as the following diagram shows,

assuring that the gel covers the bottom of each well evenly.

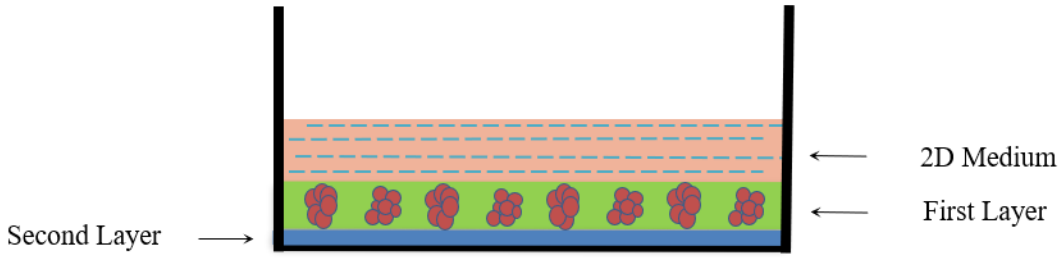

Figure 4. 3D culture diagram for each well in 12-well plate.

3. Leave the plate at 37℃ for 30 min until collagen mixture gets solidified when it is ready to seed the first layer.

4. The original concentration of collagen product is variable. It changes with Lot. Number. For example:

Components of Collagen Gel	Volume for One Well in 12-Well Plate	
	Volume for First Layer (μl)	Volume for Second Layer (μl)
10× PBS	150	50
Collagen (4 g/ml)	562.5	187.5
NaOH (1 M)	12.9	4.3
3D Culture Medium	749.6	249.9
$NaHCO_3$ (7.5%)	25	8.3

Recipe

10× PBS

Dissolve 4.775g PBS powder in sterile ddH_2O, fill up to 50 ml.

Sterilize with 0.2 μm filter, aliquot in 1.5 ml micro tube and store at 4°C

1 M NaOH

Dissolve 2 g NaOH in sterile ddH_2O, fill up to 50 ml.

Sterilize with 0.2 μm filter, aliquot in 1.5 ml micro tube and store at 4°C

7.5% $NaHCO_3$

Dissolve 3.75 g $NaHCO_3$ in sterile ddH_2O, fill up to 50 ml.

Sterilize with 0.2 μm filter, aliquot in 1.5 ml micro tube and store at 4°C

3.5.4 Seeding of acinar cell in collagen gel (Day 0)

1. Prepare collagen gel for the first layer on ice following the above description.
2. Transfer acinar cell suspension to a new 50 ml Falcon tube, centrifuge at 300 rpm for 5 minutes. Discard the supernatant, wash acinar cell pellet with the same protocol mentioned above.
3. Re-suspend acinar cell clusters with collagen gel, pipet up and down gently with 1 ml tip for short time, seed 1.5 ml mixture in each collagen-coated well.
4. Leave 12-well plates at 37℃, 5% CO_2 for 60 min until the solidification of collagen-cell mixture.
5. Add 2 ml 2D culture medium with substances into each well and incubate at 37℃, 5% CO_2 condition until time point. The substances list is in Table 2.

Table 2. List of pharmaceutical inhibitors or activators used in this study

Name	Catalogue number	Concentration	Company
Ck666	SML0006	100 μM	Sigma-Aldrich (Munich, Germany)
Cytochalasin D (Cyt D)	C8273	0.2 μM	Sigma-Aldrich
Rapamycin	553210	100 nM	Sigma-Aldrich
Akt inhibitor (Akti 1/2)	Ab142088	5 μM	Abcam (Cambridge, UK)
Bisindolylmaleimide XI	Ab143783	3 μM	Abcam

hydrochloride (BIM XI)			
EHT1864	3872	50 μM	TOCRIS Bioscience (Wiesbaden-Nordenstadt, Germany)
SC79	SML0749	11 μM	Sigma-Aldrich
Cycloheximide (CHX)	46401	178 μM	Sigma-Aldrich
TGF-α	239-A	100 ng/ml	R&D Systems, Minneapolis, USA

Recipe

TGF-α stock solution

Add 6 μl acetic acid to 10 ml sterile PBS solution to prepare 10 mM acetic acid solution, filter with 0.2 μm strainer, pipet 1 ml liquid to 100 μg recombinant human TGF-α to reconstitute at 100 μg /ml, aliquot in 1.5 ml micro tube and store at -80°C less than 3 months.

3.6 RNA isolation from 3D culture (Day 2)

1. Aspirate 2D culture medium from the well, pinch the collagen gel with disposable plastic forceps and transfer to 1.5 ml micro tube, centrifuge at 1200 rpm for 2 minutes.
2. Discard the supernatant in the micro tube, move the gel pellet to a new 2 ml micro tube with a small steel bead inside.
3. Lyse collagen-cell mixture with 1 ml TRLzol reagent, oscillate at 50 times per minute for 5 minutes until the mixture is homogeneous.
4. Pipet the homogeneous mixture to a new 1.5 ml RNase-free micro tube. Incubate 5 minutes to dissociate the nucleoproteins complex completely.
5. Add 200 μl chloroform, then cap the tube tightly, shake with hands strongly for 15 seconds.
6. Incubate at room temperature for 2-3 minutes.
7. Centrifuge at 12,000g at 4°C for 15 minutes. The mixture is separated into 3

layers, the upper aqueous phase, the lower organic phase and interphase.

8. The rest procedure was performed with RNeasy mini kit (Qiagen, Venlo, Netherlands), according to the manufacturer's procedures.

3.7 Reverse transcription

The RNA samples from 3D culture were processed for first strand cDNA synthesis with reverse transcriptase. The concentration of RNA samples was measured by Nanodrop 2000, the following procedure is done by RevertAid H Minus First Strand cDNA Synthesis Kit (Thermoscientific, Germany). Add 0.1-1 μg total RNA and 1 μl oligo$(dT)_{18}$ primer to a sterile, nuclease-free tube on ice, fill up with nuclease-free water to 12 μl. Then add 4 μl 5× Reaction Buffer, 1 μl RiboLock RNase Inhibitor, 2 μl 10 mM dNTP Mix, 1 μl Reverse Transcriptase to the above tube. Mix gently and centrifuge. Incubate for 60 min at 42℃.Terminate the reaction by heating at 70℃ for 5 min. Dilute cDNA sample with 100 μl ddH_2O for the following use. Store at -20℃ for less than one week.

3.8 Quantitative real-time polymerase chain reaction (QRT-PCR)

5 μl of diluted cDNA samples were mixed with 10 μl SYBR green master mix, 1 μl forward primer, 1 μl reverse primer and 3 μl ddH_2O. QRT-PCR was performed using the LightCycler480. cDNA samples were incubated at 95℃ for 5 min to denature, then amplified for 45 cycles, each composed of incubation at 95℃ for 15 seconds and at 60℃ for 45 seconds. The mRNA expression level of the target gene was normalized by the mouse housekeeping gene Rps29 (ribosomal protein S29) using the LightCycler^{TM}480 software.[153] The primer sequences are showing in Table 3.

Table 3. Sequences of primers used for QRT-PCR analysis of mouse genes

Gene Name	Sense (5'→3')	Antisense (5'→3')

Amylase-m	CGAGAACTACCAAGATGCTGCT	TCCATCCCACTTGCGCATAA
Krt19-m	CCCAGGTCGCCGTCCACTCTGAGC	GCGTGCCTTCCAGGGCAGCTTTCATG
Rps29-m	TCTACTGGAGTCACCCACGGAA	GGAAGCACTGGCGGCACA
Rbpjl-m	GTATCGAAGTCAGTGGCGGT	GCAGGCTCAGGTGAGTCAAA
Rbpj-m	ACTGTAAGTGCCACTGCGAA	ACAACGGAACTGCAAACTGC
mTOR-m	CCGCTACTGTGTCTTGGCAT	CAGCTCGCGGATCTCAAAGA
Rptor-m	GCCAAGAGCATCTTCCCTGT	TGCTCTATGGCCCAACCAAG
Rictor-m	GAATGCACCCGTCCTTGTCT	TCATAAACCTGCTTGGCGTC
Pdx1-m	GCGTTGAGTCACCCAAACAT	AATTGCAACAGCTGCTCGTC
Mist-m	GGAAGCACATCATGGGTCAGA	TACGCATCTTCATCTTCCTCCATT
Arp3-m	TAAGCGAGGAGCTGAGTGGT	TAGAACTCAGGCGTGGAAGC
Rac1-m	ACAGACGCTTCCTGTCATGG	GTGGTTGAAAGGCCCAACAC

3.9 Paraformaldehyde (PFA) fixation of 3D culture (Day 2)

1. Discard culture medium from the well, pinch the collagen gel from two ends of the diameter gently with disposable plastic forceps and lie it in cassette rapidly.
2. Put the cassette into 4% PFA solution and incubate at room temperature overnight.
3. Transfer the cassette to PBS, after washing, go through dehydration machine.
4. Cut the dehydrated collagen gel into 4 pieces with a scalpel. Embed them in paraffin

3.10 Protein isolation from 3D culture and frozen tissue

Proteins were extracted from 3D culture with 1 x RIPA buffer containing phosphatase and protease inhibitors. Transfer collagen gel to 1.5 ml tube with forceps, centrifuge at 12,000g for 2 minutes. Remove the supernatant and wash the collagen pellet with PBS for 2 times. From this step forward, the protein isolation from 3D culture and frozen tissue were performed using the same experimental procedures. Oscillate the pellet strongly at 50 times per minute for 5 minutes with steel beads in 100 µl RIPA buffer. Incubate protein samples on ice for 40 min to get complete homogenized. The samples were then centrifuged at full speed at 4℃ for 20 minutes. Transfer the supernatant (protein lysate) to a new tube on ice. Measure protein concentration using the BCA kit.

Recipe

1× RIPA buffer

Dilute 1 ml 10× RIPA stock solution in 9 ml ddH2O, dissolve one tablet of phosphatase inhibitor and one tablet of protease inhibitor in the mixture. Store at 4℃ less than 2 weeks.

3.11 Western-blot analysis

After measurement of protein concentration, denature the same amount of protein and run polyacrylamide gel to separate it, and then transfer to a nitrocellulose (NC) membrane. 5% milk incubation for 1 hour at room temperature was used to block unspecific binding on the membrane. Then transfer the membrane to the primary antibody in blocking buffer for overnight incubation at 4°C. The concentration of primary antibody and secondary antibody is displayed in Table 4 and 5. After washing, incubate the membrane with secondary antibody in 5% milk for 1 hour at room temperature. Wash the membrane and add on detection solution evenly. Develop the image on x-ray film in the darkroom by means of chemiluminescence technique.

Recipe

10× Running buffer

Dissolve 30.0 g of Tris base, 144.0 g of glycine in dH_2O, fill up to 1000 ml. Store at room temperature and dilute to 1× before use.

1× Running buffer

Dilute 100 ml 10× running buffer to 900 ml dH_2O, add 10 ml 10% SDS to the mixture.

1× Blotting buffer

Mix 200 ml methanol with 100 ml 10x running buffer, add 700ml dH_2O to 1 L.

Table 4. Primary antibody list

Antibody name	Catalog number	Application	Producer
Rabbit Anti-mTOR mAb#	2983	WB	Cell Signaling Technology (NEB, Frankfurt/Main, Germany)
Rabbit Anti-Rptor mAb#	2280	WB	Cell Signaling Technology
Rabbit Anti-Rptor pAb#	20984-1-AP	IHC	Proteintech
Rabbit Anti-Rictor mAb#	2140	WB	Cell Signaling Technology
Rabbit Anti-p-mTOR^{S2448} mAb#	5536	WB	Cell Signaling Technology
Rabbit Anti-p-mTOR^{S2448} mAb#	2976	IHC	Cell Signaling Technology
Rabbit Anti-p-Akt^{S473} mAb#	4060	WB, IHC	Cell Signaling Technology
Rabbit Anti-p-Akt^{T308} mAb#	4056	WB	Cell Signaling Technology
Rabbit Anti-Akt mAb#	9272	WB	Cell Signaling Technology
Rabbit Anti-p-S6$^{S235/236}$	4858	WB, IHC	Cell Signaling Technology

mAb#			
Rabbit Anti-t-S6 mAb#	2217	WB	Cell Signaling Technology
Rabbit Anti-p-Ndrg 1^{T346} mAb#	5482	WB, IHC	Cell Signaling Technology
Rabbit Anti-t-Ndrg 1 mAb#	9408	WB	Cell Signaling Technology
Phospho-Myosin Light Chain 2 (Ser19) Mouse mAb#	3675	IF	Cell Signaling Technology
Mouse Anti-Rac1 mAb#	8815	WB	Cell Signaling Technology
Goat Anti-Arpc4 Ab#	EB08249	WB	Everest Biotech Ltd
Rabbit Anti-Arpc1b pAb#	AP4321	WB	ECM Biosciences
Rabbit Anti-Arp2 pAb#	AP3861	WB, IHC	ECM Biosciences
Rabbit Anti-Arp3 pAb#	AP4581	WB, IHC	ECM Biosciences
Rabbit Anti-α-Amylase mAb#	3796	IHC, IF	Cell Signaling Technology
Rat Anti-Krt19 mAb#	AB_2133570	IHC, IF	Developmental Studies Hybridoma Bank
Rabbit Anti-Claudin 18 mAb#	700178	IHC	Invitrogen
Rabbit Anti-Glucagon mAb#	2760	IHC	Cell Signaling Technology
Rabbit Anti-Insulin mAb#	4590	IHC	Cell Signaling Technology
Mouse Anti-Muc5AC mAb#	MA5-12178	IHC	Invitrogen
Mouse Anti-F-actin	Ab205	IF	Abcam

mAb#			
Rabbit Anti-Hsp90 mAb#	4877	WB	Cell Signaling Technology
Mouse Anti-β-actin Ab#	SC-1615	WB	Santa Cruz Biotechnology
Mouse Anti-GAPDH mAb#	SC-32233	WB	Santa Cruz Biotechnology
Rabbit Anti-p-PKCα/βII (T638/641) mAb#	9375	WB	Cell Signaling Technology
Rabbit Anti-PKCα mAb#	2056	WB	Cell Signaling Technology

WB = western blot; IHC = Immunohistochemistry; IF = Immunofluorescence; Ab# = antibody

Table 5. Secondary antibody list

Antibody name	Catalog number	Application	Producer
Rabbit HRP (horseradish peroxidase)-labelled Anti-Rat IgG Ab#	P0450	IHC	Dako Deutschland GmbH
Goat HRP-Labelled Polymer Anti-Mouse Ab#	K4001	IHC	Dako Deutschland GmbH
Goat HRP-Labelled Polymer Anti-Rabbit Ab#	K4003	IHC	Dako Deutschland GmbH
Simple StainTM MAX PO	414141F	IHC	Nichirei Bioscience
Simple Stain Mouse MAX PO	414341F	IHC	Nichirei Bioscience
Goat Alexa Fluor 488 Anti-Mouse IgG Ab#	115-546-062	IF	Dianova
Goat Alexa Fluor 594 Anti-Rat	A-11007	IF	Invitrogen

IgG Ab#			
Goat Alexa Fluor 594 Anti-Rabbit IgG Ab#	A-11034	IF	Invitrogen
Goat Alexa Fluor 488 Anti-Rabbit IgG Ab#	A-11012	IF	Invitrogen
Goat Alexa Fluor 488 Anti-Rat IgG Ab#	A-11006	IF	Invitrogen
Goat Alexa Fluor 594 Anti-Mouse IgG Ab#	A-11005	IF	Invitrogen
Anti-Mouse IgG HRP Conjugate	W4028	WB	PROMEGA, Madison, USA
Anti-Rabbit IgG HRP Conjugate	W4018	WB	PROMEGA, Madison, USA
Mouse anti-goat IgG-HRP Conjugate	SC-2354	WB	Santa Cruz Biotechnology

WB = western blot; IHC = Immunohistochemistry; IF = Immunofluorescence; Ab# = antibody

3.12 Active Rac1 pull-down assay

GTP-bound Rac1 was detected in whole pancreas tissue lysate or acinar explants using a commercially available kit (Active Rac1 Detection Kit, #8815, Cell Signaling Technology, NEB, Frankfurt/Main, Germany) according to the manufacturer's instruction. The visualization of total and GTP-bound Rac1 was performed using western-blot analysis.

3.13 Immunohistochemistry (IHC) and immunofluorescence (IF)

Obtained organ were preserved in 4% PFA overnight, then embedded in paraffin and cut into slices with 2 µm thickness. Sections were subjected to Hematoxylin and eosin (H&E), IHC and IF staining. Generally, citrate buffer was used for heat-induced epitope

retrieval. Briefly, IHC and IF staining was performed with 10% goat serum in PBST as blocking. Primary antibody was diluted in antibody dilution and incubate at 4℃ overnight. The respective secondary antibody was added on the slice and incubate at room temperature for 1 hour. The primary and secondary antibody is displayed in Table 3 and 4. After washing, for IHC staining, DAB diluent was used to display the positive staining, for IF, DAPI was add on the slice before mounting. For quantification of IHC staining, sections were scanned by microscope under 5× magnification. The analysis was done by Image J.

Recipe

Citrate buffer

Dissolve 2.94 g Citrate powder in dH2O, adjust the pH to 6, fill with water up to 1L. Store at room temperature less than 2 weeks.

10% Goat serum

Dilute 100 µl goat serum in 900 µl PBST before using, keep it on ice.

3.14 Mass spectrometry-based proteomics

For mass spectrometry, the protein was isolated with urea lysis buffer. After measuring protein concentration with BCA kit, Coomassie stain was performed to show proteins on the polyacrylamide gel before sending for protein mass spectrometry analysis (Figure 5). It was done in cooperation with Dr. Christina Ludwig by HF-KMS01 (Thermo Fisher Scientific, USA) instrument in Bavarian Center for Biomolecular Mass Spectrometry of Technical University of Munich.

Recipe

8 M Urea lysis buffer

Dissolve 2.4 g urea, 9.3 mg EDTA, 39.53 mg NH_4HCO_3, 5 µl 1M DTT stock solution and half tablet of protease inhibitor cocktail in H_2O, fill up to 5 ml. Store at room temperature, always prepares fresh buffer before use.

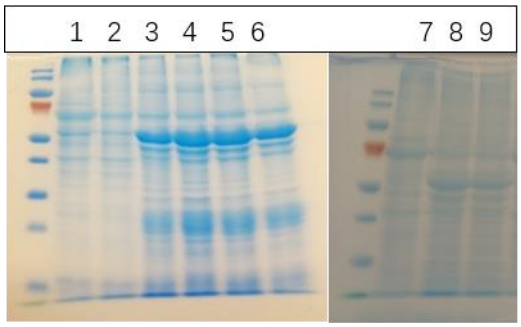

1: 9652 $Kras^{G12D}$
2: 9990 $Kras^{G12D}$
3: 10020 $Kras^{G12D}$; $Rptor^{-/-}$
4: 10023 $Kras^{G12D}$; $Rptor^{-/-}$
5: 10230 $Kras^{G12D}$; $Rictor^{-/-}$
6: 10232 $Kras^{G12D}$; $Rictor^{-/-}$
7: 9299 $Kras^{G12D}$
8: 10015 $Kras^{G12D}$; $Rptor^{-/}$
9: 10106 $Kras^{G12D}$; $Rictor^{-/-}$

Figure 5. Coomassie stain of protein samples used for mass spectrometry analysis.

3.15 Downstream differential abundance analysis

The quantitative proteomic results were further statistically analysed using the Perseus software (Version: 1.6.10.43, http://www.coxdocs.org/doku.php?id=perseus:start),[158] to obtain mTORC1 and mTORC2 proteomic signatures and related KEGG pathways using the default setting. In brief, LFQ intensities were transformed by $Log_2(x)$ and the missing values were imputed and replaced according to the normal distribution. For the generation heatmap, a multiple-sample test was applied to $Kras^{G12D}$, $Kras^{G12D}$; $Rptor^{-/-}$ and $Kras^{G12D}$; $Rictor^{-/-}$ samples to yield differentially expressed proteins using ANOVA test followed by Permutation-based *p*-value correction (cut-off FDR: 0.05). To obtain mTORC1- or mTORC2-specific proteomic signature, a two-sample test (Student's T-test) was applied and p-value is followed by Permutation-based correction (cut-off FDR: 0.01, fold change S0=0.1) to generate a list of differentially expressed proteins between $Kras^{G12D}$ and $Kras^{G12D}$; $Rptor^{-/-}$ samples as well as between $Kras^{G12D}$ and $Kras^{G12D}$; $Rictor^{-/-}$ samples (Figure 25). The list of upregulated proteins ($Kras^{G12D}$ vs. $Kras^{G12D}$; $Rptor^{-/-}$ and $Kras^{G12D}$ vs. $Kras^{G12D}$; $Rictor^{-/-}$) was considered as specific proteomic signatures (Figure 26) and they were subjected to KEGG pathway enrichment analysis. As such, p values were calculated by Fisher exact test and followed by Benjamini-Hochberg correction to generate final FDRs (Figure 27; Table 6, 7), as previously described.[158]

3.16 Quantification of ADM and PanIN

For ADM quantification in 3D culture, 5 pictures were taken from one well of each mouse on day2. The area of ADM was calculated by ImageJ (Maryland, USA). For PanIN and α-Amylase percentage quantification *in vivo*, the whole slide of relative IHC staining was scanned, the area calculation was done by ImageJ, the number of lesions was calculated manually.

3.17 Statistical analysis

GraphPad Prism V.5 Software (GraphPad, San Diego, California, USA) was used for the statistical analysis. All experiments were repeated for three times. An unpaired Student's *t*-test was used to evaluate the difference between the two groups. $P < 0.05$ was considered as statistical significance standard. Results are expressed as mean ± SD.

4. Results

4.1 mTOR signalling is activated in ADM *in vivo*

Firstly, we stained histological sections of normal pancreas (n=5), chronic pancreatitis (CP) (n=10) and PDAC (n=20) for a number of activation markers for mTORC1 (p-mTOR^{S2448}, RPTOR and p-S6$^{S235/236}$) and mTORC2 (p-mTOR^{S2448} and p-NDRG1^{T346}) signaling. In accordance with previously published data[128, 153], we observed that acinar cells in normal pancreas were weakly stained, but PDAC cells were in general positive, indicating a dual activation of mTORC1 and mTORC2 signalling in established PDAC (Figure 6). To our special attention, ADM lesions in CP sections were particularly stained for these activation markers of mTORC1 and mTORC2 (Figure 6). To further validate this, we compared their expressions in normal pancreas and CP tissues using western-blot analysis in humans. Indeed, the expression of activation markers for mTORC1 (p-mTOR^{S2448}, RPTOR and p-S6$^{S235/236}$) and mTORC2 (p-mTOR^{S2448}, RICTOR, p-AKT^{S473} and p-NDRG1^{T346}) were increased in CP tissues comparing to the normal pancreas (Figure 7).

Besides, we tested whether mTORC1 and mTORC2 were also activated in a mouse model of early pancreatic carcinogenesis driven by Kras^{G12D} and caerulein-induced pancreatitis. Here, we observed that both mTORC1 and mTORC2 were activated in these mouse ADM lesions, which is consistent with the findings in human chronic pancreatitis (Figure 8). These *in vivo* data suggest that mTOR signalling is activated in precursor lesion of PDAC.

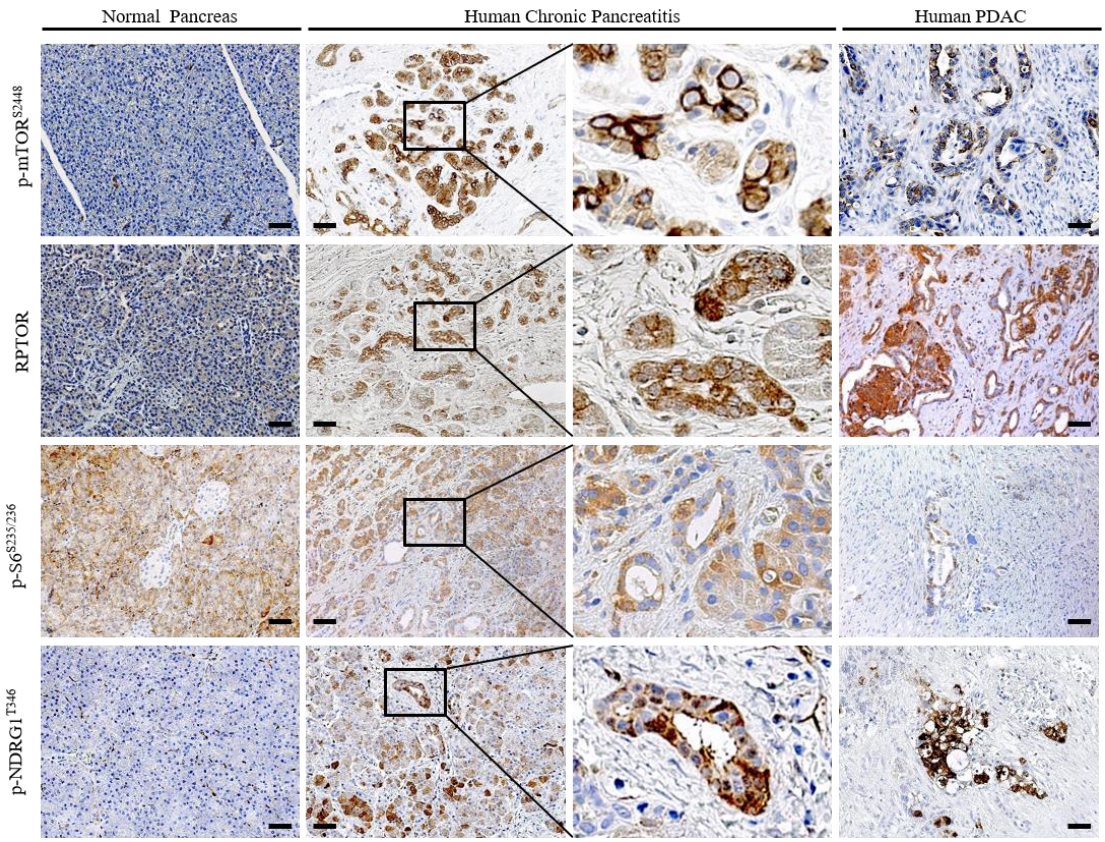

Figure 6. Representative IHC pictures show p-mTOR^{S2448}, RPTOR, p-S6$^{S235/236}$ and p-NDRG1^{T346} in the ADM lesions of human chronic pancreatitis and PDAC; Scale bars:50 μm.

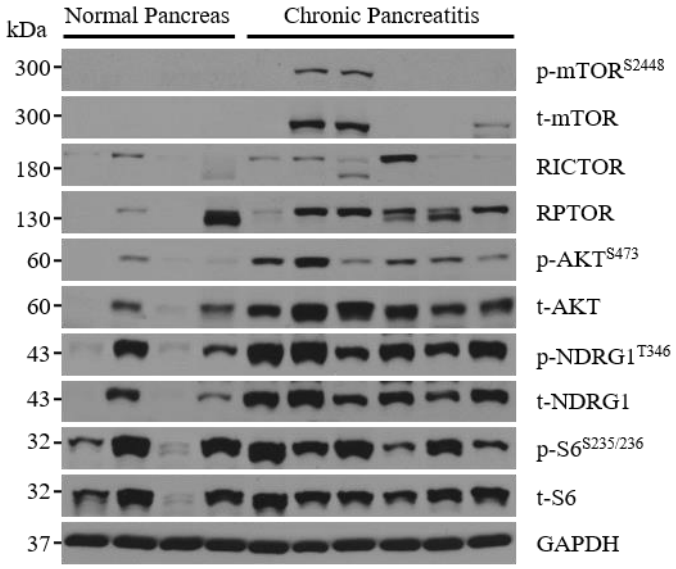

Figure 7. Western-blot analysis demonstrates the expression of p-mTOR^{S2448}, RPTOR, RICTOR, p-S6$^{S235/236}$ and p-AKT^{S473} and p-NDRG1^{T346} in normal (n=4) and chronic pancreatitis (n=6) tissues.

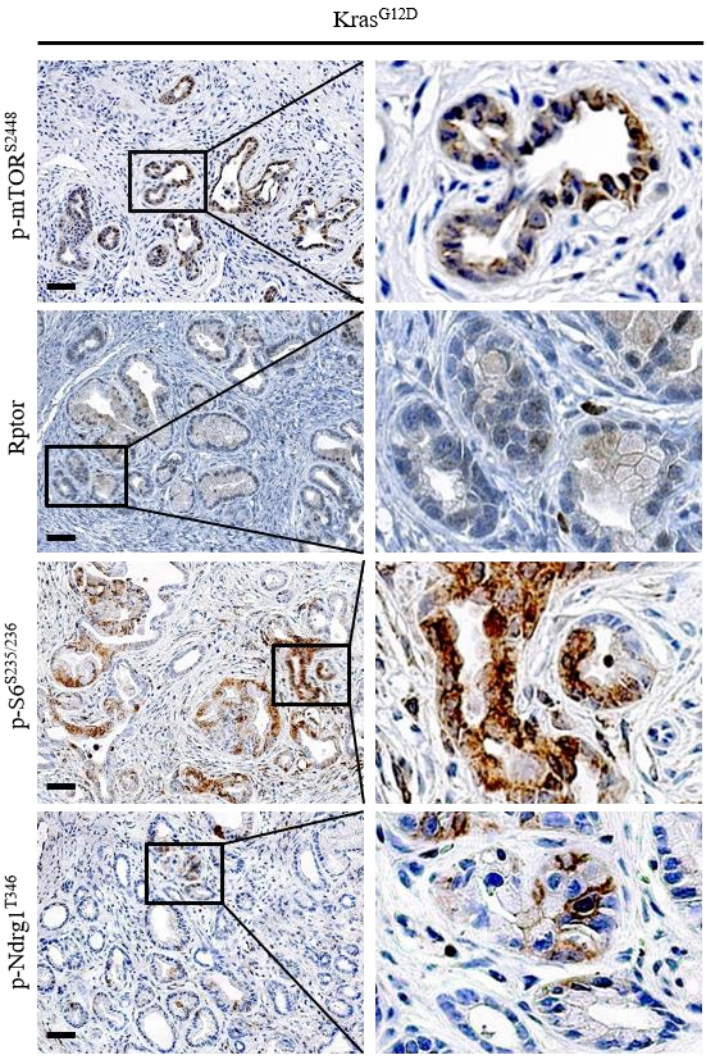

Figure 8. Representative IHC pictures show p-mTOR^{S2448}, RPTOR, p-S6$^{S235/236}$ and p-NDRG1^{T346} in the ADM lesions of Kras^{G12D} mouse model; Scale bars: 50 μm.

4.2 mTOR signalling is involved in ADM formation *in vitro*

To clarify if mTOR signalling is involved in ADM *in vitro*, we performed a ADM formation assay in 3D culture system. It was reported that isolated wild-type acinar cells treated with TGF-α or acinar clusters with spontaneous oncogenic Kras expression were able to differentiate to duct-like structures in the collagen matrix.[31] In the current study, we further optimized the protocol and stimulated explanted wild-type cells with 2 ng/ml caerulein for 24 h before implantation into the 3D culture. As such, the isolated acinar clusters are able to differentiate to metaplastic ductal lesions even in the absence

of TGF-α treatment (Figure 10A). This result was confirmed by QRT-PCR. We isolated RNA from TGF-α-mediated and control ADM (PBS treated) at 48h and also from fresh wide-type acinar cells, and checked mRNA expression level of α-Amylase, the marker of acinar cell; Krt19, the marker of ductal cell; Rbpjl and Mist1, acinar cell identity factors; Rbpj and Pdx1, acinar cell dedifferentiation factors.[159, 160] The expression of α-Amylase, Rbpjl, Mist1 reduced dramatically in TGF-α-mediated and control ADM compared to fresh acinar cell, also the expression of Krt19, Rbpj, Pdx1 increased significantly (Figure 9), which indicated acinar cell dedifferentiation to ductal phenotype in 3D culture. However, TGF-α-induced and oncogenic $Kras^{G12D}$-driven ADM are bigger than control ADM in the 3D culture at 48h (Figure 10A). These data suggested that TGF-α stimulation and oncogenic Kras promote ADM formation *in vitro* (Figure 10A). On this basis, we checked mTOR, Rptor, Rictor mRNA expression level in these ADM. QRT-PCR results showed that both Rptor and Rictor increased significantly in TGF-α-induced and $Kras^{G12D}$-driven ADM compared with control, also mTOR was upregulated in TGF-α-mediated ADM compared with control (Figure 10B). Also, proteins were isolated from these ADM, and western blot was implied to analyze the activation of mTOR signalling. It shows that p-$mTOR^{S2448}$, Rptor and Rictor, members of mTOR complexes, are overexpressed in $Kras^{G12D}$-mediated and TGF-α-induced ADM compared with control, also, p-$Pkc\alpha^{T638}$, p-$Ndrg1^{T346}$ and p-$S6^{S235/236}$, the downstream targets of mTOR signalling upregulate significantly; p-Akt^{S473}, the target of mTORC2, increases in $Kras^{G12D}$-mediated ADM (Figure 11). Therefore, these data indicate that mTORC1 and mTORC2 signalling are involved in ADM formation *in vitro*.

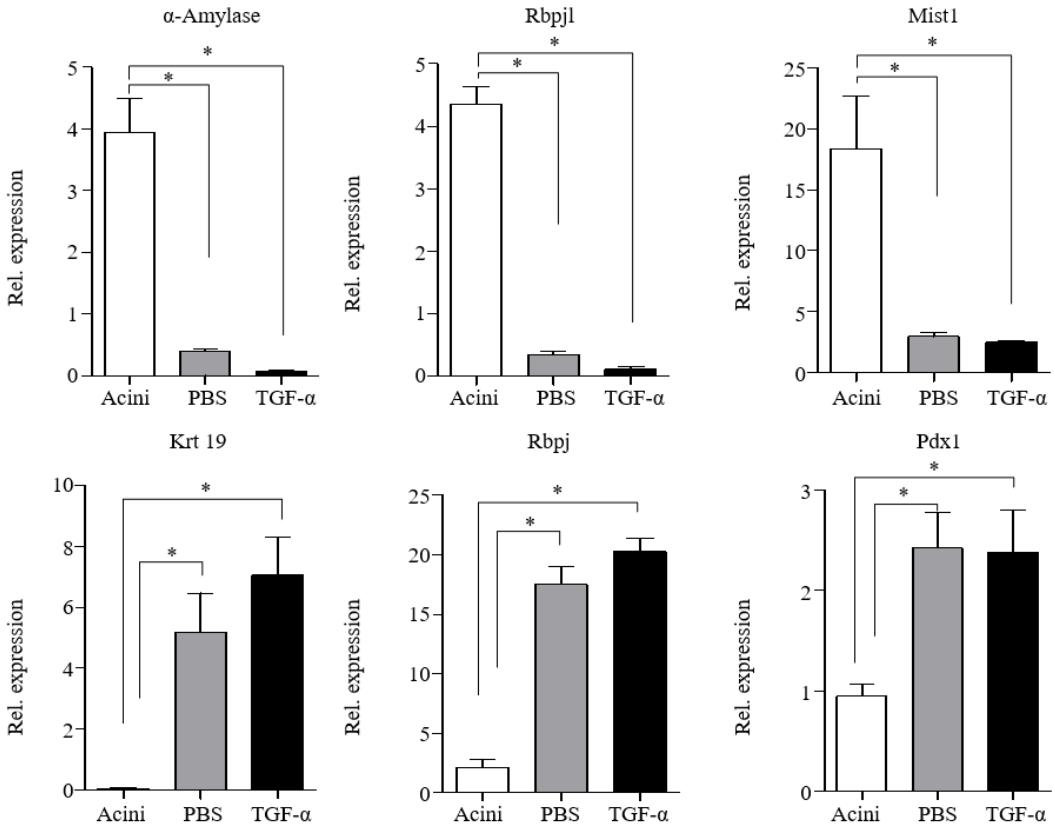

Figure 9. QRT-PCR demonstrates the mRNA expression level of α-Amylase, Rbpjl, Mist1, Krt19, Rbpj and Pdx1 in fresh acinar cells, PBS- and TGF-α-mediated ADM; n=3, *: <0.05, unpaired *t*-test.

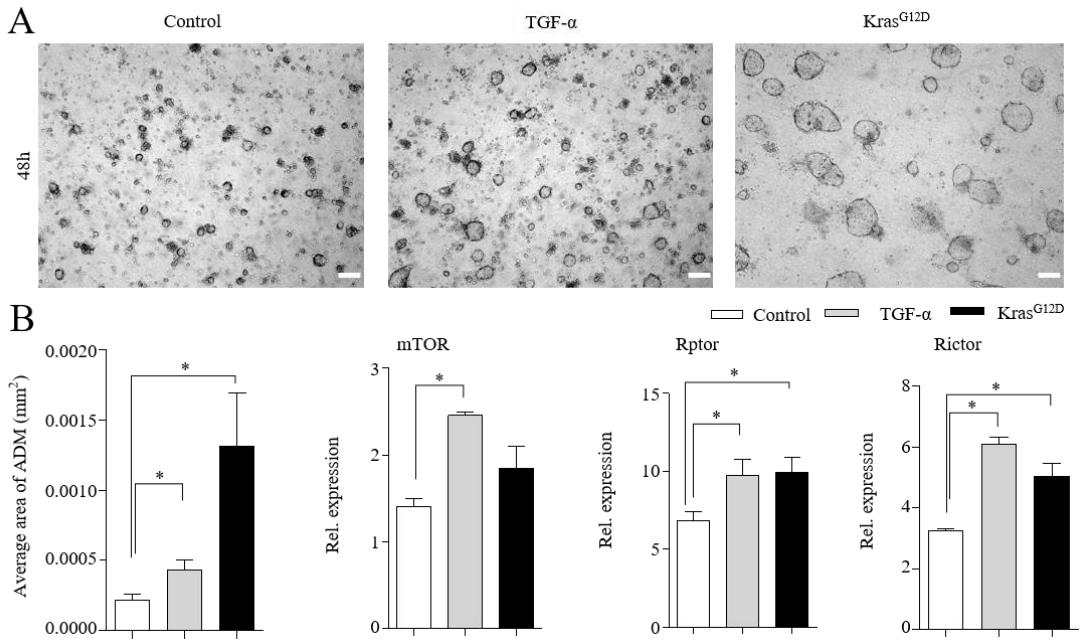

Figure 10. (**A** and **B**) Representative phase-contrast pictures show oncogenic $Kras^{G12D}$-induced ADM lesions, TGF-α-induced ADM lesions from wild-type acinar cells and ADM lesions from wild-type acinar cells (control) in 3D culture; quantitative data show the area of ADM lesions in vitro, n=3, *:

<0.05, unpaired *t*-test; QRT-PCR demonstrates the mRNA expression level of mTOR, Rptor and Rictor in oncogenic $Kras^{G12D}$-mediated ADM lesions, TGF-α-mediated ADM lesions from wild-type acinar cells and control ADM lesions in 3D culture; n=3, *: <0.05, unpaired *t*-test.

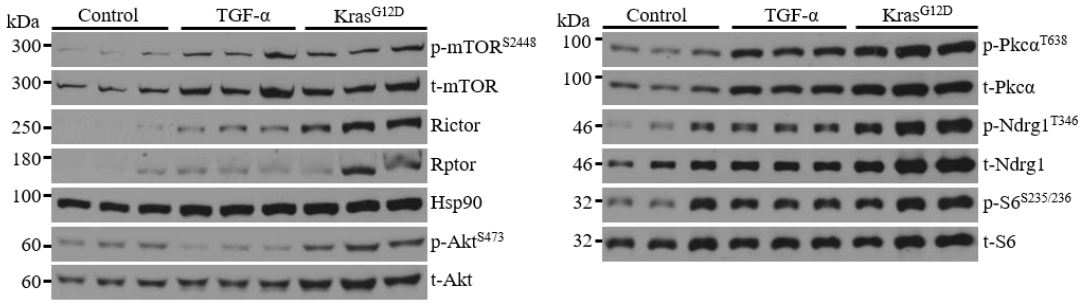

Figure 11. Western-blot analysis demonstrates the expression of p-$mTOR^{S2448}$, t-mTOR, Rptor, Rictor, p-$S6^{S235/236}$, p-Akt^{S473} and p-$Ndrg1^{T346}$ in oncogenic $Kras^{G12D}$-induced ADM lesions, TGF-α-induced ADM lesions from wild-type acinar cells and controls ADM lesions, *in vitro*.

4.3 Loss of Rptor or Rictor displays no pancreatic abnormalities

From *in vivo* and *in vitro* data, we might conclude that mTOR signalling plays a vital role in precursor lesion of PDAC. To test the functional significance of mTORC1 and mTORC2 activation in ADM lesions, we generated $p48Cre^{ERTM}$; $Rptor^{flox/flox}$ and $p48Cre^{ERTM}$; $Rictor^{flox/flox}$ to specifically deactivate mTORC1 and mTORC2 function in pancreatic acinar cells in a tamoxifen-inducible manner (Figure 12A). To trace the fate of recombined acinar cells, we crossed these lines with a Cre-dependent LSL-$Rosa26^{CAG\text{-}tdTomato}$ reporter allele to generate $p48Cre^{ERTM}$; $Rptor^{flox/flox}$; LSL-$Rosa26^{CAG\text{-}tdTomato}$ (referred to as 'Rptor$^{-/-}$' mice) and $p48Cre^{ERTM}$; $Rictorf^{lox/flox}$; LSL-$Rosa26^{CAG\text{-}tdTomato}$ (referred to as 'Rictor$^{-/-}$' mice), respectively. All recombined acinar cells were genetically labelled by a red fluorescent protein variant (RFP: tdTomato). All mice were treated with tamoxifen at 5-6 weeks of age (Figure 14). Inducible Cre-mediated recombination efficiency was assessed by RFP immunohistochemistry staining (Figure 12D). The recombination efficiency was around 95%. The results of the western-blot analysis confirmed reduced expression of Rptor and Rictor in Rptor$^{-/-}$ and Rictor$^{-/-}$ pancreas after tamoxifen treatment (Figure 12B). The loss of Rptor or Rictor in acinar cells had no physiological impact, as reflected by random blood glucose

levels and body weight analysis (Figure 12C), histological analysis (Figure 12D), staining for endocrine (Insulin and Glucagon) and exocrine (Keratin 19 (Krt19) and α-Amylase) markers (Figure 13). Therefore, we conclude that deletion of Rptor or Rictor leads to no pancreatic abnormalities.

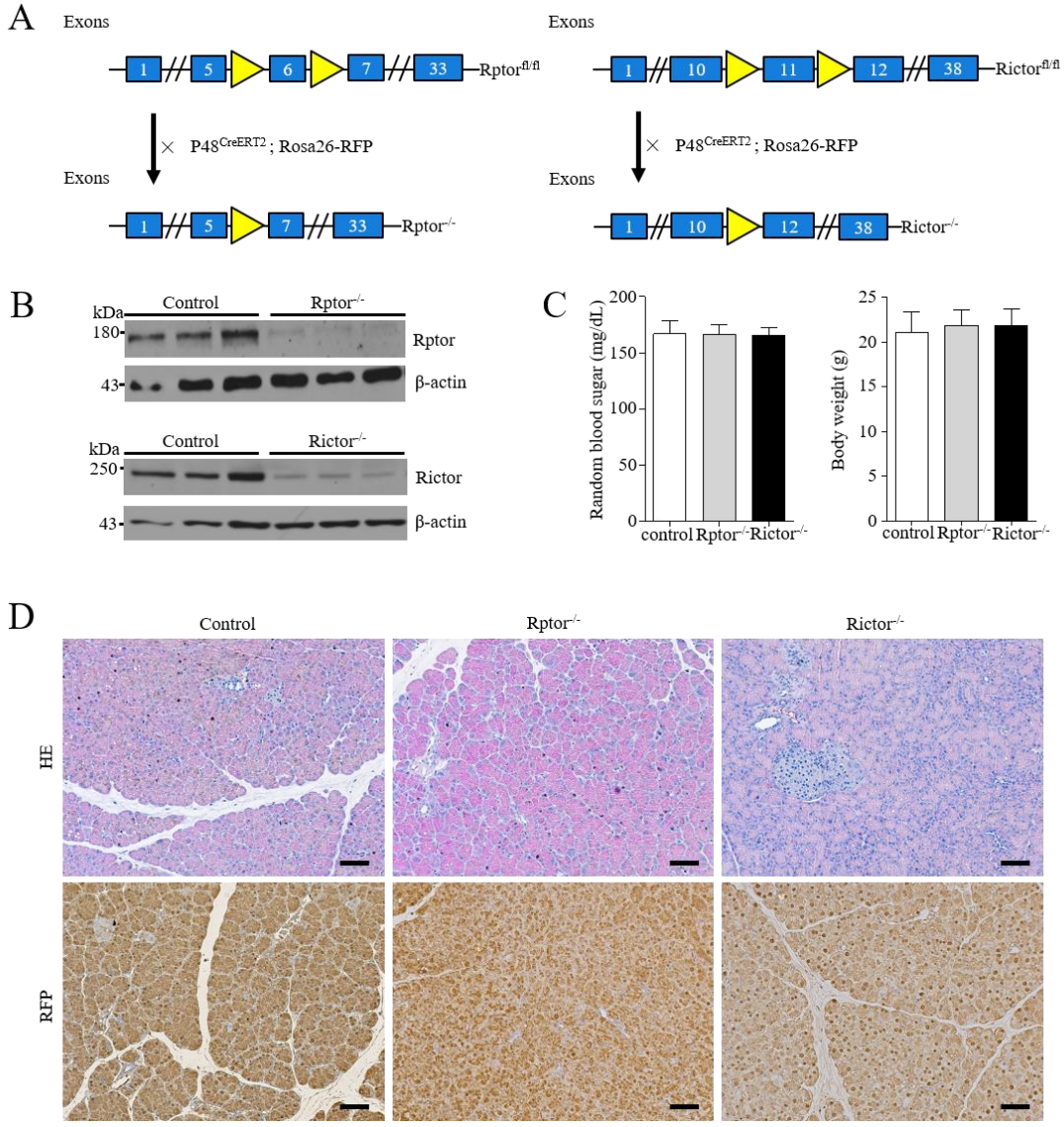

Figure 12. (**A**) Diagram of inducible Cre-mediated recombination. Rptor or Rictor is specifically ablated in pancreas at 5 weeks old, as shown by deleting exon 6 or 11; (**B**) Western-blot analysis demonstrates the expression of Rptor and Rictor in control, Rptor$^{-/-}$ and Rictor$^{-/-}$ mice at 8 weeks old; β-actin indicates equal loading; (**C**) Quantitative data show the random blood glucose (mg/dL) and the body weight (g) of control, Rptor$^{-/-}$ and Rictor$^{-/-}$ mice, n>=3, unpaired *t*-test; (**D**) H&E staining shows the histology of pancreas from 8-week-old Rptor$^{-/-}$, Rictor$^{-/-}$ and control mice; Representative IHC pictures show the expression of RFP in these animals at 8 weeks old after tamoxifen induction; Scale bars: 50 μm.

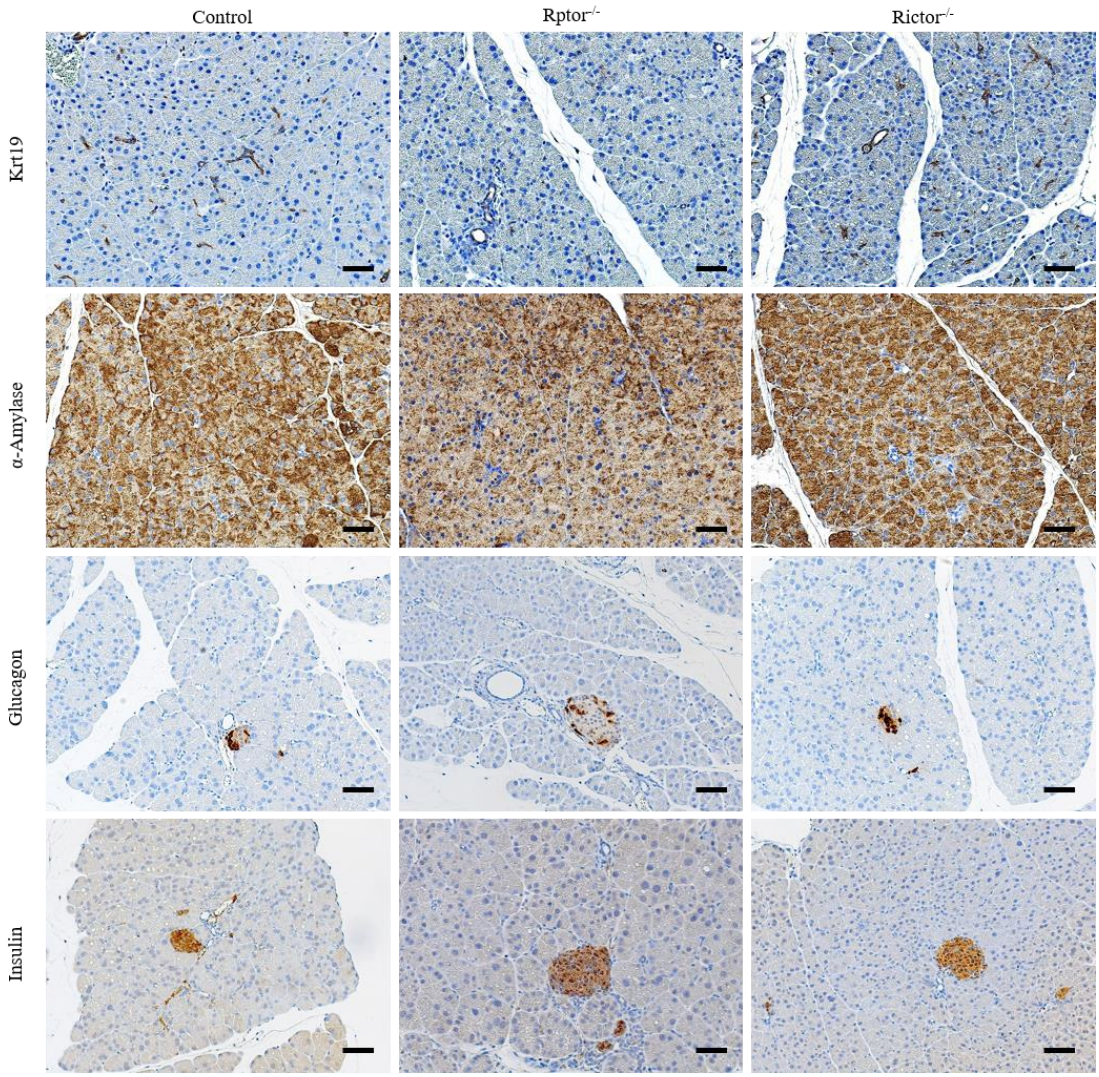

Figure 13. Representative IHC pictures show the exocrine (Krt19 and a-Amylase staining) and endocrine (Glucagon and Insulin staining) compartment of Rptor$^{-/-}$, Rictor$^{-/-}$ and control mice at 8 weeks old; Scale bar: 50 μm.

4.4 Rptor or Rictor is involved in ADM formation

To determine whether Rptor or Rictor is required for ADM formation, we examined the impact of Rptor or Rictor ablation on ADM formation *in vivo* and *in vitro*.

Firstly, we turn to caerulein induced pancreatitis mouse model. These mice were induced with tamoxifen at 5 weeks old to block mTORC1 or mTORC2 signalling separately and injected with caerulein 8 hourly for 2 consecutive days. The pancreas was harvested 2 or 14 days after caerulein injection (Figure 14A). ADM is the dominant

pancreatic responses to injury, besides leukocyte infiltration, increased separation of acinar lobules. All mice displayed similar histological changes, which were not significantly altered by Rptor or Rictor deletion (Figure 15B). In this study, 14 days post-injury, the pancreas was mostly restored as expected in control mice and also in Rptor$^{-/-}$ or Rictor$^{-/-}$ mice (Figure 15B). These data suggest that Rptor or Rictor is not required for inflammation-induced ADM formation and pancreatic regeneration *in vivo*.

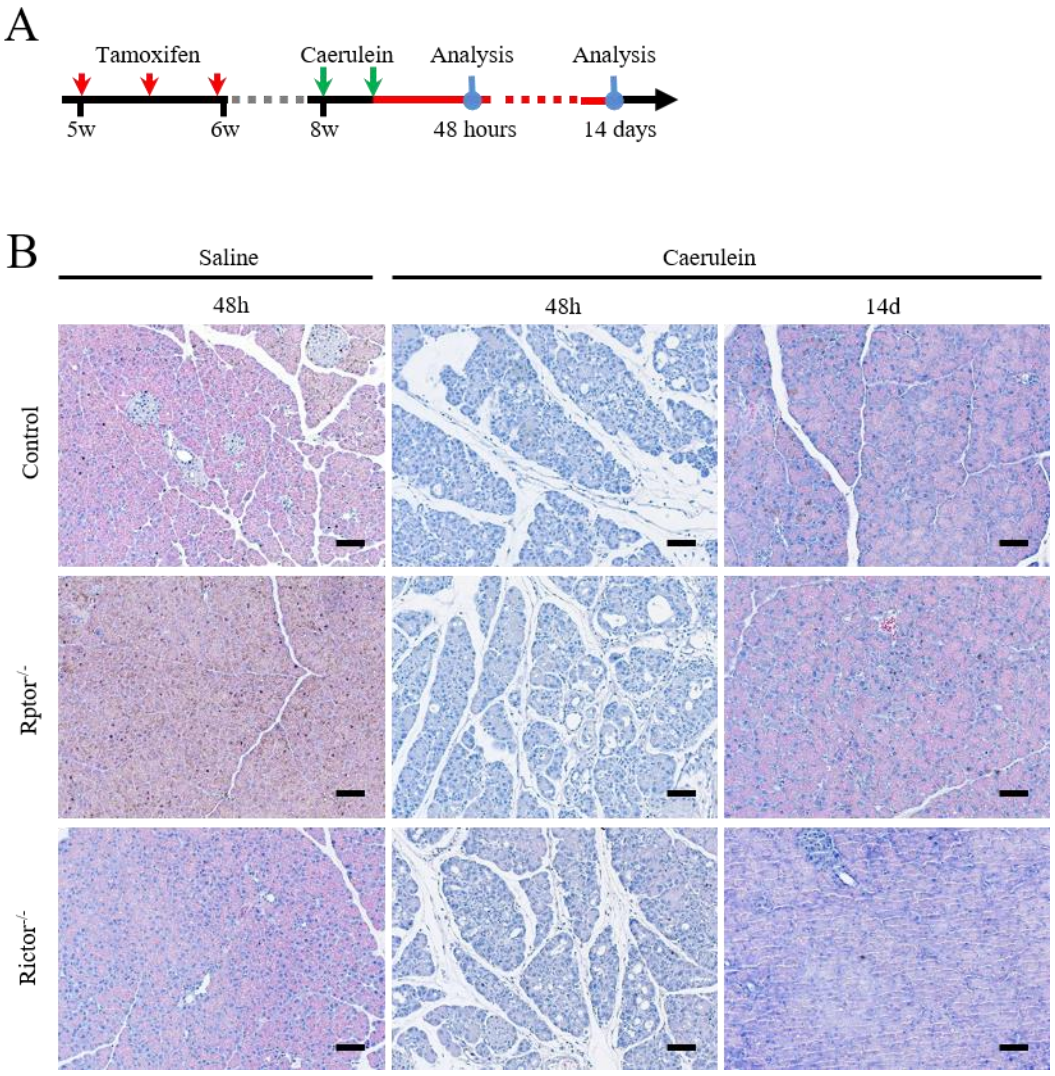

Figure 14. (**A**) 5-week-old transgenic mice were induced with tamoxifen at day 1,3,5, and injected with caerulein for 2 consecutive days at 8 weeks old. Pancreas was harvested for analysis 2 or 14 days after caerulein injection; (**B**) Representative H&E-stained sections show histological changes 48 hours and 14 days after caerulein-induced pancreatitis in control, Rptor$^{-/-}$ and Rictor$^{-/-}$ pancreas; Scale bar: 50 μm.

Secondly, we performed an ADM formation assay in 3D culture. Pancreatic acinar cells were isolated from control and Rptor or Rictor ablation mice and treated with TGF-α for 48h. Interestingly, Rptor or Rictor knock out acini still generated intact but smaller

duct-like structures compared with control acinar cells (Figures 15). Thus, this result suggests that both Rptor and Rictor are partially required for TGF-α-induced ADM formation *in vitro*.

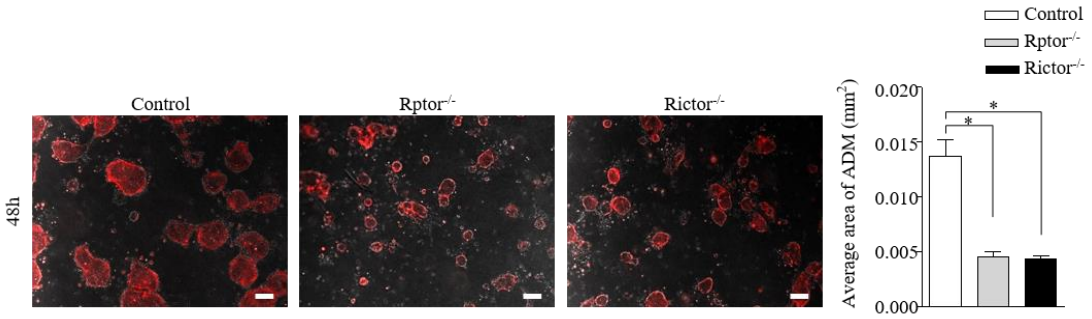

Figure 15. Representative IF pictures show the capacity of ADM formation (induced by TGF-α) of acinar cells isolated from wild type (control), Rptor$^{-/-}$ and Rictor$^{-/-}$ pancreata in 3D culture, all acinar cells are marked by RFP; Scale bar: 100 μm; Quantitative data shows the area of ADM lesions *in vitro*, n=3, *<0.05, unpaired *t*-test.

4.5 Rptor and Rictor is crucial for Kras^{G12D}-mediated ADM and PanIN formation

To investigate the oncogenic role of mTORC1 and mTORC2 in PDAC, we generated *p48^{CreERTM}; LSL-Kras$^{G12D/+}$; Rptor$^{flox/flox}$;* LSL-Rosa26$^{CAG\text{-}tdTomato}$ (referred to as 'Kras^{G12D}; Rptor$^{-/-}$' mice), *p48^{CreERTM}; LSL-Kras$^{G12D/+}$; Rictor$^{flox/flox}$;* LSL-Rosa26$^{CAG\text{-}tdTomato}$ (referred to as 'Kras^{G12D}; Rictor$^{-/-}$' mice) and *p48^{CreERTM}; LSL-Kras$^{G12D/+}$;* LSL-Rosa26$^{CAG\text{-}tdTomato}$ (referred to as 'Kras^{G12D}' mice). These animals were treated with caerulein for two days after tamoxifen induction. Here, the deactivation of mTORC1 (Kras^{G12D}; Rptor$^{-/-}$) or mTORC2 (Kras^{G12D}; Rictor$^{-/-}$) significantly inhibited ADM development 14 days after caerulein treatment in Kras^{G12D} mice (as exemplified by H&E staining, a-Amylase and Krt19 staining, Figure 16, 17, 18). Furthermore, PanIN formation (as exemplified by Claudin 18 and Muc5ac staining) in Kras^{G12D}; Rptor$^{-/-}$ and Kras^{G12D}; Rictor$^{-/-}$ was also reduced, compared to Kras^{G12D} mice (Figure 17, 18). RFP IHC staining shows that the recombination efficiency is stable on the 14th day post

caerulein injection (Figure 16). In $Kras^{G12D}$ mice treated with saline, pancreas morphology was largely normal, although occasional PanINs were already evident by 8 weeks of age (Figure 16). Indeed, the results of western-blot analysis revealed that the genetic ablation of Rptor or Rictor led to a significant reduction in the expression of Rptor, Rictor and mTOR as well as compromised activation of downstream targets of mTORC1 (p-$S6^{S235/236}$) and mTORC2 (p-Akt^{S473} and p-$Ndrg^{T346}$) in pancreas (Figure 19B). Stainings for p-$S6^{S235/236}$, p-$Ndrg^{T346}$ and p-Akt^{S473} in pancreatic sections confirmed the results of western-blot analysis (Figure 19A). These data demonstrate that the activity of mTORC1 and mTORC2 is functionally indispensable for oncogenic $Kras^{G12D}$-mediated ADM development.

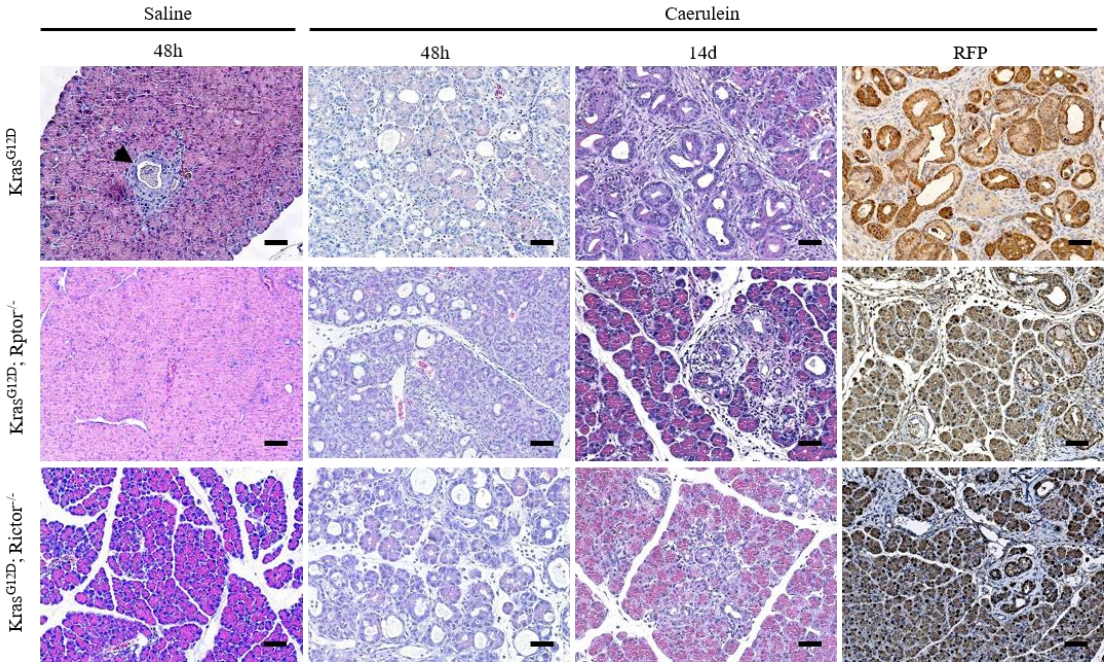

Figure 16. Occasional PanINs can be detected in $Kras^{G12D}$ mice treated with saline by 8 weeks of age (black arrow indicates low-grade PanIN). Representative H&E-stained sections show histological changes 48 hours and 14 days after caerulein-induced pancreatitis in $Kras^{G12D}$, $Kras^{G12D}$; $Rptor^{-/-}$ and $Kras^{G12D}$; $Rictor^{-/-}$ pancreas; Representative IHC pictures show the expression of RFP in these animals (scale bars: 50 µm).

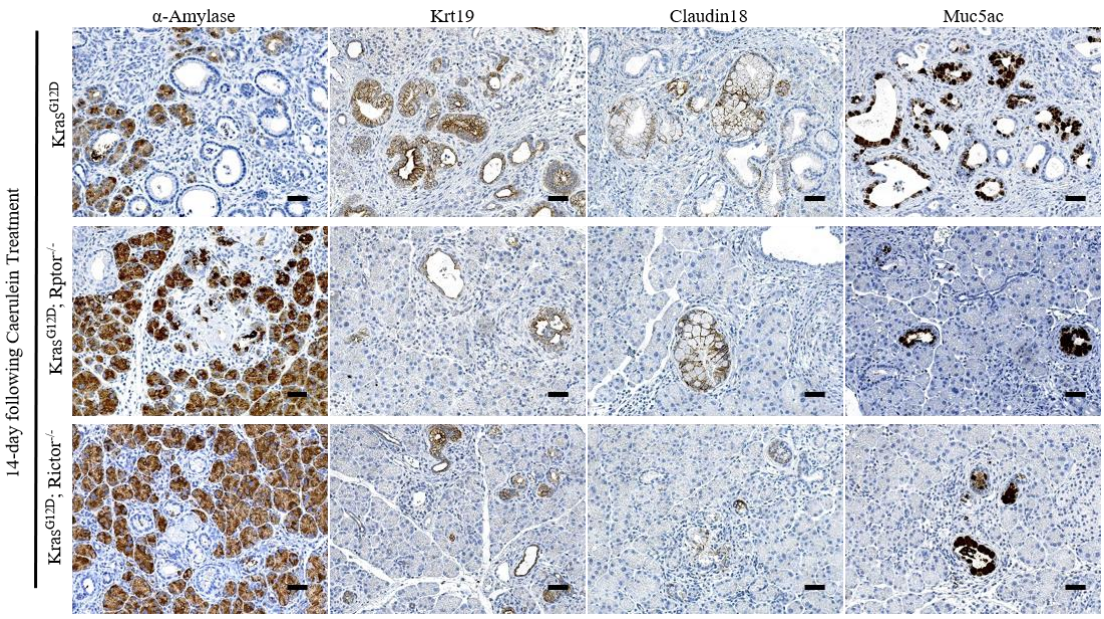

Figure 17. Representative IHC pictures show components of acinar cells (α-Amylase-positive), ADM (Krt19-positive) and PanIN (Claudin18- or Muc5ac-positive) lesions 14 days after caerulein-induced pancreatitis in $Kras^{G12D}$, $Kras^{G12D}$; $Rptor^{-/-}$ and $Kras^{G12D}$; $Rictor^{-/-}$ pancreata (scale bars: 50 µm).

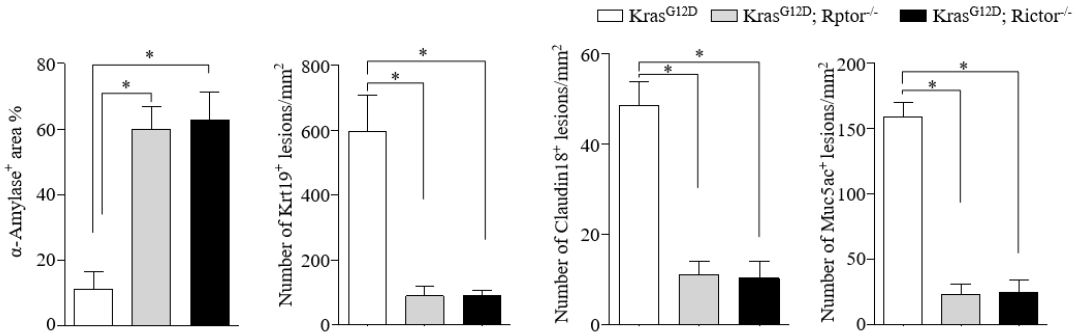

Figure 18. Quantitative data shows the area of acinar cells and the number of ADM and PanIN lesions in $Kras^{G12D}$, $Kras^{G12D}$; $Rptor^{-/-}$ and $Kras^{G12D}$; $Rictor^{-/-}$ pancreata 14 days after caerulein-induced pancreatitis, n=3, *: <0.05, unpaired *t*-test.

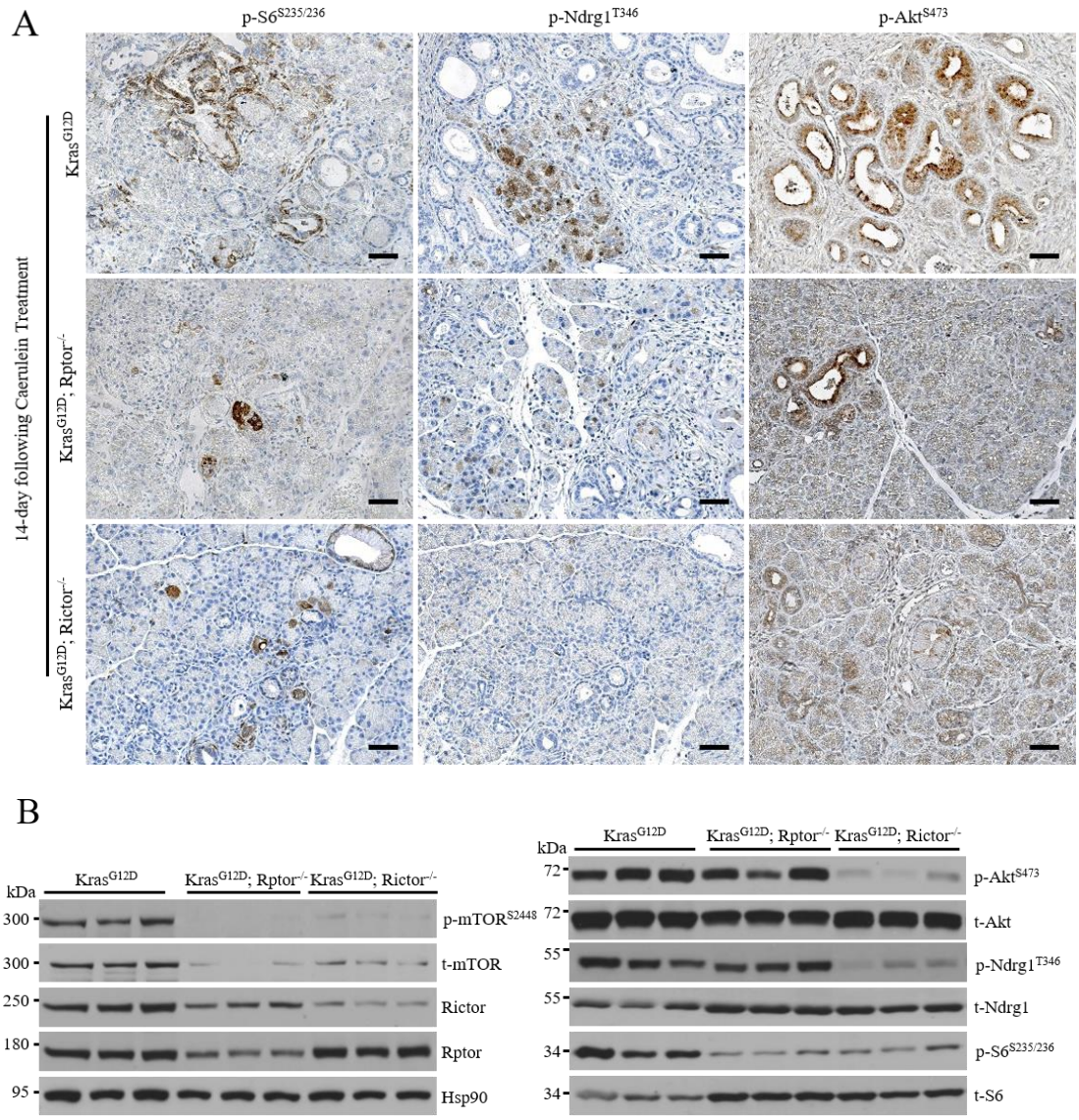

Figure 19. (**A**) Representative IHC pictures show stainings of p-S6$^{S235/236}$, p-Ndrg1^{T346} and p-Akt^{S473} 14 days after caerulein-induced pancreatitis in Kras^{G12D}, Kras^{G12D}; Rptor$^{-/-}$ and Kras^{G12D}; Rictor$^{-/-}$ pancreata (scale bars: 50 µm); (**B**) Western-blot analysis demonstrates the expression of Rptor, Rictor, and mTOR (and p-mTOR^{S2448}) as well as activation of downstream targets of mTORC1 (p-S6$^{S235/236}$) and mTORC2 (p-Ndrg1^{T346}, p-Akt^{S473}) in Kras^{G12D}, Kras^{G12D}; Rptor$^{-/-}$ and Kras^{G12D}; Rictor$^{-/-}$ pancreata.

4.6 Rptor and Rictor is critical for ADM formation in the presence of Kras^{G12D} *in vitro*

To analyze the effect of Rptor or Rictor on ADM formation in the presence of Kras^{G12D} *in vitro*, freshly harvested explants from the pancreas of Kras^{G12D}, Kras^{G12D}; Rptor$^{-/-}$ and Kras^{G12D}; Rictor$^{-/-}$ littermates were incubated with caerulein for 24 hours, we found

that a lot of dead single acinar cell suspended in the culture medium in $Kras^{G12D}$; $Rptor^{-/-}$ and $Kras^{G12D}$; $Rictor^{-/-}$ explants compared with control. Acini clusters were seeded in collagen gel at 0h. At 48h, we observed round and large ADM structures from $Kras^{G12D}$ pancreas in 3D culture, however, only irregular and small ADM-like structures from $Kras^{G12D}$; $Rptor^{-/-}$ and $Kras^{G12D}$; $Rictor^{-/-}$ explants could be observed (Figure 20). We quantified the average area of ADM lesions and found that the size of the formed structures in $Kras^{G12D}$; $Rptor^{-/-}$ and $Kras^{G12D}$; $Rictor^{-/-}$ explants is smaller at 48h compared with that from $Kras^{G12D}$samples. Taken together, the loss of Rptor or Rictor strongly inhibit the $Kras^{G12D}$-driven ADM formation *in vitro*.

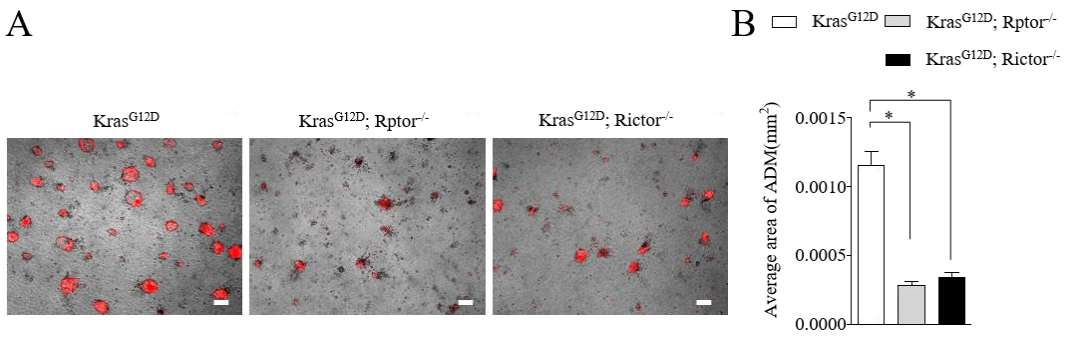

Figure 20. (**A** and **B**) Representative IF pictures show the capacity of ADM formation in acinar cells isolated from $Kras^{G12D}$, $Kras^{G12D}$; $Rptor^{-/-}$ and $Kras^{G12D}$; $Rictor^{-/-}$ pancreas in 3D culture, all acinar cells are marked by RFP; Quantitative data shows the area of ADM lesions *in vitro*, n=3, *: <0.05, unpaired *t*-test.

4.7 mTORC1 and mTORC2 synergistically promote $Kras^{G12D}$-induced ADM formation

To test if mTORC1 and mTORC2 synergistically promote $Kras^{G12D}$-induced ADM formation, we generated $p48Cre^{ERTM}$; LSL-$Kras^{G12D/+}$; $Rptor^{flox/flox}$; $Rictor^{flox/flox}$; LSL-$Rosa26^{CAG\text{-}tdTomato}$ (referred to as '$Kras^{G12D}$; $Rptor^{-/-}$; $Rictor^{-/-}$' mice) which is double-deficient for mTORC1 and mTORC2 function. All animals were treated with tamoxifen at 5-6 weeks of age, and they were treated with caerulein for two consecutive days. Better than the phenotype of $Kras^{G12D}$; $Rptor^{-/-}$ and $Kras^{G12D}$;

Rictor$^{-/-}$ mice, there was no detectable ADM lesions two weeks after caerulein treatment in Kras^{G12D}, Rptor$^{-/-}$; Rictor$^{-/-}$ pancreas (Figure 21). To investigate the long-term impact of mTORC1- or mTORC2-deficiency on pancreatic carcinogenesis, we sacrificed a set of compound mice 24 weeks after caerulein treatment. As previously described,[161] Kras^{G12D} animals developed high-grade PanIN lesions and numerous ADM lesions with occasionally visible intact acinar cells (Figure 21 and 22). The phenotype of Kras^{G12D}; Rptor$^{-/-}$ and Kras^{G12D}; Rictor$^{-/-}$ animals have slightly attenuated: more intact acinar cells (labelled by a-Amylase staining) and less ADM (labelled by Krt19 staining) lesions were observed, as compared to Kras^{G12D} mice; however, no difference in the area of PanIN lesions was observed. Strikingly, the double-deficient (Kras^{G12D}; Rptor$^{-/-}$; Rictor$^{-/-}$) mice showed only a few ADM lesions and low-grade PanIN lesions (Figure 22 and 23). Taken together, mTORC1 or mTORC2 ablation alone only transiently inhibits oncogenic Kras^{G12D}-driven ADM formation. A dual deactivation of mTORC1 and mTORC2 is required to persistently suppress oncogenic Kras^{G12D}-driven ADM development and carcinogenesis.

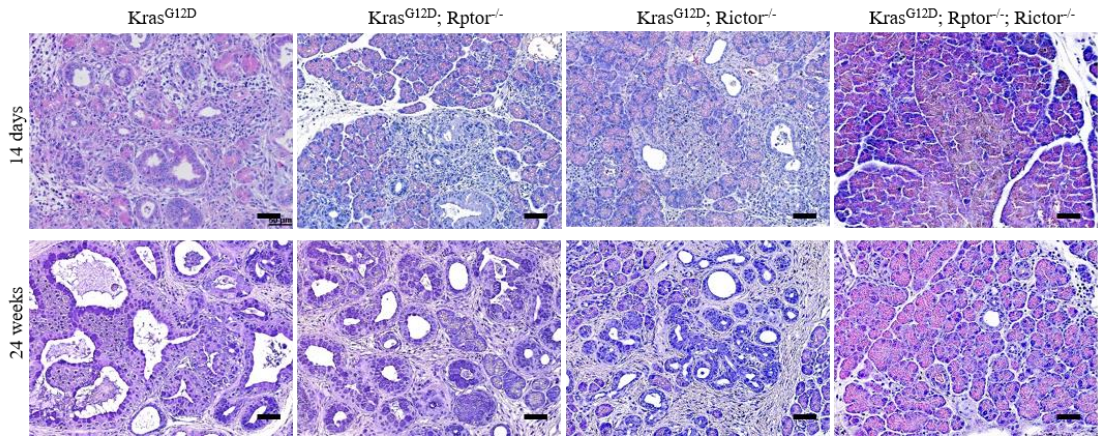

Figure 21. Representative H&E-stained sections show histological changes 14days and 24 weeks after caerulein-induced pancreatitis in Kras^{G12D}, Kras^{G12D}; Rptor$^{-/-}$, Kras^{G12D}; Rictor$^{-/-}$ and Kras^{G12D}; Rptor$^{-/-}$; Rictor$^{-/-}$ pancreas (scale bars: 50 μm).

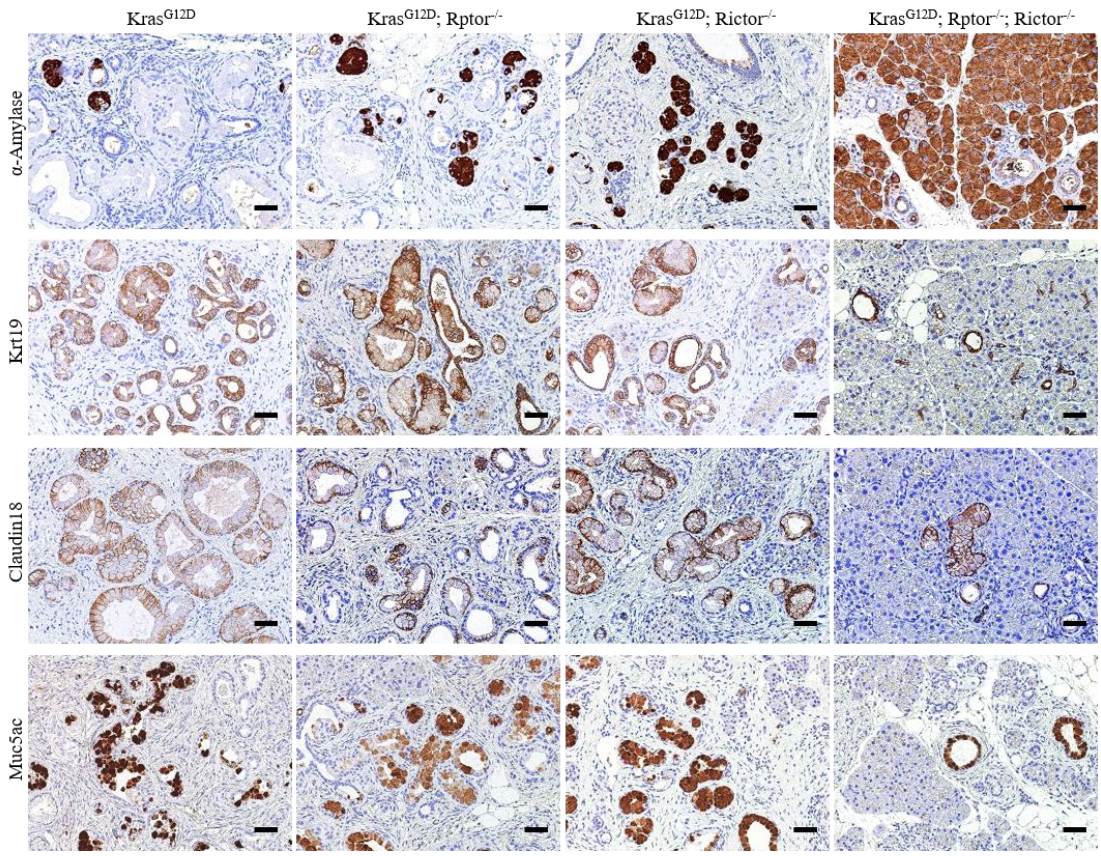

Figure 22. Representative IHC pictures show components of acinar cells (a-Amylase-positive), ADM (Krt19-positive) and PanIN (Claudin18- or Muc5ac-positive) lesions 24 weeks after caerulein-induced pancreatitis in $Kras^{G12D}$, $Kras^{G12D}$; $Rptor^{-/-}$, $Kras^{G12D}$; $Rictor^{-/-}$ and $Kras^{G12D}$; $Rptor^{-/-}$; $Rictor^{-/-}$ pancreas (scale bars: 50 µm).

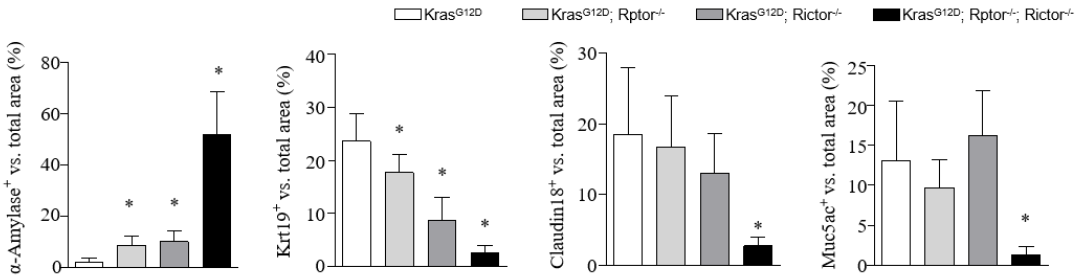

Figure 23. Quantitative data shows the number of acinar cells, ADM and PanIN lesions in $Kras^{G12D}$, $Kras^{G12D}$; $Rptor^{-/-}$, $Kras^{G12D}$; $Rictor^{-/-}$ and $Kras^{G12D}$; $Rptor^{-/-}$; $Rictor^{-/-}$ pancreas 24 weeks after caerulein-induced pancreatitis (right panel), n>=5, *: <0.05, unpaired *t*-test.

4.8 Identification of differently expressed proteins in $Kras^{G12D}$ versus Rptor or Rictor ablation -$Kras^{G12D}$ mouse model

To investigate the underlying mechanism responsible for ADM formation, we performed a mass spectrometry-based proteomic analysis using $Kras^{G12D}$, $Kras^{G12D}$; $Rptor^{-/-}$ and $Kras^{G12D}$; $Rictor^{-/-}$ pancreatic samples 14 days after caerulein treatment. Similar to histological findings, the clustering analysis revealed that the proteasomes of $Kras^{G12D}$; $Rptor^{-/-}$ and $Kras^{G12D}$; $Rictor^{-/-}$ samples were comparable, but they were highly distinctive from $Kras^{G12D}$ samples (Figure 24). Next, we performed a pairwise comparison to identify proteins that were differentially expressed between $Kras^{G12D}$ and $Kras^{G12D}$; $Rptor^{-/-}$ samples as well as between $Kras^{G12D}$ and $Kras^{G12D}$; $Rictor^{-/-}$ samples. The volcano plots show the statistical significance versus the fold change for differently expressed proteins detected in the proteomic analysis (Figure 25). The up-regulated significant proteins between $Kras^{G12D}$ and $Kras^{G12D}$; $Rptor^{-/-}$ mice or between $Kras^{G12D}$ and $Kras^{G12D}$; $Rptor^{-/-}$ animals are depicted as red solid circle and green solid circle, and the down-regulated significant proteins are displayed as black solid circles. From these upregulated proteins, we pick out all proteins that were increased in $Kras^{G12D}$ mouse model and represent the distribution of them in the Venn diagram (Figure 26). Of the 708 up-regulated proteins in $Kras^{G12D}$ animal, 578 were detected between $Kras^{G12D}$ and $Kras^{G12D}$; $Rptor^{-/-}$ mice, 440 were detected between $Kras^{G12D}$ and $Kras^{G12D}$; $Rictor^{-/-}$ mice, 310 were shared by these two sets of comparations.

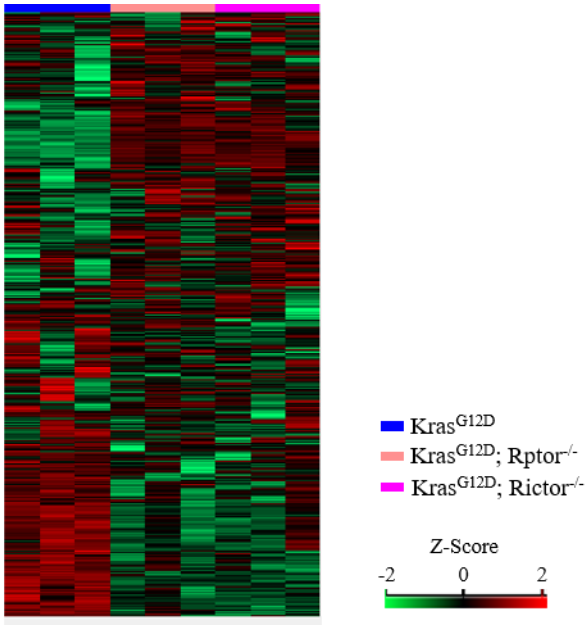

Figure 24. The heat map presents different expression profile of all proteins tested in $Kras^{G12D}$ animal compared with $Kras^{G12D}$; $Rptor^{-/-}$ and $Kras^{G12D}$; $Rictor^{-/-}$ samples (n=3).

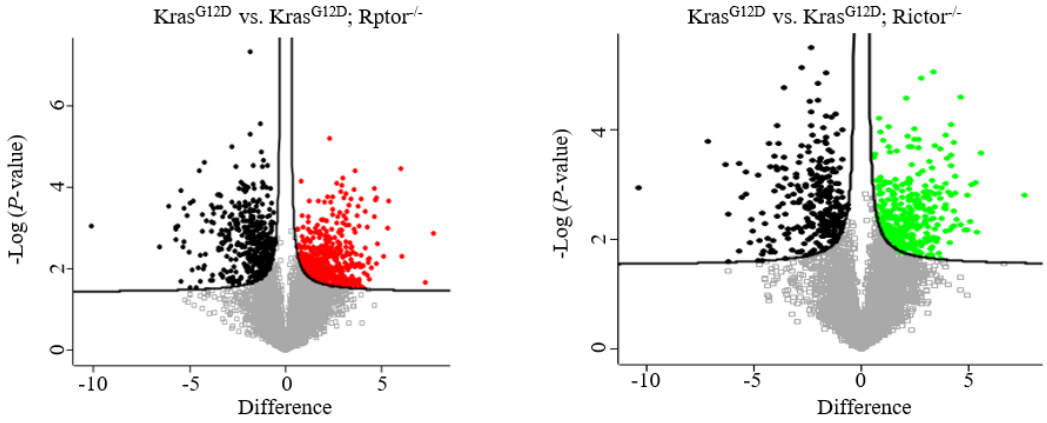

Figure 25. The volcano plots show the fold change and significance of differently expressed proteins detected in the proteomic analysis. Each dot in the right part of the volcano plot represent an up-regulated protein, displayed in red or green, each black dot represents a down-regulated protein in these two sets of comparison (n=3, FDR<0.05).

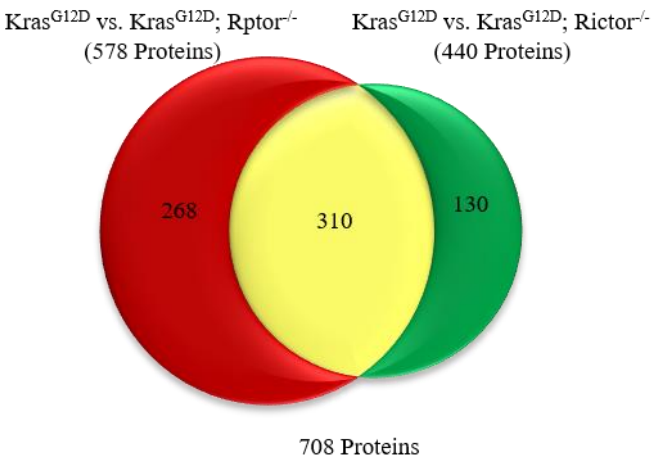

Figure 26. Venn diagram display 578 up-regulated proteins of Kras^{G12D} sample detected in Kras^{G12D} versus Kras^{G12D}; Rptor$^{-/-}$, 440 detected in Kras^{G12D} versus Kras^{G12D}; Rictor$^{-/-}$, 310 shared by the two sets of comparisons.

4.9 KEGG pathway enrichment analysis

To explore the functional relevance, we analyzed the KEGG pathways using mTORC1 and mTORC2 proteomic signatures (Figure 27; Table 6, 7). Notably, KEGG analysis identified six pathways: “Regulation of actin cytoskeleton”, “Lysosome”, “Focal adhesion” and “Fc gamma R-mediated phagocytosis”, “MAPK signaling pathway”, “Shigellosis”, which were shared by mTORC1 and mTORC2 proteomic signatures. As “Regulation of actin cytoskeleton” was the most significant pathway and as it was also known to be involved in ADM formation[54, 162], we went on to explore this pathway. In particular, Arpc1b (actin related protein 2/3 complex, subunit 1B), Arpc3 (actin related protein 2/3 complex, subunit 3) and Arpc5 (actin related protein 2/3 complex, subunit 5) are essential components of Arp2/3 complex which is an actin nucleator consisting of seven subunits.[163, 164] These data suggest that the Arp2/3 complex is involved in oncogenic Kras^{G12D}-driven ADM formation.

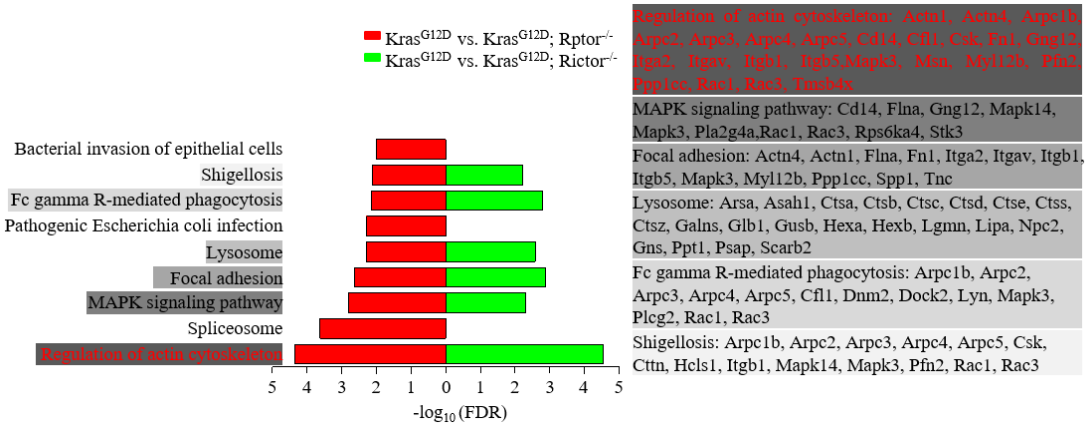

Figure 27. 9 enriched pathways were detected in Kras^{G12D} versus Kras^{G12D}; Rptor$^{-/-}$, 6 enriched pathways were detected in Kras^{G12D} to Kras^{G12D}; Rictor$^{-/-}$ comparison. Shared up-regulated proteins related to each enriched pathway are presented in the table.

Table 6. Enriched pathway in Kras^{G12D} vs. Kras^{G12D}; Rptor$^{-/-}$

KEGG name	*P value*	*Enrichment*	*Ben. Ho. FDR*
Regulation of actin cytoskeleton	5.86950000E-07	1.6353	4.48040000E-05
Spliceosome	5.17800000E-06	1.7716	2.37150000E-04
MAPK signaling pathway	5.40120000E-05	1.7716	1.54610000E-03
Focal adhesion	9.49090000E-05	1.6299	2.41490000E-03
Lysosome	2.28710000E-04	1.5748	5.23750000E-03
Pathogenic Escherichia coli infection	2.53460000E-04	1.6784	5.27670000E-03
Fc gamma R-mediated phagocytosis	4.30600000E-04	1.6732	7.04330000E-03
Shigellosis	4.30600000E-04	1.6732	7.58510000E-03
Bacterial invasion of epithelial cells	7.28690000E-04	1.6674	9.81580000E-03

Table 7. Enriched pathway in Kras^{G12D} vs. Kras^{G12D}; Rictor$^{-/-}$

KEGG name	*P value*	*Enrichment*	*Ben. Ho. FDR*
Regulation of actin cytoskeleton	4.03360000E-07	1.6705	2.94460000E-05
Focal adhesion	2.92560000E-05	1.6705	1.28140000E-03
Fc gamma R-mediated phagocytosis	4.97550000E-05	1.6705	1.55660000E-03
Lysosome	9.59690000E-05	1.5978	2.62710000E-03
MAPK signaling pathway	2.43330000E-04	1.6705	4.84450000E-03
Shigellosis	4.12230000E-04	1.6705	6.01850000E-03

4.10 Validation of mass spectrometry data *in vivo* and *in vitro*

Firstly, we investigated the expression of several Arp2/3 complex components (Arp2, Arp3 and Arpc1b) in pancreatic tissues from $Kras^{G12D}$, $Kras^{G12D}$; $Rptor^{-/-}$ and $Kras^{G12D}$; $Rictor^{-/-}$ mice 14 days after caerulein treatment. Accordingly, the results of western-blot analysis revealed that the expression of these Arp2/3 complex components was reduced in both $Kras^{G12D}$; $Rptor^{-/-}$ and $Kras^{G12D}$; $Rictor^{-/-}$ samples, compared to $Kras^{G12D}$ samples (Figure 28A). *In vitro*, Arp2, Arp3 and Arpc1b expression was higher in $Kras^{G12D}$-mediated ADM lesions, as compared to TGF-α-induced ADM lesions from wild-type acinar cells and control ADM lesions (Figure 28B). Finally, the expression of ARPC1B, ARP2 and ARP3 was also higher in human CP tissues than that in the normal pancreas (Figure 28C). Also, we confirmed these data using IHC staining analysis (Figure 28D). F-actin was localized on both apical and basal part of these ADM lesions of $Kras^{G12D}$ pancreas *in vivo* and *in vitro* (Figure 29).

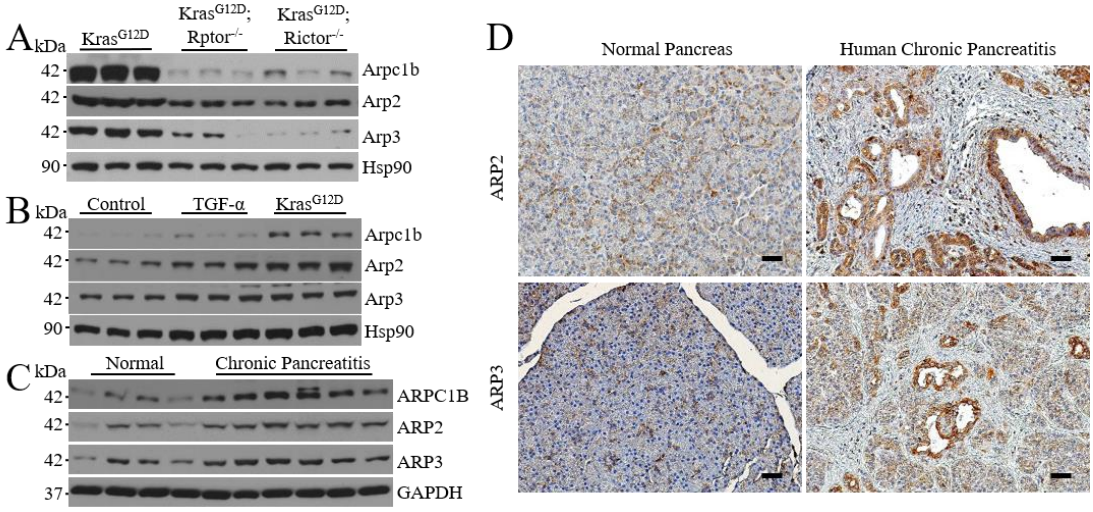

Figure 28. (**A**) Western-blot analysis confirms the reduced expression of Arpc1b, Arp2 and Arp3 in $Kras^{G12D}$; $Rptor^{-/-}$ and $Kras^{G12D}$; $Rictor^{-/-}$, compared to $Kras^{G12D}$ samples; (**B**) Western-blot analysis demonstrates the expression of Arpc1b, Arp2 and Arp3 in oncogenic $Kras^{G12D}$-induced ADM lesions, TGF-α-induced ADM lesions from wild-type acinar cells and ADM lesions from wild-type acinar cells, *in vitro*; (**C**) Western-blot analysis demonstrates the expression of ARPC1B, ARP2 and ARP3 in normal and chronic pancreatitis tissues. GAPDH is served as equal loading; (**D**) Representative IHC pictures show the staining of Arp2 andArp3 in human chronic pancreatitis tissue and normal human pancreas

(scale bars: 50 μm).

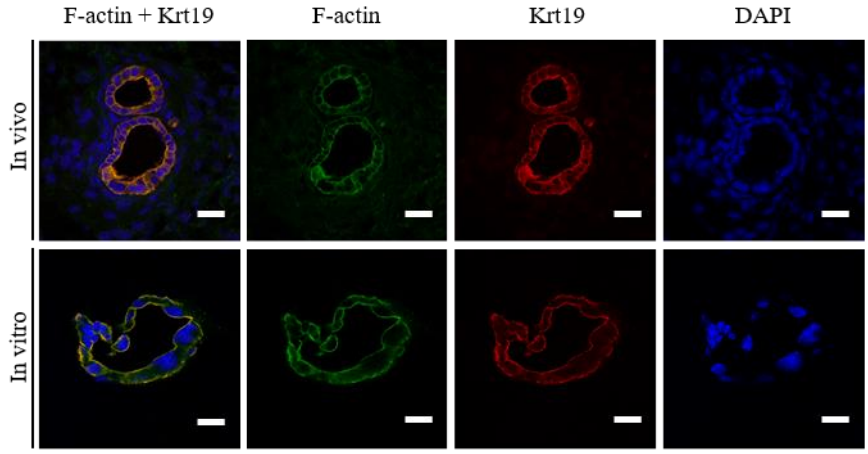

Figure 29. Representative IF pictures show the F-actin and Krt19 localization in the ADM lesions of $Kras^{G12D}$ pancreas two weeks after caerulein injection and in the ADM lesion formed by isolated $Kras^{G12D}$ acinar cells *in vitro* (scale bars: 25 μm).

4.11 Loss of Arpc4 displays no pancreatic abnormalities

From the KEGG pathway enrichment analysis, we noticed that the regulation of actin cytoskeleton is the most significant pathway involved in ADM formation. In this pathway, many proteins correlated with actin cytoskeleton are upregulated. For example, Arp2/3, Cofilin 1, Profilin 2 and Tmsb4x, most of them are actin-binding proteins. Therefore, we choose the Arp2/3 complex as the main target to study its role in precursor lesion of PDAC. Moreover, it is reported that the y-branching of actin filament network mediated by Arp2/3 complex is ideally suited for generating mechanical tension required in lamellipodia formation.[165] Thus, we hypothesized that the tension-generating property of branch network mediated by Arp2/3 complex might be responsible for creating the apico-basal tension redistribution in the process of ADM formation.

To test this, we crossed an $Arpc4^{flox/flox}$ (actin-related protein 2/3 complex, subunit 4) line with $p48Cre^{ERTM}$ to generate $p48Cre^{ERTM}$; $Arpc4^{flox/flox}$ (referred to as '$Arpc4^{-/-}$' mice). Previous studies have proved that the loss of Arpc4 subunit completely

deactivated the function of Arp2/3 complex.[157] All mice were treated as above mentioned. The results of western-blot analysis confirmed reduced expression of Arpc4, Arp2, Arp3 and Arpc1b in Arpc4$^{-/-}$ mice after tamoxifen treatment (Figure 30A). The loss of Arp2/3 complex function in acinar cells had no significant impact on pancreatic physiology, as reflected by histological analysis, staining for endocrine (Insulin and Glucagon) and exocrine (Keratin 19 (Krt19) and α-Amylase) markers, random blood glucose levels and body weight analysis (Figure 30B, 30C).

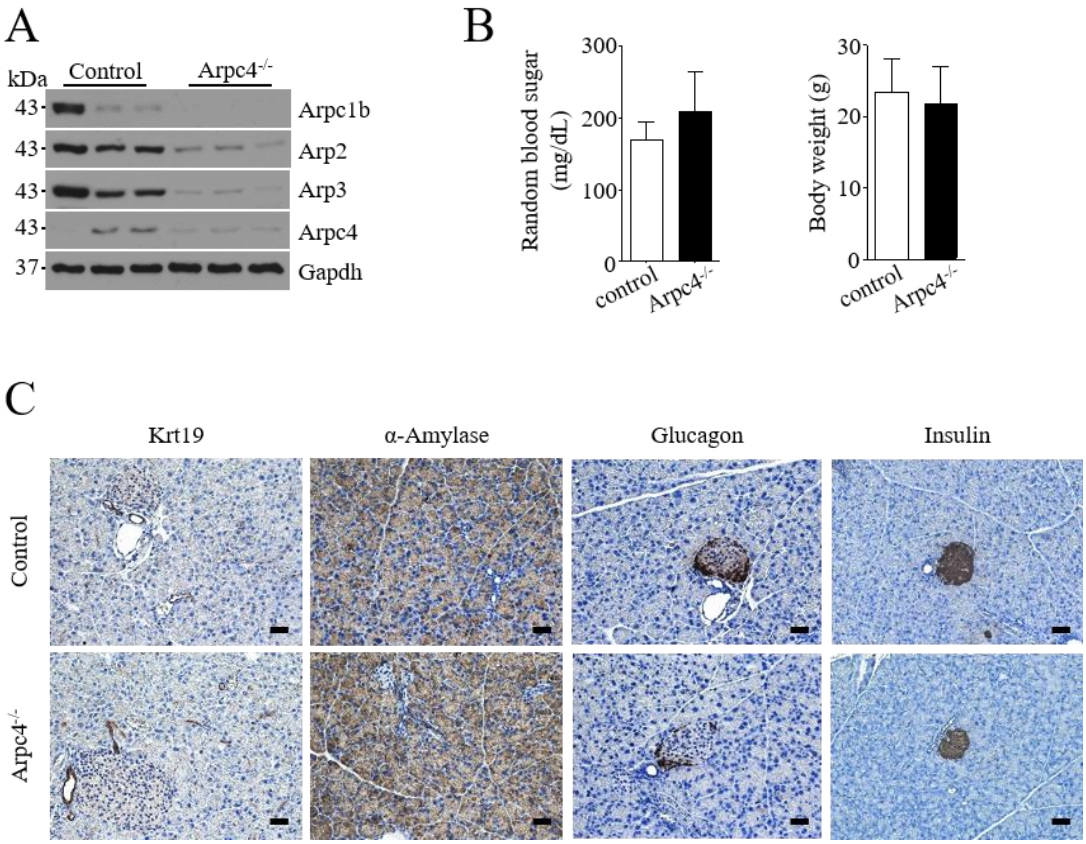

Figure 30. (**A**) Western-blot analysis demonstrates the expression of Arpc1b, Arp2, Arp3 and Arpc4 in wildtype (control) and Arpc4$^{-/-}$ pancreata; (**B**) Quantitative data show the random blood glucose (mg/dL) and the body weight (g) of control and Arpc4$^{-/-}$ mice; n=3, unpaired *t*-test; (**C**) Representative IHC pictures show the exocrine (Krt19 and α-Amylase staining) and endocrine (Glucagon and Insulin staining) compartment of these animals (scale bars: 50 µm).

4.12 Arpc4 is required for ADM formation

To test if Arpc4$^{-/-}$ mice are generally resistant to ADM formation, we treated them with

caerulein for two consecutive days and sacrificed 48 hours and 14 days after caerulein treatment. The pancreas of all Arpc4$^{-/-}$ mice was fully regenerated on day 14, indicating that the loss of Arp2/3 complex function did not influence organ regeneration. Notably, the number of ADM lesions was dramatically reduced in Arpc4$^{-/-}$ mice 48 hours after caerulein treatment, as compared to control animals (Figure 31A). Thus, acinar cells deficient for Arp2/3 complex function are protected against inflammation-induced ADM formation.

After *in vivo* experiments, pancreatic acinar cells were isolated from control and Arpc4 ablation mice and treated with TGF-α for 48h. Ductal-like structure generated from Arpc4 knock out acini is smaller compared with control (Figures 31B). This result suggests that the inhibitory effect of Arp2/3 complex on ADM formation is cell autonomous *in vitro*. Overall, the data from *in vivo* and *in vitro* indicate that Arp2/3 complex is necessary for acinar-to-ductal epithelial reprogramming.

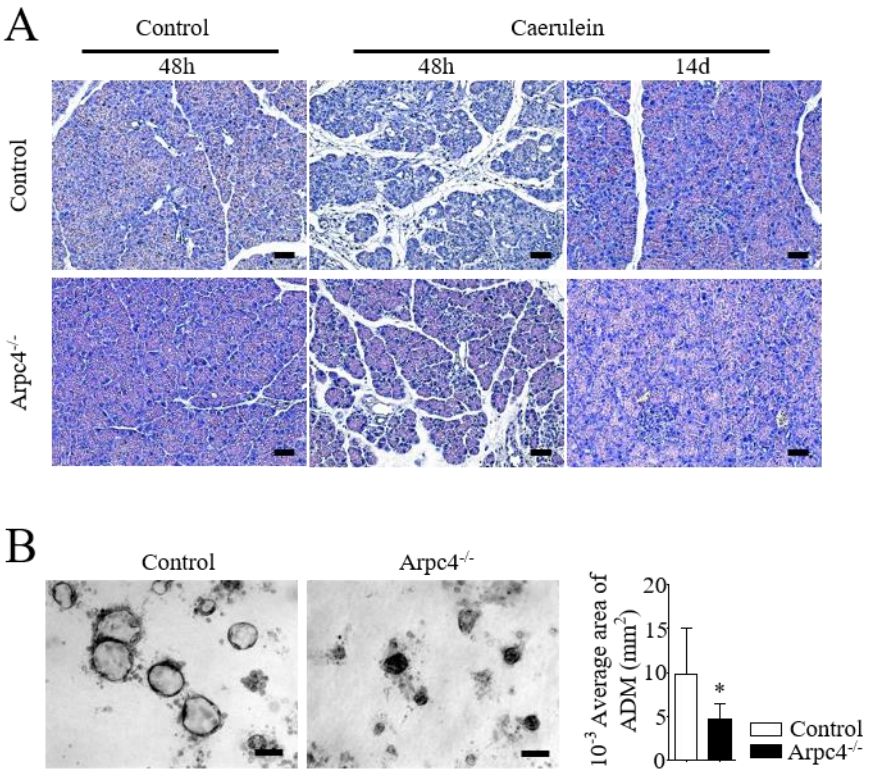

Figure 31. (**A**) Representative H&E-stained sections show histological changes 48 hours and 14 days after caerulein-induced pancreatitis in control and Arpc4$^{-/-}$ pancreas (scale bars: 50 μm); (**B**)

Representative pictures show the capacity of ADM formation (induced by TGF-α) of acinar cells isolated from control and Arpc4$^{-/-}$ pancreas in 3D culture. Quantitative data shows the area of ADM lesions *in vitro*, *<0.05, unpaired *t*-test.

4.13 The inactivation of Arp2/3 complex completely blocks oncogenic Kras^{G12D}-mediated ADM formation

To investigate the potential oncogenic role of Arp2/3 complex, we generated p48Cre^{ERTM}; LSL-Kras$^{G12D/+}$; Arpc4$^{flox/flox}$ (referred to as 'Kras^{G12D}; Arpc4$^{-/-}$' mice). After tamoxifen induction, all animals were treated with caerulein and subjected to histopathological characterization 14 days after treatment. Compellingly, all Kras^{G12D}; Arpc4$^{-/-}$ pancreas were completely devoid of ADM and PanIN lesions, as compared to Kras^{G12D} pancreas (Figure 32A, 32C, as exemplified by H&E staining, a-Amylase, Krt19, Claudin 18 and Muc5ac staining). The results of western-blot analysis revealed that the genetic ablation of Arpc4 led to a dramatic reduction in the expression of Arpc4, Arp2, Arp3 and Arpc1b in Kras^{G12D}; Arpc4$^{-/-}$ pancreas, as compared to Kras^{G12D} pancreas (Figure 32B). Besides, Rac1 expression was significantly reduced in Kras^{G12D}; Arpc4$^{-/-}$ pancreas. Except for Rictor and p-Akt^{S473} (the reduction in Kras^{G12D}; Arpc4$^{-/-}$ samples), no difference in the activation of downstream targets for mTORC1 (p-mTOR^{S2448}, Rptor and p-S6$^{S235/236}$) and mTORC2 (p-mTOR^{S2448} and p-Ndrg^{T346}) was observed between Kras^{G12D} and Kras^{G12D}; Arpc4$^{-/-}$ pancreas (Figure 32B). Consistently, Kras^{G12D}; Arpc4$^{-/-}$ acinar cells showed a compromised capacity in forming ADM lesions *in vitro*, as compared to Kras^{G12D} acinar cells (Figure 33). It is reported that the myosin activity (as exemplified by phospho-Myosin Light Chain 2^{Ser19}, p-MLC2^{S19}) is higher apically than basally in acinar cells; however, this gradient was lost in the ADM lesions of Kras^{G12D} pancreata.[166] Here IF shows that Kras^{G12D}; Arpc4$^{-/-}$ acinar cells maintained acinar phenotype (positive for α-Amylase staining) with focused myosin activity (labelled by p-MLC2^{S19}, Figure 34) in 3D culture. In comparison, Kras^{G12D} acinar cells assumed ductal phenotype (positive for Krt19) with basally enhanced myosin activity (positive for p-MLC2^{S19} staining) *in vitro*, underscoring the importance of apical-basal

tension redistribution in instructing ADM formation (Figure 34). Taken together, these data demonstrate a crucial role of Arp2/3 complex in ADM formation by redistributing apical-basal tension.

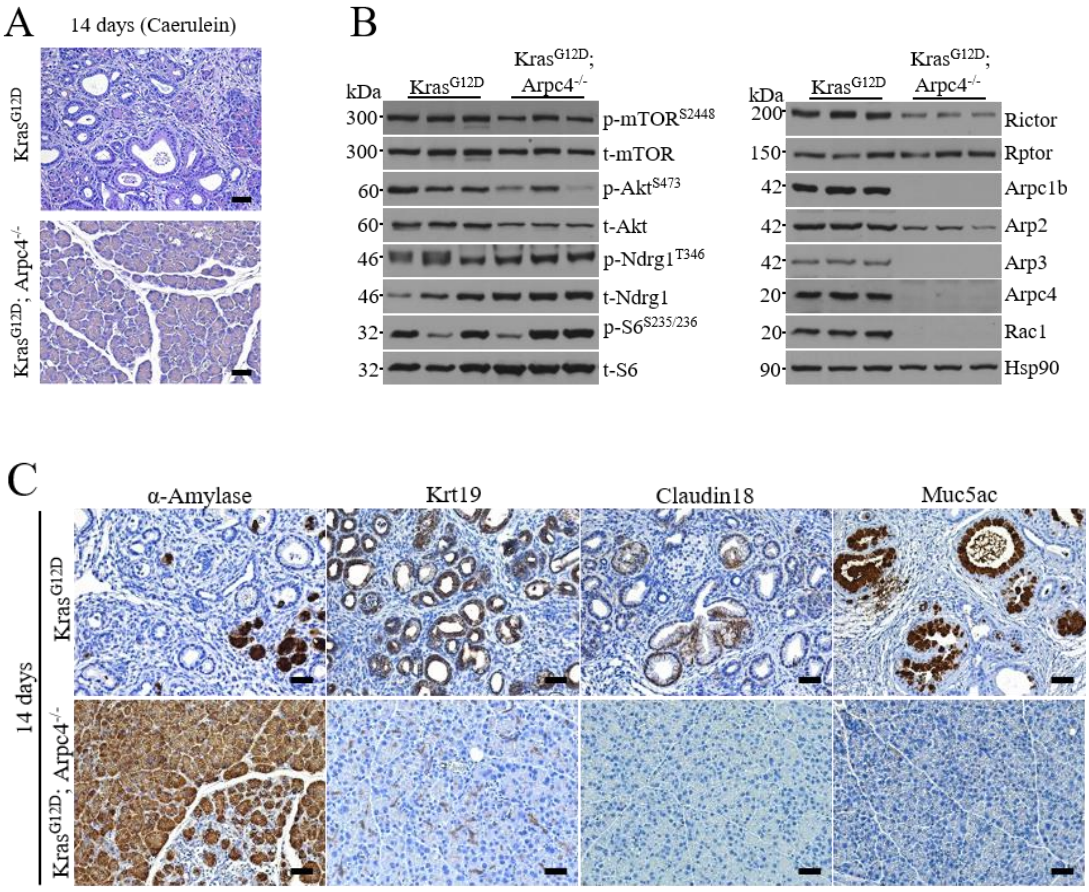

Figure 32. (**A**) Representative H&E-stained sections show histological changes 14 days after caerulein-induced pancreatitis in Kras^{G12D} and Kras^{G12D}; Arpc4$^{-/-}$ pancreas (scale bars: 50 µm); (**B**) Western-blot analysis demonstrates the expression of p-mTOR^{Ser2448}, pAkt^{S473}, p-Ndrg1^{T346}, p-S6$^{S235/236}$, Rictor, Rptor, Arpc1b, Arp2, Arp3, Arpc4 and Rac1 14 days after caerulein-induced pancreatitis in Kras^{G12D} and Kras^{G12D}; Arpc4$^{-/-}$ pancreas; (**C**) Representative IHC pictures show components of acinar cells (α-Amylase-positive), ADM (Krt19-positive) and PanIN (Claudin18- or Muc5ac-positive) lesions 14 days after caerulein-induced pancreatitis in Kras^{G12D} and Kras^{G12D}; Arpc4$^{-/-}$ pancreas (scale bars: 50 µm).

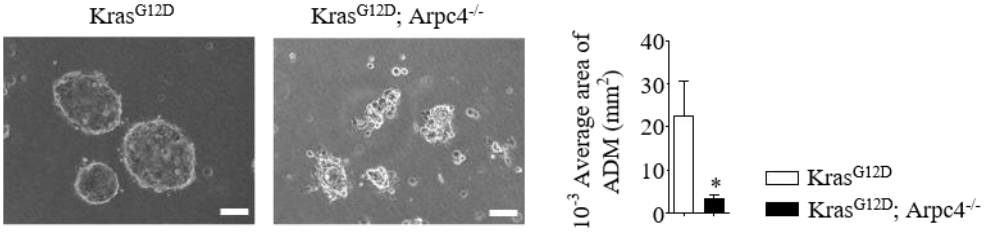

Figure 33. Representative phase contrast pictures show the capacity of ADM formation of acinar cells isolated from $Kras^{G12D}$ and $Kras^{G12D}$; $Arpc4^{-/-}$ pancreas in 3D culture; quantitative data show the area of ADM lesions *in vitro*, n=3, *: <0.05, unpaired *t*-test.

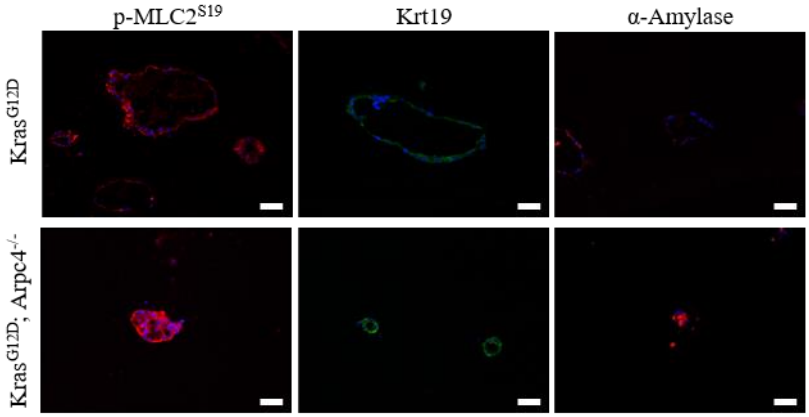

Figure 34. Representative IF pictures show p-$MLC2^{S19}$, Krt19 and a-Amylase staining in ADM lesions formed by acinar cells isolated from $Kras^{G12D}$ and $Kras^{G12D}$; $Arpc4^{-/-}$ pancreas in 3D culture.

4.14 mTORC2 activates the activity of Arp2/3 complex via Akt/Rac1 signal axis while mTORC1 controls the protein synthesis of Rac1/Arp3

We went on to investigate how mTORC1 and mTORC2 affect the activity of Arp2/3 complex. As illustrated earlier, since Rac1 is indispensable for $Kras^{G12D}$-driven ADM formation, the phenotype of mTORC2-deficient mice can be attributed to damped Rac1 activity.[54, 162] mTORC2 activates Rac1 activity through two substrates: Akt and Pkcα.[167, 168] Rac1 promotes the activity of the Arp2/3 complex via WAVE proteins (WASP-family verprolin-homologous proteins, Figure 33A).[169] Thus, we hypothesise that: 1). inhibition of these signal pathways blocks ADM formation of isolated $Kras^{G12D}$ acinar cells; 2). activation of these signal pathways reconstitutes the ADM phenotype in isolated $Kras^{G12D}$; $Rictor^{-/-}$ acinar cells *in vitro*. To test this, a variety of pharmaceutical inhibitors against Akt1/2 (Akti-1/2), Pkcα (BIM XI), Rac1 (EHT 1864), Arp2/3 (CK-666), actin polymerization (Cytochalasin D) were used to test their capacities in inhibiting $Kras^{G12D}$-induced ADM formation in 3D culture (Figure 35A). This analysis revealed that inhibition of Akt, Rac1, Arp2/3 complex and actin polymerization effectively block isolated $Kras^{G12D}$ acinar cells in forming ADM *in vitro* whereas

inhibition of Pkcα had no effect (Figure 35A). These data suggest that mTORC2/Akt/Rac1/Arp2/3 complex signal constitutes a crucial pathway mediating ADM formation in isolated $Kras^{G12D}$ acinar cells. Indeed, Rac1 pull-down activation assay confirmed that both Rac1 expression and activation (GTP-bound) were dramatically reduced in both $Kras^{G12D}$; $Rictor^{-/-}$ and $Kras^{G12D}$; $Rptor^{-/-}$ pancreatic tissues, as compared to $Kras^{G12D}$ pancreas (Figure 35B). Furthermore, inhibition of either Akt (Akti-1/2) or Rac1 (EHT 1864) reduced consistently phosphorylation levels of p-Akt^{S473} and expression levels of Rac1, Arp2, Arp3 and Arpc1b in the isolated $Kras^{G12D}$ acinar cells. No such effect was observed for Pkcα inhibition (Figure 36).

Consistently, activation of Akt signalling by an Akt activator (SC 79) reconstituted ADM phenotype in isolated $Kras^{G12D}$; $Rictor^{-/-}$ acinar cells, but not in isolated $Kras^{G12D}$; $Rptor^{-/-}$ acinar cells (Figure 37A). The SC 79 treatment increased phosphorylation levels of p-Akt^{S473} and it induced Rac1 expression and activation simultaneously in $Kras^{G12D}$; $Rictor^{-/-}$ acinar cells (Figure 37B, 38A). In addition, the SC 79 treatment activated Akt signaling in $Kras^{G12D}$; $Rptor^{-/-}$ acinar cells (Figure 37C). To confirm that Rac1 is responsible for ADM formation induced by Akt activation in $Kras^{G12D}$; $Rictor^{-/-}$ acinar cells, a combinational treatment of Akt activator and Rac1 inhibitor was applied. As such, the additional Rac1 inhibition completely blocked the ability of Akt activator in inducing ADM formation in $Kras^{G12D}$; $Rictor^{-/-}$ acinar cells (Figure 38B). Thus, mTORC2 promotes the function of Arp2/3 complex through Akt/Rac1 pathway in driving $Kras^{G12D}$-mediated ADM formation.

The Akt activity in $Kras^{G12D}$ and $Kras^{G12D}$, $Rptor^{-/-}$ pancreas was comparable, and Akt activation failed to reconstitute ADM phenotype in isolated $Kras^{G12D}$, $Rptor^{-/-}$ acinar cells (Figure 37A). However, Rac1 expression (and activity) together with components of Arp2/3 was indeed reduced in $Kras^{G12D}$, $Rptor^{-/-}$ pancreas, as compared to $Kras^{G12D}$ pancreas. Thus, these phenomena in mTORC1-deficient mice cannot be explained by Akt signalling. As mTORC1 is a master complex responsible for protein synthesis, we hypothesise mTORC1 is accountable for the protein synthesis of Rac1 and Arp2/3

complex components. To test this, we performed a protein synthesis assay using isolated $Kras^{G12D}$ acinar cells in 3D culture. As such, the freshly prepared acinar cells were added to 3D culturing condition to form ADM lesions for 12 hours. To determine the protein synthesis rates of Rac1 and Arp2/3 complex components, ADM lesions were treated with cycloheximide (CHX: an inhibitor of protein synthesis) then released from CHX and harvested at 0-, 0.5-, 1-, 2- and 3-hours in the presence of mTORC1 inhibitor (Rapamycin, Figure 39). This analysis revealed that the activity of mTORC1 is responsible for the protein synthesis of Rac1 and Arp3, but not for Arp2, Arpc1b (Figure 39). As an internal control, Rapamycin treatment reduced p-$S6^{S235/236}$ levels in these ADM cells (Figure 39).

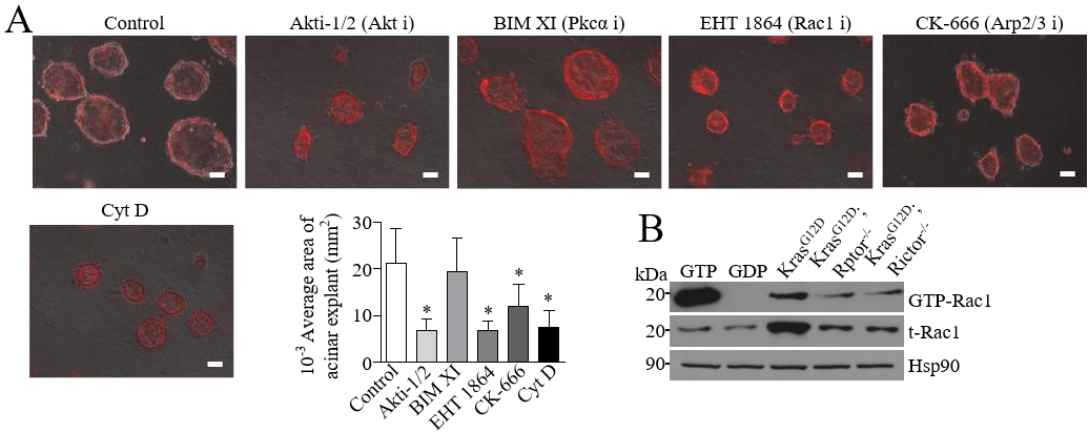

Figure 35. (**A**) Representative IF pictures show the capacity of ADM formation of acinar cells isolated from $Kras^{G12D}$ pancreas under the treatment of Pkcα (BIM XI), Akt (Akti-1/2), Rac1 (EHT1864), Arp2/3 (CK-666) and actin (Cyt D) inhibition; quantitative data shows the area of ADM lesions *in vitro* (low panel), n=3, *: <0.05, unpaired *t* test; (**B**) Rac1 pull-down assay shows Rac1 activation (GTP-Rac1) and expression 14 days after caerulein-induced pancreatitis in $Kras^{G12D}$, $Kras^{G12D}$; $Rptor^{-/-}$ and $Kras^{G12D}$; $Rictor^{-/-}$ pancreas; one out of three independent experiments is shown.

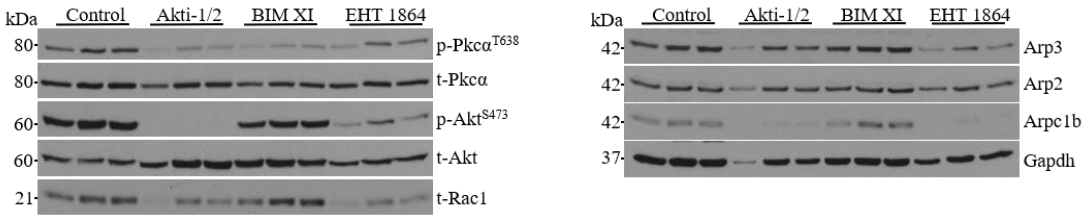

Figure 36. Western-blot analysis show the expression of p-Akt^{S473}, Rac1, Arp2, Arp3, Arpc1b in $Kras^{G12D}$-induced ADM cells treated with control (PBS), or Akt1/2 (Akti-1/2), or p-Pkcα (BIM XI) or Rac1 inhibitor (EHT 1864).

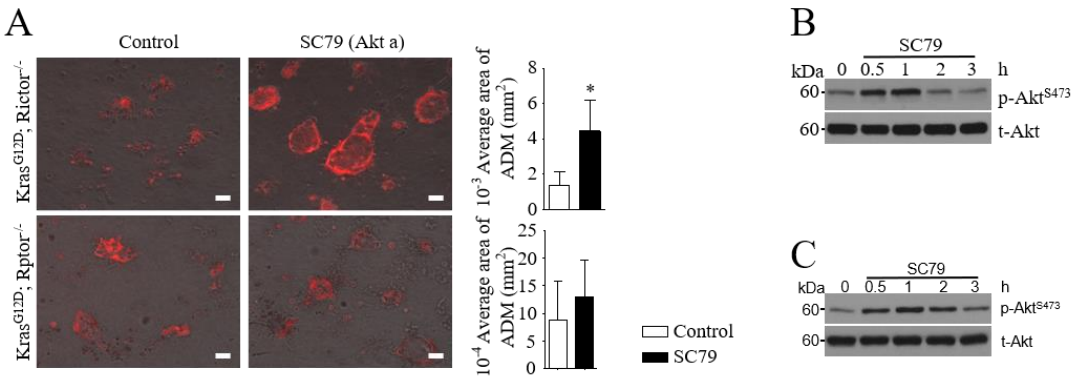

Figure 37. (**A**) Representative IF pictures show the capacity of ADM formation of acinar cells isolated from Kras^{G12D}; Rictor$^{-/-}$ and Kras^{G12D}; Rptor$^{-/-}$ pancreas under the treatment of control and Akt activator (SC79); quantitative data shows the area of ADM lesions *in vitro* (low panel), n=3, *: <0.05, unpaired *t* test; (**B**) Western-blot analysis shows the activation of Akt pathways (p-Akt^{S473}) in Kras^{G12D}; Rictor$^{-/-}$ acinar cells after the treatment of Akt acivator (SC79); (**C**) Western-blot analysis shows the activation of Akt pathways (p-Akt^{S473}) in Kras^{G12D}; Rptor$^{-/-}$ acinar cells after the treatment of Akt acivator (SC79).

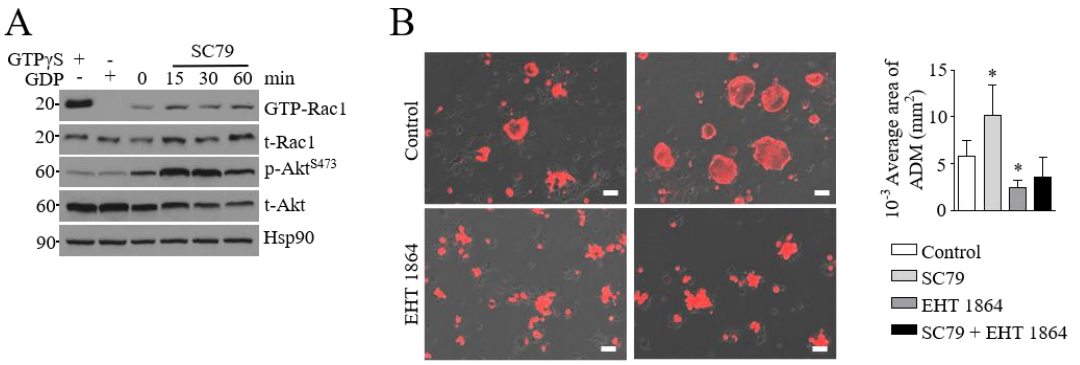

Figure 38. (A) Rac1 pull-down assay shows the active Rac1 (GTP-Rac1) in Kras^{G12D}; Rictor$^{-/-}$ acinar cells after the treatment of Akt acivator (SC79); (**B**) Representative IF pictures show the capacity of ADM formation of acinar cells isolated from Kras^{G12D}; Rictor$^{-/-}$ pancreata under the treatment of control, Akt activator (SC79), Rac1 inhibtor (EHT 1864) and both; quantitative data shows the area of ADM lesions *in vitro* (low panel), n=3, *: <0.05, unpaired *t* test.

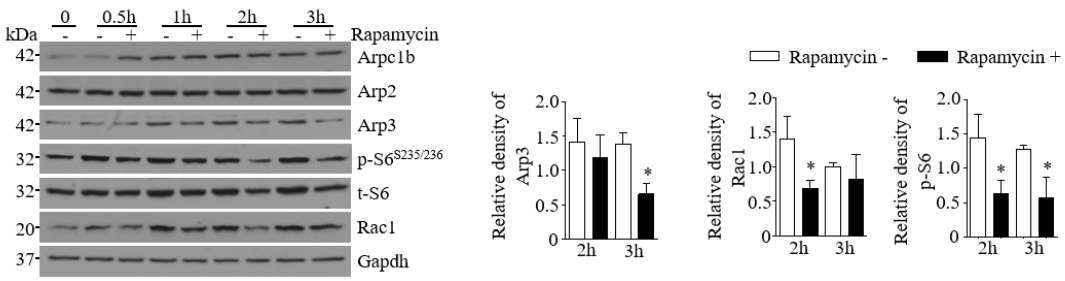

Figure 39. Western-blot analysis of block-and-release assay shows the expression of Arpc1b, Arp2, Arp3, Rac1, p-S6$^{S235/236}$ and S6 under the treatment of control or Rapamycin; one out of three independent experiments is shown, quantitative data shows the relative density of Arp3, Rac1 and p-S6$^{S234/236}$ at 2h and 3h timepoint, n=3, *: <0.05, unpaired *t*-test.

5. Discussion

In human PDAC, more than 80% of cases carry Kras mutation which persistently activates the downstream effectors to promote tumour growth, and metastasis.[170] mTOR signalling is a downstream pathway of MAPK pathway and vital for cell growth and survival. mTOR activation is widely implicated in tumorigenesis. The fatality of PDAC urges researchers to find a solution to make early diagnosis and treatment. In our previous study, mTOR signalling promotes PDAC development in the mouse model and is overexpressed in most human PDAC samples.[171] In this study, we observed that the activation of mTOR signaling is an early event associated with pancreatic carcinogenesis that is visible already in pre-neoplastic ADM lesions.

Previously, it has been published that the TGF-α treatment or the expression of oncogenic Kras promotes ADM formation at a conversion rate of around 75% without the pre-treatment of caerulein.[172-175] Here, we optimized the assay protocol by incubating the isolated pancreatic acinar cells in 2D culture medium with caerulein for 24 hours before seeding them in collagen gel. As such, the ADM formation at higher conversion rate (data is not shown) is observed in the absence of mutant Kras expression or TGF-α stimulation. It was verified by measuring the ADM markers via QRT-PCR assay. This optimized assay protocol enabled us to investigate the phenotypic difference between the physiological ADM lesions formed by wild-type acinar cells and the oncogenic ADM lesions by acinar cells with oncogenic $Kras^{G12D}$ expression. However, how caerulein promotes the ability of acinar cells to form ADM lesions *in vitro* is still elusive.

In this study, *in vivo* and *in vitro* data indicate that the mTOR signaling is implicated in the precursor lesion of PDAC. Hence, we used the transgenic mouse model to study the impact of mTORC1 and mTORC2 on the $Kras^{G12D}$-driven ADM formation. Given the

known important physiological function of mTORC1 and mTORC2 in pancreas (e.g. endocrine function[107, 108]), we did not use the conventional pancreas-specific Cre such as $p48^{Cre}$ to ablate Rptor and Rictor, respectively. Instead, we turned to an inducible mouse model. It was reported that the $Ptf1a^{CreER}$ allele specifically targets the acinar cell compartments and recombine the $Kras^{G12D}$ allele effectively.[15] In this study, RFP, as a reporter, is employed to monitor the $creER^{TM}$-mediated recombination efficiency. After the TAM induction, the pancreas of the reporter strain appears to be red. Based on the immunohistochemistry analysis of RFP, he recombination efficiency is as high as approximately 95%. Previously, it has been reported that the conventional creER-mediated recombination efficiency in the pancreatic acinar cell is as low as 10%.[15] The published experience showed that the $creER^{TM}$ construct is about 10-fold more sensitive to induction than the creER.[21] Moreover, in smooth muscle, the $creER^{TM}$-mediated recombination efficiency is up to 100% .[176] In this study, the $creER^{TM}$-mediated recombination efficiency is sufficient and stable, which is the experimental prerequisite to stably reproduce the presented results

In this study, we found that the inhibition of mTORC1 or mTORC2 signalling alone only partially block the $Kras^{G12D}$-driven ADM formation *in vivo*; however, the dual inhibition of mTORC1 and mTORC2 was required to persistently inhibit the ADM and PanIN formation. These findings are similar to the observations of mTOR inhibitor in clinical trials: rapalogs, as the first generation of mTOR inhibitor, is sensitive to mTORC1. The monotherapy with rapalogs failed in the majority of primary solid tumours due to the feedback activation of insulin/PI3K/Akt signaling when mTORC1 signalling is blocked for a long time.[177] Later on, the dual mTORC1/2 inhibitors were developed as targeted anticancer agents. The ATP-competitive mTOR kinase inhibitor, the second-generation inhibitor, blocks the activity of mTORC1 and mTORC2 entirely by inhibiting the catalytic activity of mTOR.[123] In preclinical research, the dual mTORC1/2 inhibitor was used in mouse model, and PDAC progression was significantly delayed.[156] The results of clinical trial testing the effectiveness of dual mTORC1/2 inhibitor are also promising.[178, 179] All these findings support that both

mTORC1 and mTORC2 signalling play an essential role in promoting oncogenic Kras-mediated PDAC onset and progression. .

Based on KEGG pathway enrichment analysis, we identified the regulation of actin cytoskeleton is the most correlated pathway in the oncogenic $Kras^{G12D}$-mediated ADM formation. This finding is consistent with the previous study.[54, 166] It is reported that the actin rearrangement is strongly associated with ADM formation. F-actin redistributes to the basolateral side from the apical, leading to the loss of cell polarity during the ADM formation. The inhibition of actin cytoskeleton results in an impaired ADM formation. In our study, we verified these findings in our 3D culture system. It is reported that the actin cytoskeleton remodeling is not only critical in the ADM formation, but also in the epithelial-mesenchymal transition (EMT) and cancer metastasis.[180] During EMT, the actin rearrangement support the dynamic cell elongation and provide the directional motility, contributing to a migratory phenotype of cancer cells.[181] In metastasis, cancer cell has a high plasticity to migrate from primary tumour site to distant tissue; the acquisition of migratory capacity dependents on the actin reorganization.

Cell morphology altered in the process of ADM formation, EMT and cancer metastasis. It is reported that of several cellular forces drive morphogenesis. The genetic screens uncover that the key driver underpinning morphogenesis is the actomyosin cytoskeleton, composed of actin and myosin. In the network, myosin can generate contractile force.[182] Hendrik A. and his colleagues found that the myosin activity was mainly apically located in pancreatic acinar cells, but upon transformation, it redistributes to the basolateral side and concentrates on both sides of duct-like cells.[166] In this study, we identified the same distribution of myosin activity in oncogenic $Kras^{G12D}$-mediated ADM lesions. Actin filaments can produce pushing (protrusive) forces on the leading edge of cells. Branched network-mediated protrusion (lamellipodia) generates more pushing forces than parallel bundles-mediated protrusion (filopodia), and function as a main cellular motor to move the cutting edge forward in cell migration.[183] In

lamellipodia, Arp2/3 complex, one regulator of the actin cytoskeleton, promote dendritic nucleation and generate the branched network. It creates a daughter filament on the side of mother filament at an angle of around 70°.[184, 185] In this way, being anchored on mother filament, daughter filament transmits the force of actin polymerization onto membrane much more effectively. Also, according to the calculation in a specific model, pushing force imposed at an angle to the membrane also promote protrusion much better.[183, 186] From previous study, we can conclude that Arp2/3 complex play an essential role in cell morphogenesis. In this study, we confirmed this view by finding that impaired Arp2/3 complex blocked oncogenic $Kras^{G12D}$-mediated ADM formation *in vivo* and *in vitro*.

In the KEGG pathway enrichment analysis, the expression of Rac1is also increased in in $Kras^{G12D}$ pancreata. RAC1 is widely involved in solid tumours; it promotes cancer cell proliferation, metastasis and drug-resistance.[187] Around three decades ago, it was found that Rac1 regulates the actin cytoskeleton organization in fibroblast.[188] In gastric adenocarcinoma, Rac1 inhibition block the EMT process and the acquisition of stem-like cells phenotype.[189] In colorectal cancer, mTORC1 and mTORC2 promote EMT, motility and metastasis via Rac1 signalling.[190] Moreover, in breast cancer, mTORC2 activates Akt and PKC pathways, both of which converge on the Rac1 to promote cell invasion and motility.[168] Besides, in our study, Rac1 activity is upregulated in $Kras^{G12D}$ pancreata after caerulein treatment. It was reported that Rac1 promotes the $Kras^{G12D}$-mediated ADM formation by regulating actin cytoskeleton,[54] however, the mechanism underlying the Rac1-mediated actin rearrangement was not well addressed.

Nevertheless, the downstream of Rac1 is well studied in lamellipodia, which provides the dominant force in cell motility as we discussed above. It was found that activated Rac1 directly recruits the WAVE complex at the plasma membrane, and subsequently activates Arp2/3 complex, which mediates the branched actin network.[191] In the KEGG pathway enrichment analysis, both of Rac1 and Arp2/3 complex are increased in Kras-mediated ADM formation, imply the critical role of Rac1-WAVE-Arp2/3-mediated cytoskeleton reorganization in this particular scenario. Another alternative mechanism

for Rac1-mediated actin rearrangement is by activating PAK (p21-activated kinase). PAK1 is a known regulator of actin dynamics and cell motility.[192] Since PAK1 is not appeared in our proteomic analysis , the Rac1-PAK-mediated actin polymerization may not be involved in the $Kras^{G12D}$-mediated ADM formation.

In this study, we provided descriptive and functional evidence delineating a crucial role of Arp2/3 complex in oncogenic $Kras^{G12D}$-mediated ADM formation. Through a non-redundant regulatory system, the function of the Arp2/3 complex is controlled by oncogenic mTORC1 and mTORC2. In particular, the Arp2/3 complex-mediated actin polymerization is responsible for generating apical-basal tension redistribution, it acts as an "incipient" instruction cue for inducing ductal morphology of acinar cells.

Previously, we demonstrated an oncogenic property of mTORC1 signalling in established PDAC. As such, the $Kras^{G12D}$/Mek-mediated mTORC1 signalling promotes a highly metastatic subtype of PDAC.[153] Further analysis uncovered that the oncogenic activity of $Kras^{G12D}$/Mek-mediated mTORC1 signalling partially relied on Aldh1a3 (aldehyde dehydrogenase 1 family member A3) function. Here, we demonstrated that the oncogenic activity of mTORC1 in early carcinogenesis rather depended on its regulatory function on Rac1 and Arp2/3 complex in polymerizing actin cytoskeleton. Thus, the oncogenic Kras-mediated mTORC1 signalling is per se oncogenic; however, it may use distinct downstream effector to promote tumour progression depending on the specific stage of PDAC development. Compared to mTORC1 signalling, the function of mTORC2 signalling is less pleiotropic. Previously, Driscoll and co-workers reported that deactivation of mTORC2 signalling by Rictor deletion specifically impaired PanIN progression to invasive carcinoma in a well-defined mouse model of PDAC.[156] It is observed that mTORC2 deactivation led to an elevation of multiple CDK (Cyclin-dependent kinase) inhibitors such as $p16^{Ink4a}$ and $p21^{Cip1}$ in PanIN lesions, thereby, blunted PanIN progression. However, it remains elusive how mTORC2 signalling would affect the function of CDK inhibitors. Alternatively, we provided evidence that the oncogenic activity of mTORC2 signalling could also be attributed to

its classic role in regulating actin cytoskeleton via Akt/Rac1 signal axis. However, this oncogenic function of mTORC2 signalling is particularly crucial for oncogenic Kras-driven ADM formation rather than PanIN progression. Collectively, these data argue for a context-dependent role of oncogenic mTORC1 and mTORC2 signalling in a different stage of PDAC development.

The Arp2/3 complex is the first identified actin nucleator whose function is unique that it binds to the sides of existing actin filament and promotes novel actin polymerization to form branching filament network, leading to so-called y-branching.[193, 194] Notably, this y-branching of filament network by Arp2/3 complex is ideally suited for generating mechanical tension required in a variety of biological circumstances such as lamellipodia formation.[165] Thus, it is conceivable that this tension-generating property of y-branching filament is responsible for creating the apico-basal tension redistribution in the process of oncogenic ADM formation. For the first time, we demonstrated that the Arp2/3 complex is the converging point of two major oncogenic pathways of PDAC: mTORC1 and mTORC2. Thus, targeting of the Arp2/3 complex may circumvent the feedback responses elicited by direct mTOR inhibition.[153, 195] The effectiveness of such therapies should be tested in a translational setting. Certainly, the function of the Arp2/3 complex in established PDAC needs to be further addressed.

6. Summary

Previously, we and others have provided genetic evidence defining the oncogenic function of both mTORC1 and mTORC2 in PDAC. Now, we observed that mTORC1 and mTORC2 were particularly activated in pre-neoplastic ADM lesions. The deactivation of mTORC1 or mTORC2 activity compromised oncogenic $Kras^{G12D}$-induced ADM development. The proteomic analyses identified the Arp2/3 complex, as the common downstream effector of mTORC1 and mTORC2 signalling. The Arp2/3 complex is the first identified actin nucleator consisting of seven proteins: Arp2, Arp3 and Arpc1-Arpc5. In the ADM development, it mediates y-branching of actin filament responsible for generating apical-basal tension redistribution. Mechanistically, mTORC1 is responsible for the direct protein synthesis of Rac1 and Arp3 while mTORC2 promotes the activity of Arp2/3 complex by Akt/Rac1 signal axis. Finally, deactivation of Arp2/3 complex by pancreas-specific Arpc4 ablation completely blocks oncogenic $Kras^{G12D}$-induced ADM formation. Thus, we defined a dual, yet non-redundant, regulatory function of mTORC1 and mTORC2 on Arp2/3 complex in promoting ADM formation.

7. References

1. Siegel R, Ma J, Zou Z, et al. Cancer statistics, 2014. CA Cancer J Clin 2014;64:9-29.
2. Kamisawa T, Wood LD, Itoi T, et al. Pancreatic cancer. Lancet 2016;388:73-85.
3. Gillen S, Schuster T, Meyer Zum Buschenfelde C, et al. Preoperative/neoadjuvant therapy in pancreatic cancer: a systematic review and meta-analysis of response and resection percentages. PLoS Med 2010;7:e1000267.
4. Spanknebel K, Conlon KC. Advances in the surgical management of pancreatic cancer. Cancer J 2001;7:312-23.
5. Rahib L, Smith BD, Aizenberg R, et al. Projecting cancer incidence and deaths to 2030: the unexpected burden of thyroid, liver, and pancreas cancers in the United States. Cancer Res 2014;74:2913-21.
6. Luttges J. [What's new? The 2010 WHO classification for tumours of the pancreas]. Pathologe 2011;32 Suppl 2:332-6.
7. Wood LD, Hruban RH. Pathology and molecular genetics of pancreatic neoplasms. Cancer J 2012;18:492-501.
8. Le N, Sund M, Vinci A. Prognostic and predictive markers in pancreatic adenocarcinoma. Dig Liver Dis 2016;48:223-30.
9. Perkhofer L, Ettrich TJ, Seufferlein T. Pancreatic Cancer: Progress in Systemic Therapy. Gastrointest Tumors 2014;1:167-79.
10. Smit VT, Boot AJ, Smits AM, et al. KRAS codon 12 mutations occur very frequently in pancreatic adenocarcinomas. Nucleic Acids Res 1988;16:7773-82.
11. Almoguera C, Shibata D, Forrester K, et al. Most human carcinomas of the exocrine pancreas contain mutant c-K-ras genes. Cell 1988;53:549-54.
12. Noe M, Brosens LA. Pathology of Pancreatic Cancer Precursor Lesions. Surg Pathol Clin 2016;9:561-580.
13. Pin CL, Ryan JF, Mehmood R. Acinar cell reprogramming: a clinically important target in pancreatic disease. Epigenomics 2015;7:267-81.
14. Yamaguchi J, Yokoyama Y, Kokuryo T, et al. Cells of origin of pancreatic neoplasms. Surg Today 2018;48:9-17.
15. Kopp JL, von Figura G, Mayes E, et al. Identification of Sox9-dependent acinar-to-ductal reprogramming as the principal mechanism for initiation of pancreatic ductal adenocarcinoma. Cancer Cell 2012;22:737-50.
16. Gidekel Friedlander SY, Chu GC, Snyder EL, et al. Context-dependent transformation of adult pancreatic cells by oncogenic K-Ras. Cancer Cell 2009;16:379-89.
17. Hingorani SR, Wang L, Multani AS, et al. Trp53R172H and KrasG12D cooperate to promote chromosomal instability and widely metastatic pancreatic

ductal adenocarcinoma in mice. Cancer Cell 2005;7:469-83.
18. Lee JW, Komar CA, Bengsch F, et al. Genetically Engineered Mouse Models of Pancreatic Cancer: The KPC Model (LSL-Kras(G12D/+) ;LSL-Trp53(R172H/+) ;Pdx-1-Cre), Its Variants, and Their Application in Immuno-oncology Drug Discovery. Curr Protoc Pharmacol 2016;73:14.39.1-14.39.20.
19. Feil R, Brocard J, Mascrez B, et al. Ligand-activated site-specific recombination in mice. Proc Natl Acad Sci U S A 1996;93:10887-90.
20. Feil S, Valtcheva N, Feil R. Inducible Cre mice. Methods Mol Biol 2009;530:343-63.
21. Indra AK, Warot X, Brocard J, et al. Temporally-controlled site-specific mutagenesis in the basal layer of the epidermis: comparison of the recombinase activity of the tamoxifen-inducible Cre-ER(T) and Cre-ER(T2) recombinases. Nucleic Acids Res 1999;27:4324-7.
22. Kuhbandner S, Brummer S, Metzger D, et al. Temporally controlled somatic mutagenesis in smooth muscle. Genesis 2000;28:15-22.
23. Kopinke D, Brailsford M, Pan FC, et al. Ongoing Notch signaling maintains phenotypic fidelity in the adult exocrine pancreas. Dev Biol 2012;362:57-64.
24. Desai BM, Oliver-Krasinski J, De Leon DD, et al. Preexisting pancreatic acinar cells contribute to acinar cell, but not islet beta cell, regeneration. J Clin Invest 2007;117:971-7.
25. De La OJ, Emerson LL, Goodman JL, et al. Notch and Kras reprogram pancreatic acinar cells to ductal intraepithelial neoplasia. Proc Natl Acad Sci U S A 2008;105:18907-12.
26. Bouabe H, Okkenhaug K. Gene targeting in mice: a review. Methods Mol Biol 2013;1064:315-36.
27. Pan FC, Bankaitis ED, Boyer D, et al. Spatiotemporal patterns of multipotentiality in Ptf1a-expressing cells during pancreas organogenesis and injury-induced facultative restoration. Development 2013;140:751-64.
28. Rooman I, Real FX. Pancreatic ductal adenocarcinoma and acinar cells: a matter of differentiation and development? Gut 2012;61:449-58.
29. Baer R, Cintas C, Dufresne M, et al. Pancreatic cell plasticity and cancer initiation induced by oncogenic Kras is completely dependent on wild-type PI 3-kinase p110alpha. Genes Dev 2014;28:2621-35.
30. Shi G, DiRenzo D, Qu C, et al. Maintenance of acinar cell organization is critical to preventing Kras-induced acinar-ductal metaplasia. Oncogene 2013;32:1950-8.
31. Means AL, Meszoely IM, Suzuki K, et al. Pancreatic epithelial plasticity mediated by acinar cell transdifferentiation and generation of nestin-positive intermediates. Development 2005;132:3767-76.
32. Liu J, Akanuma N, Liu C, et al. TGF-beta1 promotes acinar to ductal metaplasia of human pancreatic acinar cells. Sci Rep 2016;6:30904.
33. Krah NM, De La OJ, Swift GH, et al. The acinar differentiation determinant PTF1A inhibits initiation of pancreatic ductal adenocarcinoma. Elife 2015;4.
34. Martinelli P, Madriles F, Canamero M, et al. The acinar regulator Gata6

suppresses KrasG12V-driven pancreatic tumorigenesis in mice. Gut 2016;65:476-86.
35. Zhu L, Tran T, Rukstalis JM, et al. Inhibition of Mist1 homodimer formation induces pancreatic acinar-to-ductal metaplasia. Mol Cell Biol 2004;24:2673-81.
36. Hendley AM, Provost E, Bailey JM, et al. p120 Catenin is required for normal tubulogenesis but not epithelial integrity in developing mouse pancreas. Dev Biol 2015;399:41-53.
37. Kopp JL, Dubois CL, Schaffer AE, et al. Sox9+ ductal cells are multipotent progenitors throughout development but do not produce new endocrine cells in the normal or injured adult pancreas. Development 2011;138:653-65.
38. Furuyama K, Kawaguchi Y, Akiyama H, et al. Continuous cell supply from a Sox9-expressing progenitor zone in adult liver, exocrine pancreas and intestine. Nat Genet 2011;43:34-41.
39. Prevot PP, Simion A, Grimont A, et al. Role of the ductal transcription factors HNF6 and Sox9 in pancreatic acinar-to-ductal metaplasia. Gut 2012;61:1723-32.
40. Park JY, Hong SM, Klimstra DS, et al. Pdx1 expression in pancreatic precursor lesions and neoplasms. Appl Immunohistochem Mol Morphol 2011;19:444-9.
41. Rose SD, Swift GH, Peyton MJ, et al. The role of PTF1-P48 in pancreatic acinar gene expression. J Biol Chem 2001;276:44018-26.
42. Miyatsuka T, Kaneto H, Shiraiwa T, et al. Persistent expression of PDX-1 in the pancreas causes acinar-to-ductal metaplasia through Stat3 activation. Genes Dev 2006;20:1435-40.
43. Liou GY, Doppler H, Necela B, et al. Macrophage-secreted cytokines drive pancreatic acinar-to-ductal metaplasia through NF-kappaB and MMPs. J Cell Biol 2013;202:563-77.
44. Murtaugh LC, Keefe MD. Regeneration and repair of the exocrine pancreas. Annu Rev Physiol 2015;77:229-49.
45. Greer RL, Staley BK, Liou A, et al. Numb regulates acinar cell dedifferentiation and survival during pancreatic damage and acinar-to-ductal metaplasia. Gastroenterology 2013;145:1088-1097.e8.
46. Zhou Q, Melton DA. Pancreas regeneration. Nature 2018;557:351-358.
47. Hidalgo-Sastre A, Brodylo RL, Lubeseder-Martellato C, et al. Hes1 Controls Exocrine Cell Plasticity and Restricts Development of Pancreatic Ductal Adenocarcinoma in a Mouse Model. The American journal of pathology 2016;186:2934-2944.
48. Wang W, Friedland SC, Guo B, et al. ARID1A, a SWI/SNF subunit, is critical to acinar cell homeostasis and regeneration and is a barrier to transformation and epithelial-mesenchymal transition in the pancreas. Gut 2019;68:1245-1258.
49. Fendrich V, Esni F, Garay MV, et al. Hedgehog signaling is required for effective regeneration of exocrine pancreas. Gastroenterology 2008;135:621-31.
50. Dhillon AS, Hagan S, Rath O, et al. MAP kinase signalling pathways in cancer. Oncogene 2007;26:3279-90.
51. Collins MA, Yan W, Sebolt-Leopold JS, et al. MAPK signaling is required for

dedifferentiation of acinar cells and development of pancreatic intraepithelial neoplasia in mice. Gastroenterology 2014;146:822-834.e7.
52. Payne SN, Maher ME, Tran NH, et al. PIK3CA mutations can initiate pancreatic tumorigenesis and are targetable with PI3K inhibitors. Oncogenesis 2015;4:e169.
53. Elghazi L, Weiss AJ, Barker DJ, et al. Regulation of pancreas plasticity and malignant transformation by Akt signaling. Gastroenterology 2009;136:1091-103.
54. Heid I, Lubeseder-Martellato C, Sipos B, et al. Early requirement of Rac1 in a mouse model of pancreatic cancer. Gastroenterology 2011;141:719-30, 730 e1-7.
55. Liou GY, Doppler H, DelGiorno KE, et al. Mutant KRas-Induced Mitochondrial Oxidative Stress in Acinar Cells Upregulates EGFR Signaling to Drive Formation of Pancreatic Precancerous Lesions. Cell Rep 2016;14:2325-36.
56. Liou GY, Doppler H, Braun UB, et al. Protein kinase D1 drives pancreatic acinar cell reprogramming and progression to intraepithelial neoplasia. Nat Commun 2015;6:6200.
57. Sawey ET, Johnson JA, Crawford HC. Matrix metalloproteinase 7 controls pancreatic acinar cell transdifferentiation by activating the Notch signaling pathway. Proc Natl Acad Sci U S A 2007;104:19327-32.
58. Morton JP, Timpson P, Karim SA, et al. Mutant p53 drives metastasis and overcomes growth arrest/senescence in pancreatic cancer. Proc Natl Acad Sci U S A 2010;107:246-51.
59. Bardeesy N, Aguirre AJ, Chu GC, et al. Both p16(Ink4a) and the p19(Arf)-p53 pathway constrain progression of pancreatic adenocarcinoma in the mouse. Proc Natl Acad Sci U S A 2006;103:5947-52.
60. Kojima K, Vickers SM, Adsay NV, et al. Inactivation of Smad4 accelerates Kras(G12D)-mediated pancreatic neoplasia. Cancer Res 2007;67:8121-30.
61. Lerch MM, Gorelick FS. Models of acute and chronic pancreatitis. Gastroenterology 2013;144:1180-93.
62. Siveke JT, Lubeseder-Martellato C, Lee M, et al. Notch signaling is required for exocrine regeneration after acute pancreatitis. Gastroenterology 2008;134:544-55.
63. Jensen JN, Cameron E, Garay MV, et al. Recapitulation of elements of embryonic development in adult mouse pancreatic regeneration. Gastroenterology 2005;128:728-41.
64. Morris JPt, Cano DA, Sekine S, et al. Beta-catenin blocks Kras-dependent reprogramming of acini into pancreatic cancer precursor lesions in mice. J Clin Invest 2010;120:508-20.
65. Kim DH, Sarbassov DD, Ali SM, et al. mTOR interacts with raptor to form a nutrient-sensitive complex that signals to the cell growth machinery. Cell 2002;110:163-75.
66. Kim DH, Sarbassov DD, Ali SM, et al. GbetaL, a positive regulator of the rapamycin-sensitive pathway required for the nutrient-sensitive interaction

between raptor and mTOR. Mol Cell 2003;11:895-904.
67. Sancak Y, Thoreen CC, Peterson TR, et al. PRAS40 is an insulin-regulated inhibitor of the mTORC1 protein kinase. Mol Cell 2007;25:903-15.
68. Vander Haar E, Lee SI, Bandhakavi S, et al. Insulin signalling to mTOR mediated by the Akt/PKB substrate PRAS40. Nat Cell Biol 2007;9:316-23.
69. Peterson TR, Laplante M, Thoreen CC, et al. DEPTOR is an mTOR inhibitor frequently overexpressed in multiple myeloma cells and required for their survival. Cell 2009;137:873-86.
70. Nojima H, Tokunaga C, Eguchi S, et al. The mammalian target of rapamycin (mTOR) partner, raptor, binds the mTOR substrates p70 S6 kinase and 4E-BP1 through their TOR signaling (TOS) motif. J Biol Chem 2003;278:15461-4.
71. Schalm SS, Fingar DC, Sabatini DM, et al. TOS motif-mediated raptor binding regulates 4E-BP1 multisite phosphorylation and function. Curr Biol 2003;13:797-806.
72. Yang H, Rudge DG, Koos JD, et al. mTOR kinase structure, mechanism and regulation. Nature 2013;497:217-23.
73. Long X, Lin Y, Ortiz-Vega S, et al. Rheb binds and regulates the mTOR kinase. Curr Biol 2005;15:702-13.
74. Huang J, Manning BD. The TSC1-TSC2 complex: a molecular switchboard controlling cell growth. Biochem J 2008;412:179-90.
75. Xie J, Proud CG. Signaling crosstalk between the mTOR complexes. Translation (Austin) 2014;2:e28174.
76. Gwinn DM, Shackelford DB, Egan DF, et al. AMPK phosphorylation of raptor mediates a metabolic checkpoint. Mol Cell 2008;30:214-26.
77. Brugarolas J, Lei K, Hurley RL, et al. Regulation of mTOR function in response to hypoxia by REDD1 and the TSC1/TSC2 tumor suppressor complex. Genes Dev 2004;18:2893-904.
78. Feng Z, Hu W, de Stanchina E, et al. The regulation of AMPK beta1, TSC2, and PTEN expression by p53: stress, cell and tissue specificity, and the role of these gene products in modulating the IGF-1-AKT-mTOR pathways. Cancer Res 2007;67:3043-53.
79. Kim E, Goraksha-Hicks P, Li L, et al. Regulation of TORC1 by Rag GTPases in nutrient response. Nat Cell Biol 2008;10:935-45.
80. Sancak Y, Peterson TR, Shaul YD, et al. The Rag GTPases bind raptor and mediate amino acid signaling to mTORC1. Science 2008;320:1496-501.
81. Holz MK, Ballif BA, Gygi SP, et al. mTOR and S6K1 mediate assembly of the translation preinitiation complex through dynamic protein interchange and ordered phosphorylation events. Cell 2005;123:569-80.
82. Dorrello NV, Peschiaroli A, Guardavaccaro D, et al. S6K1- and betaTRCP-mediated degradation of PDCD4 promotes protein translation and cell growth. Science 2006;314:467-71.
83. Pende M, Um SH, Mieulet V, et al. S6K1(-/-)/S6K2(-/-) mice exhibit perinatal lethality and rapamycin-sensitive 5'-terminal oligopyrimidine mRNA translation and reveal a mitogen-activated protein kinase-dependent S6 kinase

pathway. Mol Cell Biol 2004;24:3112-24.
84. Gingras AC, Gygi SP, Raught B, et al. Regulation of 4E-BP1 phosphorylation: a novel two-step mechanism. Genes Dev 1999;13:1422-37.
85. Porstmann T, Santos CR, Griffiths B, et al. SREBP activity is regulated by mTORC1 and contributes to Akt-dependent cell growth. Cell Metab 2008;8:224-36.
86. Ben-Sahra I, Howell JJ, Asara JM, et al. Stimulation of de novo pyrimidine synthesis by growth signaling through mTOR and S6K1. Science 2013;339:1323-8.
87. Duvel K, Yecies JL, Menon S, et al. Activation of a metabolic gene regulatory network downstream of mTOR complex 1. Mol Cell 2010;39:171-83.
88. Kim J, Kundu M, Viollet B, et al. AMPK and mTOR regulate autophagy through direct phosphorylation of Ulk1. Nat Cell Biol 2011;13:132-41.
89. Roczniak-Ferguson A, Petit CS, Froehlich F, et al. The transcription factor TFEB links mTORC1 signaling to transcriptional control of lysosome homeostasis. Sci Signal 2012;5:ra42.
90. Settembre C, Zoncu R, Medina DL, et al. A lysosome-to-nucleus signalling mechanism senses and regulates the lysosome via mTOR and TFEB. Embo j 2012;31:1095-108.
91. Guertin DA, Stevens DM, Thoreen CC, et al. Ablation in mice of the mTORC components raptor, rictor, or mLST8 reveals that mTORC2 is required for signaling to Akt-FOXO and PKCalpha, but not S6K1. Dev Cell 2006;11:859-71.
92. Lamming DW, Mihaylova MM, Katajisto P, et al. Depletion of Rictor, an essential protein component of mTORC2, decreases male lifespan. Aging Cell 2014;13:911-7.
93. Frias MA, Thoreen CC, Jaffe JD, et al. mSin1 is necessary for Akt/PKB phosphorylation, and its isoforms define three distinct mTORC2s. Curr Biol 2006;16:1865-70.
94. Pearce LR, Huang X, Boudeau J, et al. Identification of Protor as a novel Rictor-binding component of mTOR complex-2. Biochem J 2007;405:513-22.
95. Liu P, Gan W, Chin YR, et al. PtdIns(3,4,5)P3-Dependent Activation of the mTORC2 Kinase Complex. Cancer Discov 2015;5:1194-209.
96. Zinzalla V, Stracka D, Oppliger W, et al. Activation of mTORC2 by association with the ribosome. Cell 2011;144:757-68.
97. Yang G, Murashige DS, Humphrey SJ, et al. A Positive Feedback Loop between Akt and mTORC2 via SIN1 Phosphorylation. Cell Rep 2015;12:937-43.
98. Jacinto E, Loewith R, Schmidt A, et al. Mammalian TOR complex 2 controls the actin cytoskeleton and is rapamycin insensitive. Nat Cell Biol 2004;6:1122-8.
99. Li X, Gao T. mTORC2 phosphorylates protein kinase Czeta to regulate its stability and activity. EMBO Rep 2014;15:191-8.
100. Gan X, Wang J, Wang C, et al. PRR5L degradation promotes mTORC2-mediated PKC-delta phosphorylation and cell migration downstream of

Galpha12. Nat Cell Biol 2012;14:686-96.
101. Thomanetz V, Angliker N, Cloetta D, et al. Ablation of the mTORC2 component rictor in brain or Purkinje cells affects size and neuron morphology. J Cell Biol 2013;201:293-308.
102. Sarbassov DD, Guertin DA, Ali SM, et al. Phosphorylation and regulation of Akt/PKB by the rictor-mTOR complex. Science 2005;307:1098-101.
103. Jacinto E, Facchinetti V, Liu D, et al. SIN1/MIP1 maintains rictor-mTOR complex integrity and regulates Akt phosphorylation and substrate specificity. Cell 2006;127:125-37.
104. Garcia-Martinez JM, Alessi DR. mTOR complex 2 (mTORC2) controls hydrophobic motif phosphorylation and activation of serum- and glucocorticoid-induced protein kinase 1 (SGK1). Biochem J 2008;416:375-85.
105. Efeyan A, Zoncu R, Chang S, et al. Regulation of mTORC1 by the Rag GTPases is necessary for neonatal autophagy and survival. Nature 2013;493:679-83.
106. Kuma A, Hatano M, Matsui M, et al. The role of autophagy during the early neonatal starvation period. Nature 2004;432:1032-6.
107. Mori H, Inoki K, Opland D, et al. Critical roles for the TSC-mTOR pathway in beta-cell function. Am J Physiol Endocrinol Metab 2009;297:E1013-22.
108. Shigeyama Y, Kobayashi T, Kido Y, et al. Biphasic response of pancreatic beta-cell mass to ablation of tuberous sclerosis complex 2 in mice. Mol Cell Biol 2008;28:2971-9.
109. Bodine SC, Stitt TN, Gonzalez M, et al. Akt/mTOR pathway is a crucial regulator of skeletal muscle hypertrophy and can prevent muscle atrophy in vivo. Nat Cell Biol 2001;3:1014-9.
110. Bentzinger CF, Romanino K, Cloetta D, et al. Skeletal muscle-specific ablation of raptor, but not of rictor, causes metabolic changes and results in muscle dystrophy. Cell Metab 2008;8:411-24.
111. Lee PL, Tang Y, Li H, et al. Raptor/mTORC1 loss in adipocytes causes progressive lipodystrophy and fatty liver disease. Mol Metab 2016;5:422-432.
112. Hagiwara A, Cornu M, Cybulski N, et al. Hepatic mTORC2 activates glycolysis and lipogenesis through Akt, glucokinase, and SREBP1c. Cell Metab 2012;15:725-38.
113. Zheng Y, Collins SL, Lutz MA, et al. A role for mammalian target of rapamycin in regulating T cell activation versus anergy. J Immunol 2007;178:2163-70.
114. Araki K, Turner AP, Shaffer VO, et al. mTOR regulates memory CD8 T-cell differentiation. Nature 2009;460:108-12.
115. Haxhinasto S, Mathis D, Benoist C. The AKT-mTOR axis regulates de novo differentiation of CD4+Foxp3+ cells. J Exp Med 2008;205:565-74.
116. Lipton JO, Sahin M. The neurology of mTOR. Neuron 2014;84:275-91.
117. Crunkhorn S. mTOR inhibition curbs colorectal cancer. Nature Reviews Drug Discovery 2015;14:15-15.
118. Guerrero-Zotano A, Mayer IA, Arteaga CL. PI3K/AKT/mTOR: role in breast cancer progression, drug resistance, and treatment. Cancer Metastasis Rev 2016;35:515-524.

119. Tan FH, Bai Y, Saintigny P, et al. mTOR Signalling in Head and Neck Cancer: Heads Up. Cells 2019;8.
120. Chen H, Zhou L, Wu X, et al. The PI3K/AKT pathway in the pathogenesis of prostate cancer. Front Biosci (Landmark Ed) 2016;21:1084-91.
121. Mann KM, Ying H, Juan J, et al. KRAS-related proteins in pancreatic cancer. Pharmacol Ther 2016;168:29-42.
122. Faller WJ, Jackson TJ, Knight JR, et al. mTORC1-mediated translational elongation limits intestinal tumour initiation and growth. Nature 2015;517:497-500.
123. Saxton RA, Sabatini DM. mTOR Signaling in Growth, Metabolism, and Disease. Cell 2017;169:361-371.
124. Agarwal S, Bell CM, Taylor SM, et al. p53 Deletion or Hotspot Mutations Enhance mTORC1 Activity by Altering Lysosomal Dynamics of TSC2 and Rheb. Mol Cancer Res 2016;14:66-77.
125. Grabiner BC, Nardi V, Birsoy K, et al. A diverse array of cancer-associated MTOR mutations are hyperactivating and can predict rapamycin sensitivity. Cancer Discov 2014;4:554-63.
126. Guertin DA, Stevens DM, Saitoh M, et al. mTOR complex 2 is required for the development of prostate cancer induced by Pten loss in mice. Cancer Cell 2009;15:148-59.
127. Werfel TA, Wang S, Jackson MA, et al. Selective mTORC2 Inhibitor Therapeutically Blocks Breast Cancer Cell Growth and Survival. Cancer Res 2018;78:1845-1858.
128. Schmidt KM, Hellerbrand C, Ruemmele P, et al. Inhibition of mTORC2 component RICTOR impairs tumor growth in pancreatic cancer models. Oncotarget 2017;8:24491-24505.
129. Sabatini DM, Erdjument-Bromage H, Lui M, et al. RAFT1: a mammalian protein that binds to FKBP12 in a rapamycin-dependent fashion and is homologous to yeast TORs. Cell 1994;78:35-43.
130. Lamming DW, Ye L, Katajisto P, et al. Rapamycin-induced insulin resistance is mediated by mTORC2 loss and uncoupled from longevity. Science 2012;335:1638-43.
131. Ohtsu A, Ajani JA, Bai YX, et al. Everolimus for previously treated advanced gastric cancer: results of the randomized, double-blind, phase III GRANITE-1 study. J Clin Oncol 2013;31:3935-43.
132. Zhu AX, Kudo M, Assenat E, et al. Effect of everolimus on survival in advanced hepatocellular carcinoma after failure of sorafenib: the EVOLVE-1 randomized clinical trial. Jama 2014;312:57-67.
133. Fenner M, Oing C, Dieing A, et al. Everolimus in patients with multiply relapsed or cisplatin refractory germ cell tumors: results of a phase II, single-arm, open-label multicenter trial (RADIT) of the German Testicular Cancer Study Group. J Cancer Res Clin Oncol 2019;145:717-723.
134. Geiger JL, Bauman JE, Gibson MK, et al. Phase II trial of everolimus in patients with previously treated recurrent or metastatic head and neck squamous cell

carcinoma. Head Neck 2016;38:1759-1764.
135. Javle MM, Shroff RT, Xiong H, et al. Inhibition of the mammalian target of rapamycin (mTOR) in advanced pancreatic cancer: results of two phase II studies. BMC Cancer 2010;10:368.
136. Tabernero J, Rojo F, Calvo E, et al. Dose- and schedule-dependent inhibition of the mammalian target of rapamycin pathway with everolimus: a phase I tumor pharmacodynamic study in patients with advanced solid tumors. J Clin Oncol 2008;26:1603-10.
137. Kang SA, Pacold ME, Cervantes CL, et al. mTORC1 phosphorylation sites encode their sensitivity to starvation and rapamycin. Science 2013;341:1236566.
138. Thoreen CC, Kang SA, Chang JW, et al. An ATP-competitive mammalian target of rapamycin inhibitor reveals rapamycin-resistant functions of mTORC1. J Biol Chem 2009;284:8023-32.
139. Palm W, Park Y, Wright K, et al. The Utilization of Extracellular Proteins as Nutrients Is Suppressed by mTORC1. Cell 2015;162:259-270.
140. Rangwala R, Chang YC, Hu J, et al. Combined MTOR and autophagy inhibition: phase I trial of hydroxychloroquine and temsirolimus in patients with advanced solid tumors and melanoma. Autophagy 2014;10:1391-402.
141. Rodrik-Outmezguine VS, Chandarlapaty S, Pagano NC, et al. mTOR kinase inhibition causes feedback-dependent biphasic regulation of AKT signaling. Cancer Discov 2011;1:248-59.
142. Abella JV, Galloni C, Pernier J, et al. Isoform diversity in the Arp2/3 complex determines actin filament dynamics. Nat Cell Biol 2016;18:76-86.
143. Nolen BJ, Pollard TD. Insights into the influence of nucleotides on actin family proteins from seven structures of Arp2/3 complex. Mol Cell 2007;26:449-57.
144. Rouiller I, Xu XP, Amann KJ, et al. The structural basis of actin filament branching by the Arp2/3 complex. J Cell Biol 2008;180:887-95.
145. Goley ED, Rodenbusch SE, Martin AC, et al. Critical conformational changes in the Arp2/3 complex are induced by nucleotide and nucleation promoting factor. Mol Cell 2004;16:269-79.
146. Rodal AA, Sokolova O, Robins DB, et al. Conformational changes in the Arp2/3 complex leading to actin nucleation. Nat Struct Mol Biol 2005;12:26-31.
147. LeClaire LL, 3rd, Baumgartner M, Iwasa JH, et al. Phosphorylation of the Arp2/3 complex is necessary to nucleate actin filaments. J Cell Biol 2008;182:647-54.
148. Laurila E, Savinainen K, Kuuselo R, et al. Characterization of the 7q21-q22 amplicon identifies ARPC1A, a subunit of the Arp2/3 complex, as a regulator of cell migration and invasion in pancreatic cancer. Genes Chromosomes Cancer 2009;48:330-9.
149. Rauhala HE, Teppo S, Niemela S, et al. Silencing of the ARP2/3 complex disturbs pancreatic cancer cell migration. Anticancer Res 2013;33:45-52.
150. Iwaya K, Oikawa K, Semba S, et al. Correlation between liver metastasis of the colocalization of actin-related protein 2 and 3 complex and WAVE2 in colorectal carcinoma. Cancer Sci 2007;98:992-9.

151. Semba S, Iwaya K, Matsubayashi J, et al. Coexpression of actin-related protein 2 and Wiskott-Aldrich syndrome family verproline-homologous protein 2 in adenocarcinoma of the lung. Clin Cancer Res 2006;12:2449-54.
152. Iwaya K, Norio K, Mukai K. Coexpression of Arp2 and WAVE2 predicts poor outcome in invasive breast carcinoma. Mod Pathol 2007;20:339-43.
153. Kong B, Wu W, Cheng T, et al. A subset of metastatic pancreatic ductal adenocarcinomas depends quantitatively on oncogenic Kras/Mek/Erk-induced hyperactive mTOR signalling. Gut 2016;65:647-57.
154. Kong B, Cheng T, Wu W, et al. Hypoxia-induced endoplasmic reticulum stress characterizes a necrotic phenotype of pancreatic cancer. Oncotarget 2015;6:32154-60.
155. Cheng T, Jian Z, Li K, et al. In vivo functional dissection of a context-dependent role for Hif1alpha in pancreatic tumorigenesis. Oncogenesis 2016;5:e278.
156. Driscoll DR, Karim SA, Sano M, et al. mTORC2 Signaling Drives the Development and Progression of Pancreatic Cancer. Cancer Res 2016;76:6911-6923.
157. van der Kammen R, Song JY, de Rink I, et al. Knockout of the Arp2/3 complex in epidermis causes a psoriasis-like disease hallmarked by hyperactivation of transcription factor Nrf2. Development 2017;144:4588-4603.
158. Tyanova S, Temu T, Sinitcyn P, et al. The Perseus computational platform for comprehensive analysis of (prote)omics data. Nat Methods 2016;13:731-40.
159. Beres TM, Masui T, Swift GH, et al. PTF1 is an organ-specific and Notch-independent basic helix-loop-helix complex containing the mammalian Suppressor of Hairless (RBP-J) or its paralogue, RBP-L. Mol Cell Biol 2006;26:117-30.
160. Storz P. Acinar cell plasticity and development of pancreatic ductal adenocarcinoma. Nat Rev Gastroenterol Hepatol 2017;14:296-304.
161. Cheng T, Zhang Z, Jian Z, et al. Ductal obstruction promotes formation of preneoplastic lesions from the pancreatic ductal compartment. Int J Cancer 2019;144:2529-2538.
162. Wu CY, Carpenter ES, Takeuchi KK, et al. PI3K regulation of RAC1 is required for KRAS-induced pancreatic tumorigenesis in mice. Gastroenterology 2014;147:1405-16 e7.
163. Blanchoin L, Amann KJ, Higgs HN, et al. Direct observation of dendritic actin filament networks nucleated by Arp2/3 complex and WASP/Scar proteins. Nature 2000;404:1007-11.
164. Robinson RC, Turbedsky K, Kaiser DA, et al. Crystal structure of Arp2/3 complex. Science 2001;294:1679-84.
165. Goley ED, Welch MD. The ARP2/3 complex: an actin nucleator comes of age. Nat Rev Mol Cell Biol 2006;7:713-26.
166. Messal HA, Alt S, Ferreira RMM, et al. Tissue curvature and apicobasal mechanical tension imbalance instruct cancer morphogenesis. Nature 2019;566:126-130.
167. Morrison MM, Young CD, Wang S, et al. mTOR Directs Breast Morphogenesis

through the PKC-alpha-Rac1 Signaling Axis. PLoS Genet 2015;11:e1005291.
168. Morrison Joly M, Williams MM, Hicks DJ, et al. Two distinct mTORC2-dependent pathways converge on Rac1 to drive breast cancer metastasis. Breast Cancer Res 2017;19:74.
169. Bompard G, Caron E. Regulation of WASP/WAVE proteins: making a long story short. J Cell Biol 2004;166:957-62.
170. Hruban RH, van Mansfeld AD, Offerhaus GJ, et al. K-ras oncogene activation in adenocarcinoma of the human pancreas. A study of 82 carcinomas using a combination of mutant-enriched polymerase chain reaction analysis and allele-specific oligonucleotide hybridization. Am J Pathol 1993;143:545-54.
171. Kong B, Wu W, Cheng T, et al. A subset of metastatic pancreatic ductal adenocarcinomas depends quantitatively on oncogenic Kras/Mek/Erk-induced hyperactive mTOR signalling. Gut 2016;65:647-57.
172. Benitz S, Regel I, Reinhard T, et al. Polycomb repressor complex 1 promotes gene silencing through H2AK119 mono-ubiquitination in acinar-to-ductal metaplasia and pancreatic cancer cells. Oncotarget 2016;7:11424-33.
173. Kong B, Bruns P, Behler NA, et al. Dynamic landscape of pancreatic carcinogenesis reveals early molecular networks of malignancy. Gut 2018;67:146-156.
174. Qu C, Konieczny SF. Pancreatic Acinar Cell 3-Dimensional Culture. Bio Protoc 2013;3.
175. Fleming Martinez AK, Storz P. Mimicking and Manipulating Pancreatic Acinar-to-Ductal Metaplasia in 3-dimensional Cell Culture. J Vis Exp 2019.
176. Kühbandner S, Brummer S, Metzger D, et al. Temporally controlled somatic mutagenesis in smooth muscle. Genesis 2000;28:15-22.
177. Zhang YJ, Duan Y, Zheng XF. Targeting the mTOR kinase domain: the second generation of mTOR inhibitors. Drug Discov Today 2011;16:325-31.
178. Basu B, Krebs MG, Sundar R, et al. Vistusertib (dual m-TORC1/2 inhibitor) in combination with paclitaxel in patients with high-grade serous ovarian and squamous non-small-cell lung cancer. Ann Oncol 2018;29:1918-1925.
179. MacDonald A, Scarfe G, Magirr D, et al. Phase I study of orally administered (14)Carbon-isotope labelled-vistusertib (AZD2014), a dual TORC1/2 kinase inhibitor, to assess the absorption, metabolism, excretion, and pharmacokinetics in patients with advanced solid malignancies. Cancer Chemother Pharmacol 2019;83:787-795.
180. Fife CM, McCarroll JA, Kavallaris M. Movers and shakers: cell cytoskeleton in cancer metastasis. Br J Pharmacol 2014;171:5507-23.
181. Lamouille S, Xu J, Derynck R. Molecular mechanisms of epithelial-mesenchymal transition. Nat Rev Mol Cell Biol 2014;15:178-96.
182. Heer NC, Martin AC. Tension, contraction and tissue morphogenesis. Development 2017;144:4249-4260.
183. Svitkina T. The Actin Cytoskeleton and Actin-Based Motility. Cold Spring Harb Perspect Biol 2018;10.
184. Amann KJ, Pollard TD. The Arp2/3 complex nucleates actin filament branches

from the sides of pre-existing filaments. Nat Cell Biol 2001;3:306-10.
185. Mullins RD, Heuser JA, Pollard TD. The interaction of Arp2/3 complex with actin: nucleation, high affinity pointed end capping, and formation of branching networks of filaments. Proc Natl Acad Sci U S A 1998;95:6181-6.
186. Mogilner A, Oster G. Force generation by actin polymerization II: the elastic ratchet and tethered filaments. Biophys J 2003;84:1591-605.
187. De P, Aske JC, Dey N. RAC1 Takes the Lead in Solid Tumors. Cells 2019;8.
188. Ridley AJ, Paterson HF, Johnston CL, et al. The small GTP-binding protein rac regulates growth factor-induced membrane ruffling. Cell 1992;70:401-10.
189. Yoon C, Cho SJ, Chang KK, et al. Role of Rac1 Pathway in Epithelial-to-Mesenchymal Transition and Cancer Stem-like Cell Phenotypes in Gastric Adenocarcinoma. Mol Cancer Res 2017;15:1106-1116.
190. Gulhati P, Bowen KA, Liu J, et al. mTORC1 and mTORC2 regulate EMT, motility, and metastasis of colorectal cancer via RhoA and Rac1 signaling pathways. Cancer Res 2011;71:3246-56.
191. Chen Z, Borek D, Padrick SB, et al. Structure and control of the actin regulatory WAVE complex. Nature 2010;468:533-8.
192. Dummler B, Ohshiro K, Kumar R, et al. Pak protein kinases and their role in cancer. Cancer Metastasis Rev 2009;28:51-63.
193. Ridley AJ. Rho GTPases and actin dynamics in membrane protrusions and vesicle trafficking. Trends Cell Biol 2006;16:522-9.
194. Campellone KG, Welch MD. A nucleator arms race: cellular control of actin assembly. Nat Rev Mol Cell Biol 2010;11:237-51.
195. Hassan Z, Schneeweis C, Wirth M, et al. MTOR inhibitor-based combination therapies for pancreatic cancer. Br J Cancer 2018;118:366-377.

8. Abbreviation

PDAC	Pancreatic ductal adenocarcinoma
SPNs	Solid-pseudopapillary neoplasms
PanNETs	Pancreatic neuroendocrine tumors
PanINs	Pancreatic intraepithelial neoplasias
MCNs	Mucinous cystic neoplasms
IPMNs	Intraductal papillary mucinous neoplasms
GEMMs	Genetically engineered mouse models
LBD	Ligand-binding domain
ER	Estrogen receptor
AFP	Autofluorescent proteins
FACS	Fluorescence-activated cell sorting
ADM	Acinar-to-ductal metaplasia
TGF-α	Transforming growth factor-α
HGF	Hepatocyte growth factor
MMP-9	Matrix-degrading metalloproteinases-9
Hh	Hedgehog
MAPK	Mitogen-activated protein kinase
GTPase	Guanosine triphosphatase
mROS	Mitochondrial reactive oxygen species
CCK	Cholecystokinin
mTOR	Mechanistic target of rapamycin
PIKK	PI3K-related kinase
mTORC1	mTOR complex 1
mTORC2	mTOR complex 2
Rptor	Regulatory-associated protein of mTOR

mLST8	Mammalian lethal with Sec13 protein 8
PRAS40	Proline-rich Akt substrate of 40 kDa
DEPTOR	DEP domain-containing mTOR-interacting protein
TSC	Tuberous Sclerosis Complex
IGF-1	Insulin/insulin-like growth factor-1
S6K	p70S6 Kinase
4EBP	eIF4E Binding Protein
SREBP	Sterol responsive element binding protein
CAD	Carbamoyl-phosphate synthetase
Rictor	Rapamycin insensitive companion of mTOR
SGK	Serum- and glucocorticoid-induced protein kinase
Arp2/3	Actin-related protein 2/3
NPFs	Nucleation-promoting factors
ADF	Actin depolymerizing factor
p-MLC2	Phospho-myosin light chain 2
CHX	Cycloheximide
ICAM-1	Intercellular adhesion morlecule-1
TNF	Tumor necrosis factor
KEGG	Kyoto encyclopedia of genes and genomes
PCR	Polymerase chain reaction
3D	Thress-dimentional
RFP	Red fluorescent protein
IHC	Immunohistochemistry
IF	Immunofluorescence
WB	Western blot
QRT-PCR	Quantitative real-time polymerase chain reaction
PFA	Paraformaldehyde
UV	Ultraviolet
TAM	Tamoxifen

NC	Nitrocellulose
KRAS	Kirsten rat sarcoma viral oncogene homolog
CDKN2A	Cyclin-dependent kinase inhibitor 2A
TP53	Tumor protein p53
SMAD4	Small mothers against decapentaplegic
TGF-β	Transforming growth factor-β
PI3K	Phosphoinositide 3-kinase
Rac1	Rac family small GTPase 1
PKD1	Polycystic kidney disease 1
NF-κB	Nuclear factor kappa-light-chain-enhancer of activated B cells
EGFR	Epidermal growth factor receptor
ADAM17	A disintegrin and metalloptroteinase-17
Rheb	Ras homolog enriched in brain
PIP2	Phosphatidylinositol 4,5-bisphosphate
PIP3	Phosphatidylinositol 3,4,5 trisphosphate
PDK1	Pyruvate dehydrogenase kinase 1
eIF4B	Eukaryotic translation initiation factor 4B
PDCD4	Programmed Cell Death 4
eIF4E	Eukaryotic translation initiation factor 4E
eIF4F	Eukaryotic initiation factor 4F
HIF1α	Hypoxia-inducible factor 1
ULK1	Unc-51-like kinase 1
TFEB	Transcription factor EB
mSin1	Mammalian stress-activated protein kinase interacting protein 1
Protor1/2	Protein observed with rictor 1 and 2
PH	Pleckstrin homology
PKCα	Protein kinase C alpha

Rho	Rhodopsin
Aldh1a3	Aldehyde dehydrogenase 1 family member A3
Krt19	Keratin 19
CHX	Cycloheximide
PAK	p21-activated kinase

9. Acknowledge

I am grateful to the executive committee of the human biology PhD program who gave me the opportunity to carry out my dissertation within the framework of the PhD program at the LMU. I would like to thank PD. Dr. Jan G. D'Haese who is willing to be my supervisor at LMU and to allow me to perform this doctoral work within the frame of scientific collaboration with PD. Dr. Dr. Bo Kong at the surgical department of Technische Universität München (TUM).

Firstly, I would like to thank Univ. Prof. Dr. Helmut Friess for his support of this project. My special thanks to PD. Dr. Dr. Bo Kong for the opportunity and scientific support, the preparation of my dissertation in his working group, participation at numerous national and international conferences that are very motivating, understanding, discussion-friendly support.

Many thanks to PD. Dr. Dr. Bo Kong and Dr. Kathleen Schuck for discussing, reading and correcting the final dissertation. I would like to thank Dr. Susanne Raulefs for her kindly help and scientific suggestion. Many thanks to Ms. Nadja Maeritz for her intensive scientific and dedicated support for the practical part of the work, which is crucial to success and has completed this work.

I would also like to thank Prof. Bernhard Holzmann, Prof. Klaus-Peter Janssen, and PD. Melanie Laschinger for their constant encouragement of my research work and constructive suggestions throughout my stay at surgical department, TUM and Dr. Christina Lugwig (Bavarian Biomolecular Mass Spectrometry Center, TUM) for helping to perform the proteomic analysis. Also many thanks to Dr. Metello Innocenti (BZH, Heidelberg, Germany) for sharing the Arpc4$^{flox/flox}$ line with us.

Many thanks to my colleagues of the pancreas research group, for their kindly supports

during my work.

My parents gave me abundant freedom and financial support to help me finish my PhD study abroad, which is the best love to their daughter. Without their help and understanding, I am not able to concentrate on my research and proceed with my project forward smoothly. I am so lucky to have such kind and considerate parents.

I am grateful to everybody who has been part of my life; thank you all.

Many thanks to the Scholarship Council of the Ministry of Education of China for funding my study, Chirurgische Stiftung der TUM, and the AiF Projekt (ZIM-Kooperationsprojekte, Central Innovation Program Cooperation Projects

Many thanks to all the animals, which have been sacrificed for science.

……. ……

Place, date Signature doctoral candidat